Eastern Kentucky University

# Encompass

2023

# Optimization of Electrode Configurations for Calibration-Free, Remote Sensing of Heavy Metals in Water Using Double-Potenital Step Anodic Coulometry

Jessica Bone
*Eastern Kentucky University*, jessica_bone1@icloud.com

Follow this and additional works at: https://encompass.eku.edu/etd

 Part of the Chemistry Commons

# OPTIMIATION OF ELECTRODE CONFIGURATIONS FOR CALIBRATION-FREE, REMOTE SENSING OF HEAVY METALS IN WATER USING DOUBLE POTENTIAL STEP – ANODIC STRIPPING COULOMETRY

BY

JESSICA BONE

THESIS APPROVED:

_____

Chair, Advisory Committee

_____

Member, Advisory Committee

_____

Member, Advisory Committee

_____

Dean, Graduate School

STATEMENT OF PERMISSION TO USE

In presenting this thesis in partial fulfillment of the requirements for degree conferral at Eastern Kentucky University, I agree that the Library shall make it available to borrowers under rules of the Library. Brief quotations from the documents are allowable without special permission, provided that accurate acknowledgments of the source is made. Permission for extensive quotation from or reproduction of this document may be granted by my major professor in [his/her] absence, by the Head of Interlibrary Services when, in the opinion of either, the proposed use of the material is for scholarly purposes. Any copying or use of the material in this document for financial gain shall not be allowed without written permission.

Signature:

X _Jessica Bone_____

Date:   6/5/2023

OPTIMIATION OF ELECTRODE CONFIGURATIONS FOR CALIBRATION-FREE, REMOTE SENSING OF HEAVY METALS IN WATER USING DOUBLE POTENTIAL STEP – ANODIC STRIPPING COULOMETRY

BY

JESSICA BONE

Submitted to the Faculty of the Graduate School of

Eastern Kentucky University

in partial fulfillment of the requirements for the degree of

MASTER OF SCIENCE

2023

# ACKNOWLEDGEMENTS

ABSTRACT

Many areas around the world are known and predicted to suffer from arsenic-contaminated drinking water resulting in elevated medical issues. Current arsenic detection techniques require that a sample be taken at the site, carried to the lab, and then tested by a skilled technician, which is not practical for remote, hard to reach places. In collaboration with researchers at the University of Louisville and the University of Kentucky, we are designing an electrochemical cell for a calibration-free detection technique that can be performed remotely, eliminating the need for on-site technicians, and helping to prevent chronic arsenic poisoning. A validated and patented device was developed at the University of Louisville as a proof of concept, but the cost, electrode fabrication, and complex assembly requirements limit commercial viability and motivate this work. We are targeting electrodes that can be inkjet printed directly onto a 3D-printed polymer electrochemical cell, simplifying the manufacturing processes and substantially decreasing the costs of the device. We began by investigating the impact of a membrane separating the counter electrode from the working electrode. Then the stability and electrochemical characteristics of inkjet printed gold electrodes on plastic was evaluated through cyclic voltammetry of ferricyanide and scanning electron microscopy.

TABLE OF CONTENTS

LIST OF TABLES

LIST OF FIGURES

## LIST OF COMMON ABBREVIATIONS

Abbreviation                                                                                    Term


ASV............................................................................. Anodic Stripping Voltammetry

CE ...............................................................................Counter Electrode

CV ................................................................................Cyclic Voltammetry

DPS-ASC ......................................... Double Potential Step Anodic Stripping Coulometry

PETG...........................................................Polyethylene terephthalate glycol

PLA ............................................................................... Poly vinyl acid

RE ............................................................................... Reference Electrode

WE................................................................................ Working Electrode

## I. Introduction and Background

### 1.1 Heavy Metals and Humans

Arsenic is thought to be the most carcinogenic elements in the world, naturally existing in the Earth's crust and ground water.[1] When arsenic is combined with elements such as oxygen, chlorine, or sulfur, it is referred to as inorganic arsenic.[2] If combined with carbon and hydrogen, it is termed organic arsenic.[2] There are several avenues for arsenic to enter the environment in forms that negatively impact humans. As it naturally occurs in the crust as a mineral, weathering and mining can exposure resulting in chemical reactions producing oxidized forms of arsenic.[2,3] Metal ores such as lead and copper are known to contain arsenic which is released when mined or smelted.[2] Because of this, human exposure to arsenic is not uncommon through food, water, and air.[2] Both inorganic and organic arsenic have no identifying characteristics such as color, smell, or taste, so the presence of arsenic in water or food often undetected prior to or during its consumption.[2] In the United States, surveys show that 80% of drinking water contains 1 ppb of organic arsenic.[2] The levels of inorganic arsenic in our food and water are substantially lower than organic arsenic, so exposure from food and water in these areas is not harmful.[2] However, many areas around the world experience high concentrations of the harmful, inorganic arsenic in drinking water due to geological and industrial leeching.

Oral ingestion of inorganic arsenic at 60,000 ppb (60 mg/L) or above typically results in death; while much lower concentrations, 300 − 30,000 ppb induce milder symptoms such as stomach irritations, lower production of red and white blood cells, impaired

nerve function, and bruising from blood vessel damage.[2] These mild symptoms result

from a low exposure for a small period of time.[2] Chronic, oral exposure to inorganic

arsenic, even at low concentrations, can lead to serious ailments because it accumulates

in the body overtime.[2,4] Inorganic arsenic exits in several oxidation states such as

trivalent arsenic and pentavalent arsenic.[1,3,5] In all oxidation states, inorganic arsenic is

known to be a carcinogen; specifically causing skin, lung and bladder cancer.[2,4] The most

toxic is arsenite (As3+).[1] Trivalent arsenic deactivates over 200 enzymes, through

bonding with thiol and sulfhydryl groups, leading to organ failure.[4] This has lead the

World Health Organization to create global safe water standards, which are supported

by the Food and Drug Administration in the United States. The FDA and WHO limit the

levels of arsenic in water to 10 ppb.[6]

The largest arsenic water contamination site is in the Bengal Delta Plain in southern Asia,

including India and Bangladesh.[3] In West Bengal, India many are impacted from chronic

arsenic poisoning largely from contaminated drinking water.[7] Hand tubewells used for

generating drinking water in India were installed in the 1960's, however it was unknown

that the sand and clay of the region contained large deposits of arsenic-containing

minerals.[7,8] The presence of arsenic deposits in the Bengal Delta region were not

discovered until 1993.[9] Over time, arsenic levels in the drinking water were well above

WHO guidelines due to natural processes and anthropogenic activities.[7] In 2005 it was

determined that 3200 villages in nine out of the eighteen districts of West Bengal, India

were contaminated with arsenic.[8] In these nine districts 50 million people reside, all who

are at risk for suffering from arsenic-related diseases. In 2008 to 2012, an evaluation of

medical issues due to chronic arsenic poisoning showed a significant difference between individuals with arsenic poisoning and without arsenic exposure.[7] Common medical conditions include skin lesions, hepatomegaly, alopecia, nervous system damage, and ECG abnormalities.[7] While exposure in India is very common due to large amount of arsenic in the sedimentary composition, other areas around the world experience arsenic contamination or are at risk for it. Predictive statistical software has been used to determine areas around the world that are high-risk for possible arsenic contamination based on climate, soil composition, geology, and topography, including China, South-east Asia, and the United States.[9] This prediction data provides areas that should be targeted for contamination surveys to prevent chronic poisoning as groundwater usage increases.[9] Several known areas of contamination and predicted areas of contamination would benefit from frequent water testing, which cannot be accomplished with current detection methods.

Hazardous waste sites are another source of anthropogenic leeching of heavy metals. Noteworthy is the Love Canal landfill incidence between 1942 until 1953.[10] In Niagara County, New York, a chemical company admitted to dumping 21,800 tons of chemical waste from its plant into Niagara Falls.[10] Since then, more than 200 chemicals have been identified there.[10] In 1953 the land was sold from the chemical company to the City of Niagara Falls Board of Education, and home building directly adjacent to the landfill began.[10] Eventually an elementary school opened, furthering community growth in the area.[10] Residents of the area began reporting fumes and minor explosions leading to the New York Department of Health reported significant levels of contamination in 1978.[10]

The New York Department of Health enacted a medical state of emergency, as the chemical exposure adversely affected all human physiologic systems.[10] Since this, the EPA has worked to clean up the hazardous waste at the Love Canal area. In 1979 in Bullitt County, Kentucky, oil and other hazardous materials were reported to the EPA as spilling into Wilson Creek.[11] This launched an investigation by the EPA in what is referred to as the A. L. Taylor site.[11] The owner of the land, Mr. Taylor allowed dumping of chemical waste onto this property for paint and coating industries in Louisville.[11] Many waste drums were dumped, and recycled, while others were stored on the surface.[11] In 1979, 17,051 drums were found on the surface, and 11,628 of those were empty earning this area the name of "Valley of Drums".[11] Analysis of the hazardous substances showed several heavy metals, ketones, chlorinated alkanes and alkanes, and more.[11] In this area, groundwater is not a source of drinking water for the residents, so human exposure to the hazardous waste was limited.[11] The groundwater in this area was found to contain 5 times the national drinking standard of chlorine and 30 times the amount of iron.[11]

The occurrence of these incidences led to the creation of the Comprehensive Environmental Response, Compensation, and Liability Act (CERCLA) in 1980, also called Superfund, to respond to releases of hazardous substances in the environment primarily from manufacturing facilities, processing plants, landfills and mining sites.[12] This act allows the EPA to monitor current hazardous waste sites, hold persons liable to releases of hazardous waste, and clean up waste sites.[12] A part of this program is the identification of hazardous waste sites in the United States called the National Priorities List (NPL).[12]

There are many NPL sites in the United States, represented by the yellow diamonds in Figure 1.1. Areas that have been taken off the NPL are indicated with a green circle, and proposed areas are indicated with a red square.



**Figure 1.1** Environmental Protection Agency's National Priority List (NPL) of Hazardous Waste Sites in the United States showing current sites (yellow diamonds), cleaned sites (green circles), and proposed sites (red circles) taken from Superfund National Priorities List Where You Live Map

## 1.2 Commercially Available Arsenic Detection Techniques

Heavy metals can be effectively analyzed by many instruments and portable detectors currently on the market. These instruments and detectors are chosen based on selectivity and sensitivity parameters, as well as an instrument's limits of detection and quantification for the analyte of interest. Selectivity is the ability of an instrument to differentiate between the analyte of interest and interferences.[13,14] Sensitivity is the smallest amount of change that be detected by an instrument.[13,15] For example, an

instrument that can detect a change in 1.0 ppm from 1.1 ppm is more sensitive than an instrument that can only detect a change from 1.0 ppm to 1.5 ppm. Several of these methods are summarized in Table 1. Typically, highly sensitive instruments with very low limits of detection and quantification are stationed in a laboratory and include inductively coupled plasma (ICP) with mass spectrometry (MS) or optical emission spectrometry (OES) detectors and atomic absorption and/or atomic emission spectrophotometry (AAS and AES). Analyte detection and quantification can be further improved when using chromatographic methods such as high-performance liquid chromatography (HPLC) prior to detection.[15] For these instruments, a technician must go to the site, collect the sample, and bring the sample back to the lab for analysis by a skilled technician. This method of water monitoring is only practical for areas that are easily accessible, and do not require frequent testing. High-risk areas would require frequent, possibly daily testing to measure changes in arsenic concentration in water. Portable devices on the market are also very sensitive and accurate, however many require a skilled technician to operate them correctly. Further, all these techniques only provide a small snapshot of the arsenic concentration at the time the sample was taken. Frequent sampling at high-risk sites is necessary to maintain constant monitoring of arsenic levels, which is not practical. Though the focus of this work is on electrochemical techniques for detection and quantification of arsenic, other commercially available platforms will be briefly summarized here for comparison.

Inductively coupled plasma (ICP) using either mass spectrometry (MS) or optical emission spectrometry (OES), offers detection of arsenic below 1 ppb, which is well

6

below the WHO and FDA standard of 10 ppb.[14,15] In ICP, the liquid sample is nebulized

into an aerosol mist.[15,16] The heat of the argon plasma evaporates solvent and atomizes

and/or ionizes the sample.[15] The analyte species are detected by MS or OES. The MS

detector measures the mass to charge ratio of the ions and can provide lower detections

limit than OES.[15] The selectivity of MS is based on the mass of the element, and the

ability of the mass analyzer in the MS to separate elemental species of different masses.

The heat from the plasma excites electrons, causing them to move to a higher energy

state.[15] The OES detector measures the emission from the electron relaxation.[15] The

selectivity in OES results from the differences in the electronic structures of the

elements. The electrons in one element experience different effective nuclear charges

than electrons of another element, such that the energy differences between the

ground and excited states collectively (for all electrons of a given element) yield a unique

spectral signature for the element, measurable via OES. Spectroscopic detection is

limited by a combination of factors including the background light from the plasma and

the dispersity of the sample (and therefore the emitted photons) in space.

Atomic absorption spectrophotometry (AAS) is another method for determining

the concentration of arsenic in water. The liquid sample is atomized by either a flame of

a furnace in a sample chamber.[2,15] Often for arsenic sampling, a pretreatment procedure

is needed to convert the organic arsenic to inorganic arsenic for accurate results.[2] Once

the sample is heated by the flame, a light source, usually a laser or hollow-cathode lamp

shines light on the atomized sample.[15] The transmitted light is measured by a detector,

and the absorbance is calculated.[15] The USDA reports an analytical procedure using AAS

that can detect arsenic below 1 ppb using a Perkin Elmer Analyst 300, with a Perkin-Elmer Model FIAS 400.[17] Atomic emission spectrophotometry (AES) is similar to AAS and OES. In AES, the sample is atomized by a flame or a furnace.[15] Then a light source, such as a laser, flame, hollow-cathode tube, excites the atoms causing the electrons to move to a higher energy state.[15] As the electrons relax, the emitted light is measured by the AES.[15] The EPA reports a methodology for arsenic detection with ICP-AES with a detection limit at 53 ppb.[18]

To achieve the best detection limits, these detection methods are often coupled with separation techniques such that the analyte of interest is separated from other components in the sample matrix and concentrated before detection. One of these techniques is high-performance liquid chromatography (HPLC), which when coupled with coupled with a Thermo Scientific ELEMENT 2 Sector Field ICP-MS, can detect arsenic concentrations below 1 ppb.[16] In HPLC, analytes are separated based on their relative polarities. The stationary phase (the HPLC column) is typically a silica column, and the analyte is dissolved into a mobile phase (a solvent). For example, in normal phase chromatography the HPLC column is polar, while solvent is less polar.[15] Polar molecule in the solvent will spend more time in the polar stationary phase relative to the nonpolar molecules in the solvent, such that the nonpolar molecules will elute first.[15] Interactions such as electrostatic, dipole-dipole, and Vander Waals forces drive the separation of the analytes in the column. For heavy metal analysis, hydrocarbons in the matrix sample would elute first, while the more polar metal would be retained in

the column longer.[15] Typically, a mass spectrometer or photodiode array are used to detect the analytes after the separation.[15]

**Table 1.1 Commercially Available Arsenic Detection Techniques**

| Analytical Method | Sample detection limit | Basis for Selectivity | Sensitivity | Location of Analysis |
|---|---|---|---|---|
| Inductively Coupled Plasma-Mass Spectrometry | $1.6 \times 10^{-3}$ ppb[16] | Element mass | High | Lab |
| Inductively Coupled Plasma-Optical Emission Spectroscopy | $4 \times 10^{-2}$ ppb[19] | Electronic structure | High | Lab |
| Atomic Absorption Spectrophotometry (AAS) | 1 ppb[17] | Electronic structure | High | Lab |
| Atomic Emission Spectrophotometry (AES) | 53 ppb[18] | Electronic structure | High | Lab |
| Hach Arsenic Test Kit | 10 ppb | Reaction based | Low | On-Site |
| Metal-based nanoparticles | 2 ppb[20] | Reaction based | Low | On-Site |

Several portable devices such as the Hach Arsenic Test Kit from Fondriest Environmental Products can detect arsenic at 10 ppb are commercially available at low cost.[21] With the Hach Test Kit, a test strip is inserted into the lid of the reaction vessel, then the water sample and arsenic reagents are added.[21] In the vessel, hydrogen sulfide is oxidized to sulfate, to reduce interferences in the water sample.[21] Then sulfamic acid and powered zinc reagents react, creating an environment where inorganic arsenic is reduced to arsine gas.[21] Arsine gas reacts with mercuric bromide in the test strip, which causes a color change on the test strip, ranging from yellow to dark brown depending on the inorganic arsenic concentration.[21] The test strip is then compared to a provided standard chart.[21] However, these devices still require on-site monitoring, limiting the applicability of the platform in remote areas where continual monitoring is needed. This

specific device is only capable of completing 100 tests before more supplies are needed.[21] With frequent, remote monitoring an ideal device would be capable of performing much more than 100 tests to provide accurate, real-time data of arsenic concentrations in the water. The prototype cell from the University of Louisville was shown to last for 42 uses, used three times a day for two weeks, and up to 26 days before fouling was observed.[22] Furthermore, the selectivity of this test kit relies on the oxidation of hydrogen sulfide to hydrogen sulfate to eliminate some interferences, as hydrogen sulfide, selenium, antimony, and tellurium are known to interfere with the results of the kit.[21]

Another avenue of arsenic detection is metal-based nanoparticles.[23] This approach is also colorimetric, as the interaction of arsenic and the nanoparticles causes the an observable change in colors.[23] Gold nanoparticles are easily functionalized with sulfur containing ligands, as sulfur and arsenic bonds have a strong affinity.[23] When the functionalized nanoparticles bind with arsenic, a color change occurs such as pink to blue due to localized surface plasma resonance (LSPR); accurate detection of 1 ppb arsenic has been demonstrated with this technique.[23] LSPR refers to the electronic structure of the nanoparticle, also a plasmon, which has localized electrons on the surface that move as an oscillating wave. The electrons are localized on the plasmon surface, but overall delocalized from the individual metal atom, creating resonance. The energy of these electrons is dependent on the size of the nanoparticle. When arsenic interacts with the sulfur containing ligands on the gold nanoparticles, the size of the nanoparticle changes, causing the electronic structure (LSPR) to change. This electronic

structure change is detected through spectroscopic techniques.[24] For example, Shrivas

et al. reported gold-modified lauryl sulfate nanoparticles to have a detection limit of 2

ppb.[20,23] While this is within the FDA and WHO detection limits, several issues

complicate the use of nanoparticle-based quantification techniques such as pH changes

in water and competing metal interactions that hinder accurate quantification of

arsenic.[23] The selectivity of this method depends on the uniqueness of the sulfur and

gold reaction. If another element could bind to the sulfur ligand enacting a similar

electronic structure change, then the determined arsenic calculation would be inflated.

### 1.3 Electrochemical detection and quantification of arsenic

Electrochemistry offers very sensitive and selective methods to measure heavy metal

concentrations. Electrochemistry is based on redox reactions, where electrons are

transferred between chemical species (atoms, molecules, ions) or between chemical

species and an electrode. Equation (1.1a) shows the reduction of trivalent arsenic, and

Equation (1.1b) the oxidation of trivalent arsenic.

(1.1a)  $As^{3+} (aq) + 1\ e^- \rightarrow As^{2+} (s)$

(1.1b) $As^{2+} (s) \rightarrow As^{3+} (aq) + 1\ e^-$
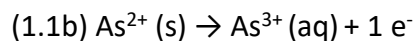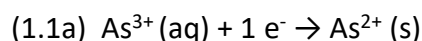
When the redox reaction occurs between a chemical species and an electrode, the

movement of electrons generates current, which can be measured in an electrical

circuit. Typically, the electrical circuit is referred to as an electrochemical cell, which is

composed of three electrodes: working electrode (WE), counter electrode (CE), and

reference electrode (RE). Figure 1.2 shows some commercially available electrodes and

a glass frit.
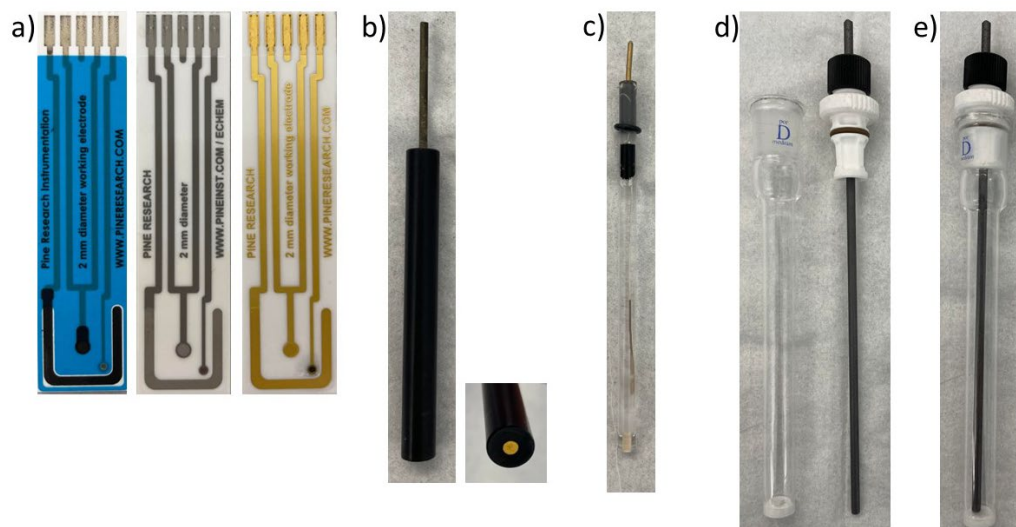
**Figure 1.2** Electrode configurations used in this work. PINE Research screen-printed planar electrodes with a reference electrode (RE), counter electrode (CE), and working electrode (WE) printed onto a substrate (a). In blue is carbon on polymer substrate, silver is platinum on ceramic substrate, and gold is gold on ceramic substrate. CHI Instrument gold rod WE (b), Ag|AgCl gel RE (c), glass frit, and graphite rod as the CE (c). The graphite rod fits into the glass frit (e).

The working electrode (WE) is where the reaction of interest occurs. The potentiostat controls the applied voltage (the potential difference between the working and reference electrodes), providing the driving force for the redox reactions.[25] Current generated from electrons in these redox reactions is referred to as faradaic current.[26] There are several common materials and characteristics that must be considered when choosing the WE. The electrode material must be conductive, electrochemically stable, allow for rapid electron transfer, and have reproductible electrical, microstructural, and chemical properties.[26] Common solid electrode materials are carbon, platinum, and gold. Choice of WE includes consideration of the reduction and oxidation potentials of the WE.[26] If the WE is electrochemically active in the same potential region that the

12

analyte of interest is electrochemically active, as signal from the WE redox events will interfere with signal from the analyte. The final electrochemical sensor will use gold as the working electrode material, is known to be electrochemically stable, allows for rapid electron transfer, and has a different reduction and oxidation potential than arsenic. Gold also has a hydrogen overpotential than platinum.[22]

The counter electrode (CE) works in conjunction with the WE by allowing electrons to flow into and out of the WE to generate current.[25] The CE should be approximately 10 times the surface area of the WE to prevent reactions occurring at the CE from inhibiting the reactions at the WE.[25] Further, the material of the CE is purposely selected to be as inert as possible. These properties help lower the noise from reactions occurring at the CE. Due to the electron flow, reactions not of interest may occur at the counter electrode and contribute to current (noise). To overcome this noise, the counter electrode is often separated from the electrochemical cell by a porous frit, such as the glass frit shown in Figure 1.2d, which allows electrons but not analyte to pass between the bulk solution and the CE surface.[25]

The reference electrode (RE) functions as a reference point for the other electrodes potential can be measured.[25] The material of the RE must have a well-defined potential and be stable so that the potential of the WE can be well regulated.[25] Common materials used are the standard hydrogen electrode or Ag|AgCl[25] In our work, the electrochemical sensor WE is gold and an Ag|AgCl gel RE is used. In the design of the electrochemical sensor, the distance between the working electrode and reference electrode will be minimized to decrease impacts of solution resistance.[26]

Current generated from processes other than redox reactions is referred to as non-faradaic current. This type of current can include capacitance current, also called charging current. Charging current refers to the current passed when charge builds up on the electrode surface in response to an applied potential. The amount of this charge depends, in part, on the magnitude of the applied potential. When a potential is applied, counter ions of the supporting electrolyte located next to the WE are electrostatically attracted to the WE surface, creating a layer of opposite charge in the solution nearest the WE. For instance, if the applied potential generates excess electrons near the electrode/solution interface, a thin layer of counter cations will be electrostatically attracted to the WE surface. This generates a small amount of current, which is measured by the potentiostat. A second layer of counter ions (in this case anions) then forms adjacent to the anions. Together, these layers of charges are termed the double layer. The double layer building is illustrated in Figure 1.3.
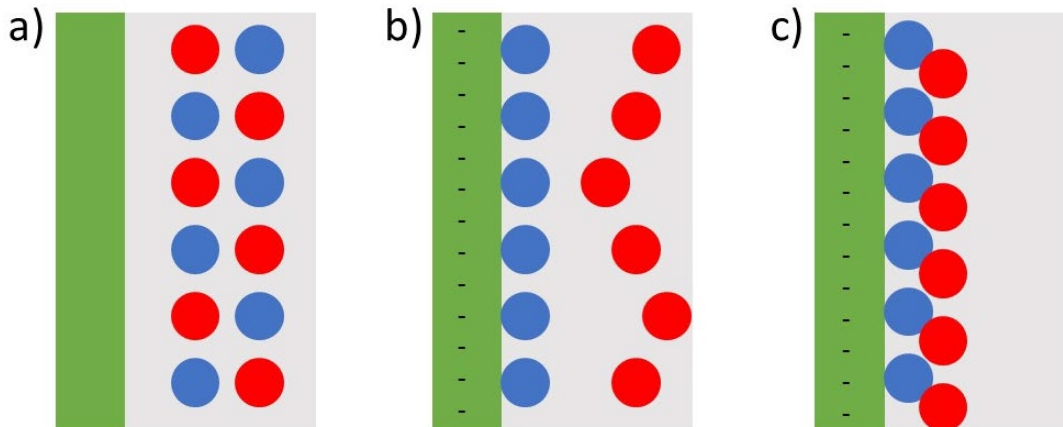
**Figure 1.3** Depiction of formation of the double layer at the WE surface (green); solvent molecules have been omitted for clarity. With no applied potential (a), the relative concentrations of anions (red) and cations (blue) near the WE surface are equivalent. When a potential is applied such that an excess of electrons are found at the WE surface (b), cations are electrostatically attracted to the WE such that the relative concentrations of cations and anions at the WE surface are no longer equivalent; a layer of anions forms adjacent to the cations (c) to yield the double layer.

The charge generated from a redox reaction is directly proportional to the amount of material undergoing the redox reaction as described by Faraday's first law, shown in Equation 1.2,

$$(1.2) \qquad\qquad m=kq$$

where the m is the mass of the electrolyzed material and q is charge. By substituting q for nFCV, analyte concentration can be quantified, as shown in Equation 1.3.

$$(1.3) \qquad\qquad q = nFCV$$

where n is the number of electrons transferred in the redox reaction of interest, F is Faraday's constant, C is the concentration of the solution, and V is the volume of the sample.[27] When the analyte is known, the number of electrons transferred by its oxidation (or reduction) is also known. The sample volume can be controlled and known,

allowing determination of analyte concentration from the measured charge. This equation allows for accurate calculations of analyte concentration from electrochemical measurements, making electrochemistry a useful technique for heavy metal analysis in water. For example, the reduction of arsenic onto a WE (plating, Figure 1.4b) and the subsequent oxidation of arsenic (stripping, Figure 1.4c) is shown in Figure 1.4.
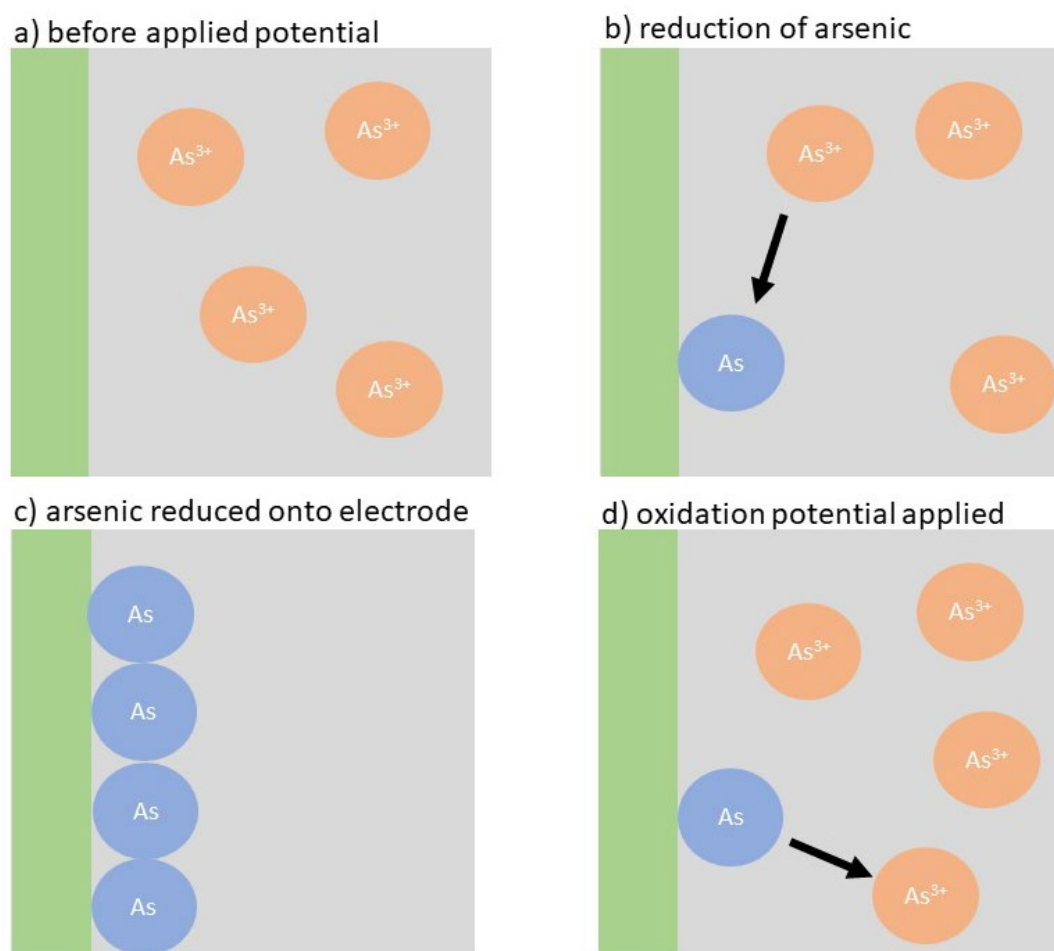


**Figure 1.4** Aqueous trivalent arsenic near the working electrode surface (a), is reduced to solid arsenic (b), and deposits onto the electrode surface (c), then deposited arsenic is oxidized off the electrode surface returning to aqueous trivalent arsenic (d). Solvent molecules and electrolyte ions have been omitted for simplicity.

For example, in Figure 1.4, there are 4 arsenic atoms plated, so the number of electrons exchanged (n) is 4. If a concentration (C) of 5 ppm, a sample volume (V) of 9.95 x 10$^{-8}$

16

nL, and exhaustive plating is assumed, Equation 1.3 can be used to determine the charge (q). Anodic Stripping Coulometry (ASC) is a two-step electrochemical technique; the applied potential steps as a function of time and the measured chronoamperogram for a typical ASC experiment are shown in Figure 1.5.[28]
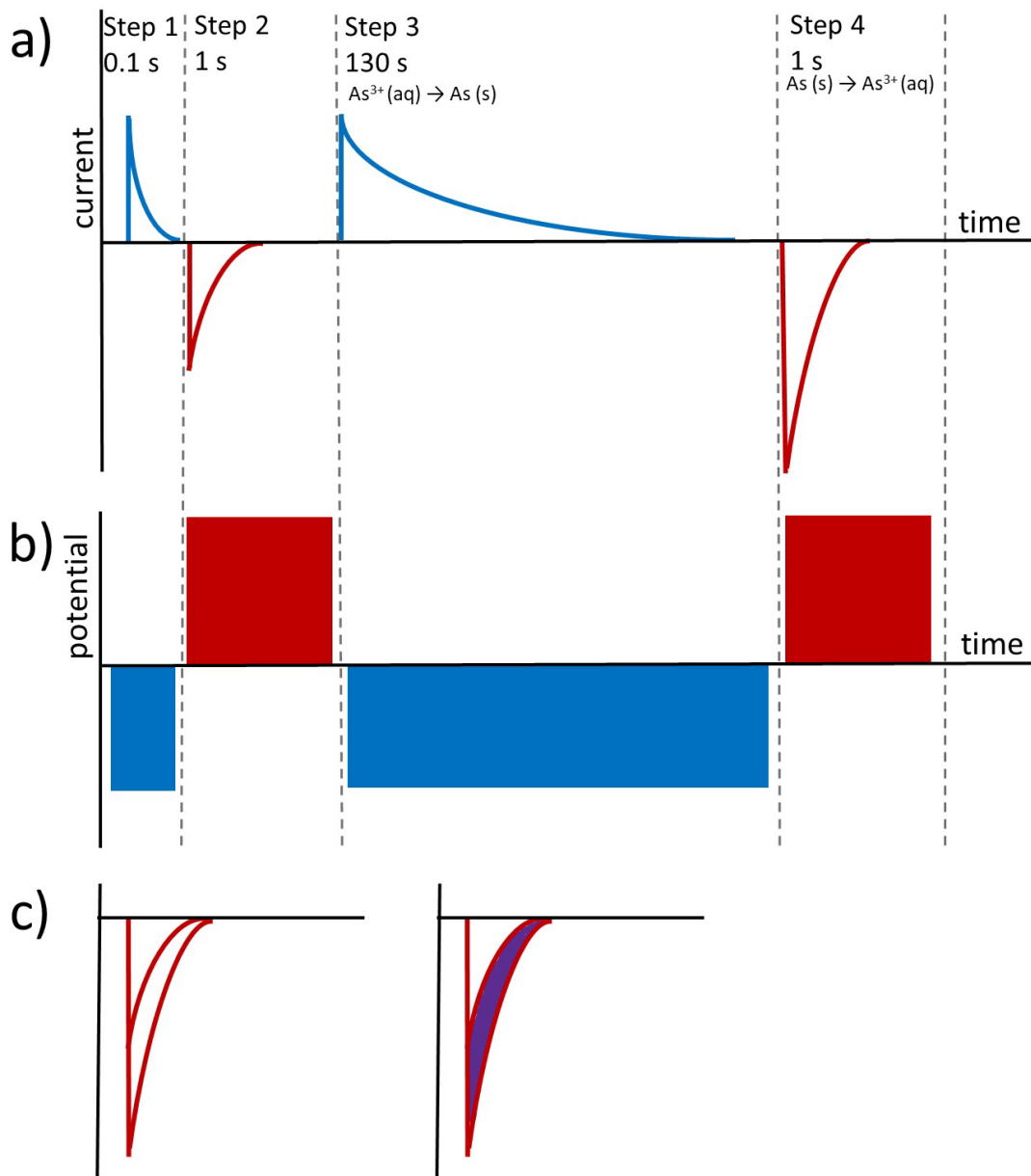
**Figure 1.5** Representative chronoamperogram (a) resulting from the double step potential – anodic stripping coulometry pulse sequence (DSP-ASC). Step 1 and Step 2 result from charging current acting as a background measurement. Step 3 allows for plating of the analyte, and Step 4 (stripping) consists of current from charging and analyte oxidation. Representative voltammetry time trace of applied potential for Step 1 – 4 (b).Subtraction of the charge passed in Step 2 from the charge passed during Step 4 enables quantification of the analyte (c). The faradaic current, current produced from the analyte is highlighted in purple.

The potential of the first step is chosen such that the metal species of interest is reduced and thereby deposited on an electrode surface.[28] Then, a potential sufficient to oxidize the analyte is applied causing the metal to be stripped off.[28] The area of the stripping peak (charge) is directly proportional to the concentration of analyte as given by Faraday's Law.[6,29] This method provides detection limits in the ppb level, which is in the range of the WHO arsenic contamination limit.

In electrochemical measurements, the measured current includes both faradaic and non-faradaic current. To quantify the amount of analyte oxidized or reduced, the non-faradaic current must first be subtracted from the total current. Both charging current and faradaic current occur during the stripping step of anodic stripping coulometry (ASC). To correct for charging current, a step sequence is applied to a blank sample (no analyte present), and the resulting current is subtracted from the total sample current to yield a background-corrected current. Subsequently, a calibration curve is generated using solutions with known concentrations of the analyte. Because this method requires preparation and measurement of solutions, ASC is not practical for a remote sensor.

A related technique, double potential step-anodic stripping coulometry (DPS-ASC) depicted in Figure 1.5, uses the analyte solution itself to measure the charging current. In the first step a suitable deposition potential is briefly applied (step 1) and then the potential is stepped to a suitable stripping potential (step 2). Step 1 is long enough for electrode charging to occur, which usually occurs in 100 ms.[6] However, step 1 is not long enough for reduction of analyte because diffusion of the analyte to the

electrode surface is slow relative to charging processes. Thus, the current generated during step 2 can be assumed to result from non-faradaic processes only. During step 3, the deposition potential is applied for a longer time allowing diffusion of analyte to the electrode surface and reduction of the analyte. During step 4, the potential is stepped to an oxidizing potential and the metal strips off the electrode producing a current that includes the faradaic current and the charging current. The faradaic current is determined by subtracting the charging current measured during step 2 from the current measured in step 4.

When the sample volume is large, meaning the only some of the analyte has time to diffuse to the electrode surface during the plating step (step 3), a calibration curve is required for accurate quantification using DPS-ASC because the measured current is proportional to concentration. However, if the sample volume is known and sufficiently small for all analyte to diffuse to the electrode surface during plating (step 3), the current measured during stripping (step 4) is *equal* to the amount of analyte present in the volume of the sample (after correction for non-faradaic processes). In this latter case, DPS-ASC can be used to quantify an analyte without need for external calibration. A DPS-ASC sensor built with a known, sufficiently small volume does not require a technician to be operational and could be operated remotely, providing frequent, operator-free testing of arsenic levels.

At the University of Louisville, a validated and patented stop flow electrochemical cell for quantification of arsenic capable of working remotely without calibration was developed.[6,27] In the prototype device a patterned gold chip functioning

as the WE and was contained in a rubber sealed compartment.[6] The counter electrode

was a pyrolytic graphite sheet contained also in a rubberized compartment.[6] The CE

compartment was housed above the working electrode compartment separated by a

200 molecular weight cut-off membrane.[6] The compartments were surrounded by two

polycarbonate fixtures.[6] The RE, a custom made Ag|AgCl miniature electrode, was

inserted into the counter electrode chamber via a small hole.[6] The working electrode

chamber of the device was designed to hold $1 - 2$ μL of sample such that exhaustive

plating and stripping occurred.[27]

However, there were several complications with this device, motivating our

work. The volume of the WE chamber can be calculated, but reassembly of the device

causes the chamber volume to change due to the compressibility of the silicone gasket

between the WE and the membrane. For commercial viability, reproduceable sample

chamber volume is key for quantification using Faraday's Laws in Equation 1.2. If the

volume is different than anticipated, the apparent analyte concentration will be

inaccurate. Further, the device contains many layers, making reassembly complicated

for users. The cost of manufacturing the cell was estimated to be over $1000 per sensor,

due primarily to the clean-room fabrication of the gold working electrodes. The

combination of complicated assembly and high cost limit the commercial viability of this

device and motivate this work.

## 1.4 Our Work

Collectively, our work aims to modify the protype electrochemical cell. In an

attempt to eliminate the variability of the sample chamber volume, we investigated the

impacts of the separation of counter electrode and working electrode to see if the

21

desired limit of detection could be reached without separation. If separation of the CE and WE is not necessary, then the compressible membrane will not be necessary. During this work an experimental and statistical methodology was developed for use in subsequent experiments. This work is described in Chapter 2. In an attempt to reduce the number of layers (for easier assembly), streamline manufacturing, and reduce costs, we investigated gold WEs, comparing various commercially available options to inkjet printed gold WEs produced at the University of Kentucky. This work is described in Chapter 3. Future directions are described in Chapter 4.

## II. Investigation of Electrode Separation as it Relates to Charging Current and

## Quantification

The electrochemical cell used in this work consists of three electrodes: working electrode (WE), counter electrode (CE) and reference electrode (CE) as described in Chapter 1.[25] Current is recorded as electrons flow between the WE and the CE. The surface area of the CE is typically larger than that of the WE so that kinetic factors do
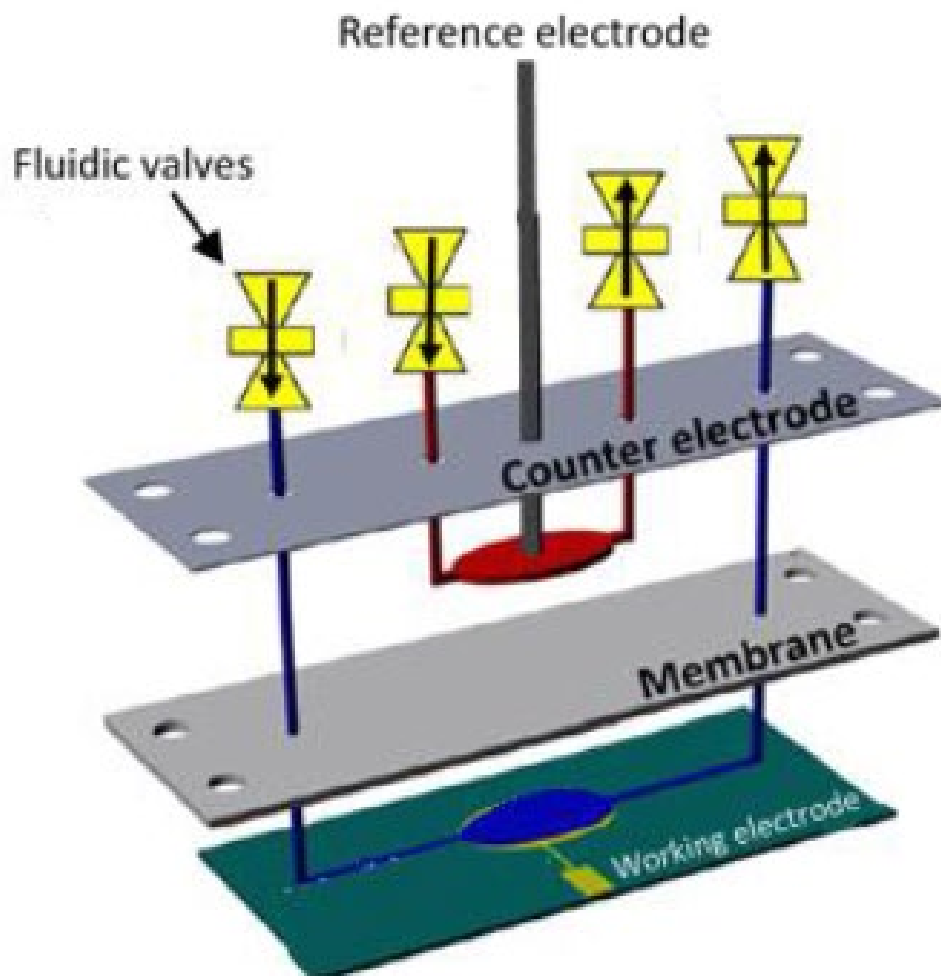


Figure 2.1. Simplified diagram of the prototype electrochemical cell patented by the University of Louisville team illustrating the membrane separating the counter electrode and working electrode chambers taken from ref Khat 2019.

not inhibit the reaction at the WE. Further, the material of the CE is purposely selected to be as inert as possible. These steps help lower the noise from reactions occurring at the counter electrode. To increase the signal to noise ratio, the WE and CE are often isolated from each other. In the electrochemical cell patented by the University of Louisville team, a membrane on top of a flexible silicone gasket separates the WE and CE chambers.

As mentioned, the flexibility and compressibility of the silicone gasket hinders reproducibility of sample chamber volume between reassemblies, which in turn hinders reproducibility for quantification of arsenic. This motivates our efforts to simplify the cell. This chapter describes our investigation into the impacts of separating the WE and CE on noise and limits of detection for quantification of lead in the 100 ppb - 1000 ppb range. In these experiments, the electrochemical cell was simplified to three electrodes in a beaker instead of the proposed device from UofL. This cell configuration allows for the counter electrode to be separated from the bulk solution or not for comparison, whereas the prototype electrochemical sensor only allows for CE separation. Our goal of the initial experiments is to determine if the CE needs to be separated from the bulk solution or not, so comparison between these configurations is necessary.

Calibration-free anodic stripping coulometry (ASC) relies on exhaustively plating the analyte. This is possible with the proposed device configurations because the sample volume is small, $1 - 2$ µL. For ease, we used a much larger cell volume (10 mL), where exhaustive plating is not practical. Anodic stripping voltammetry (ASV) is a complimentary electrochemical technique, and the chemical processes occurring during

24

the measurement are analogous to those in ASC. The first step is the same as ASC, where the potential is held at a sufficient voltage long enough to reductively plate the analyte. Then, the potential is swept positively, oxidatively stripping the analyte from the WE surface. Rather than determining the charge passed during stripping, peak currents, which are proportional to analyte concentration, are used. ASV is not a calibration-free technique, requiring analysis of known samples to generate a calibration curve before quantification is possible. Because calibration is needed, exhaustive plating is not needed, enabling analysis of larger sample volumes. The potential step sequences and representative voltammograms during ASV are shown in Figure 2.2.
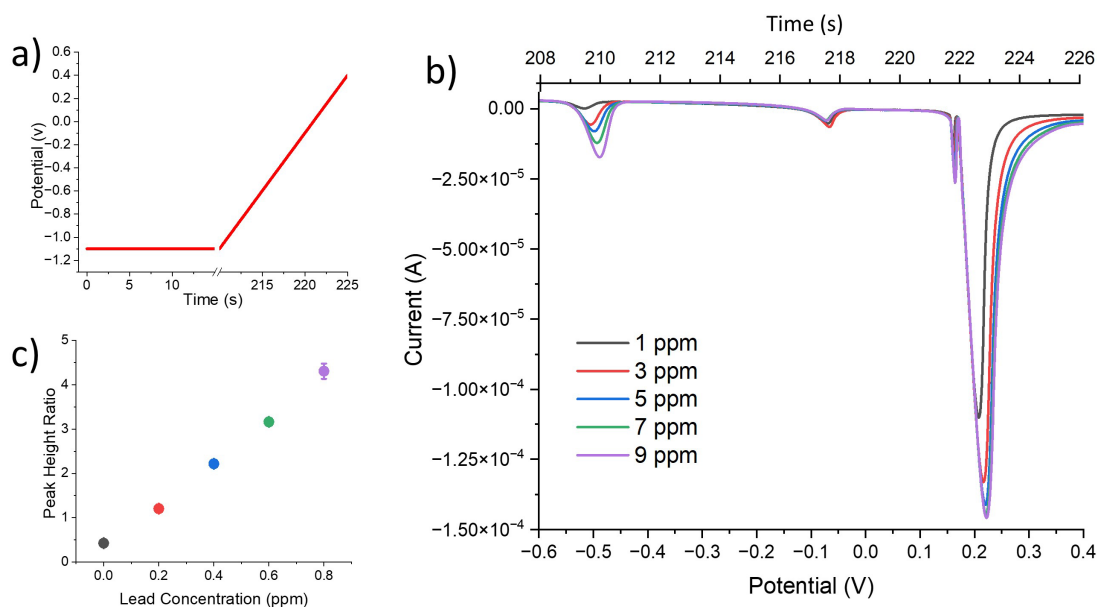
**Figure 2.2.** Anodic stripping voltammetry time trace of applied potential (a), and Anodic stripping voltammetry time trace of measured current for increasing concentrations of lead (b). Mercury, copper, and lead are plated for a sufficient amount of time at -1.1 V vs. Ag|AgCl, and then the potential is swept from -1.1 V to +0.4 V at a scan rate of 100 mV/s. Peak height ratio of lead peak height/copper peak height versus lead concentration (c)

## 2.1 Materials and Methods

*Reagents:* Sodium citrate from Fisher Chemical ACS grade, citric acid monohydrate from Fischer Chemical certified ACS grade, 1000 ppm mercury from Fisher Chemical, 1000 ppm lead from Fluka Analytical AAS grade in 2% w/w nitric acid, 1000 ppm copper in 3% nitric acid from Fisher Chemical, 1000 ppm arsenic standard for ICP from Sigma-Aldrich in 2% w/w nitric acid, potassium chloride from Fischer Chemical, concentrated nitric acid from Fisher Chemical certified ASC plus, concentrated hydrochloric acid from Fisher Chemical certified ASC plus, 18 MΩ water.

*Instrumentation:* All electrochemical measurements were performed using a CHI 760E bipotentiostat.

*Three electrode electrochemical cell:* A 3-electrode electrochemical cell, which consists of a WE, CE, and RE, was used for the electrochemical studies described here. Several WE were used: a fixed disc, non-rotating, 2 mm diameter gold rod from CHI, Inc, gold screen-printed electrode on ceramic from Pine Research, platinum screen-printed electrode on ceramic from Pine Research, and carbon screen-printed electrode on polyethylene terephthalate from Pine Research, gold inkjet printed, thermally annealed on glass manufactured at the University of Kentucky, gold inkjet printed, photoannealed on glass manufactured at the University of Kentucky, and gold inkjet printed, photoannealed on PLA substrate manufactured at the University of Kentucky. The counter electrode was a graphite rod. The reference electrode was an Ag|AgCl gel electrode. All potentials here are reported with respect to Ag|AgCl unless otherwise noted. A glass-fritted isolation tube was used to separate the counter electrode from the solution containing the WE and RE. The CE, WE, RE, and glass-fritted isolation tube are shown in Figure 2.3. The gold working electrode was polished with MicroPolish Powder of 0.05 micron particle size from CH Instruments, INC on a polishing pad. The electrode was moved in a figure-eight motion for three minutes and then rinsed thoroughly with copious amounts of 18 M$\Omega$ water.
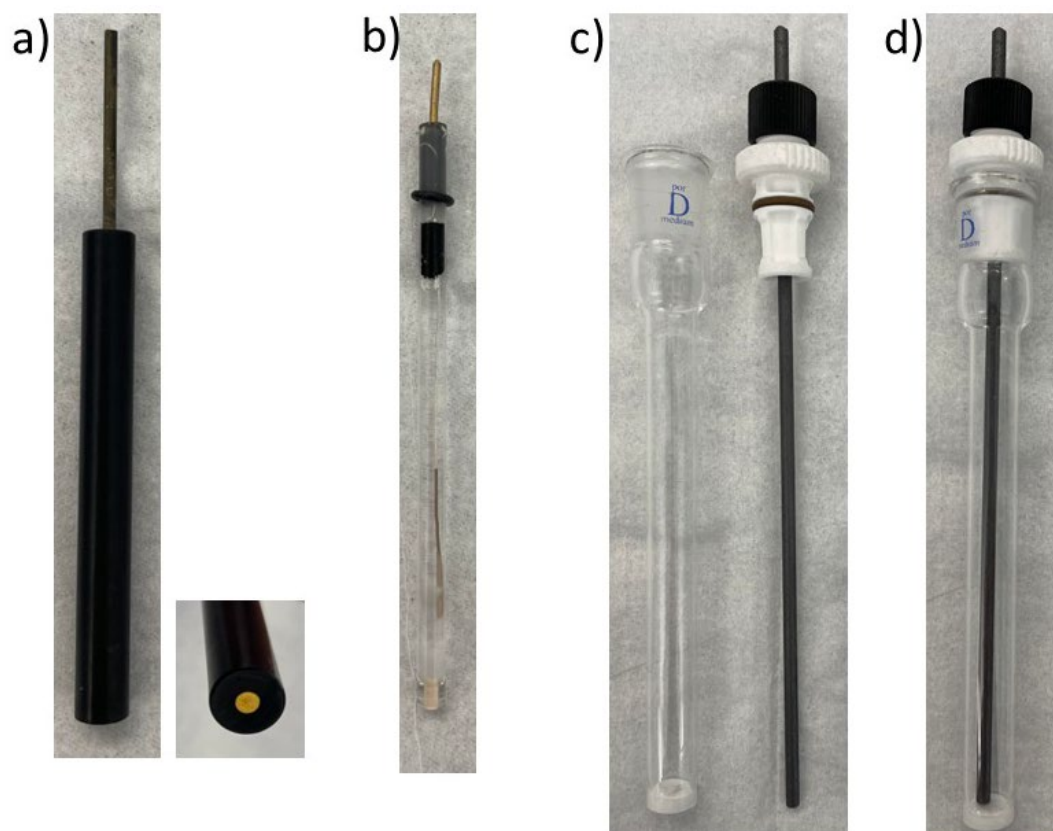
**Figure 2.3** Electrodes and frit. Shown is the working electrode as a fixed disc, non-rotating, 2 mm diameter gold rod (a), the reference electrode as an Ag|AgCl gel electrode (b), and the graphite rod counter electrode and a glass-fritted isolation tube (c), and the CE inserted into the glass-fritted isolation tube (d).

Further evaluation of counter electrode separation was completed using a screen-printed carbon electrode from Pine Research. Screen-printed Pine electrodes contain the WE, CE, and RE electrode assemblies screen printed onto a planar substrate as shown in Figure 2.4. For these electrodes, the WE and CE were of the same material (carbon, platinum, or gold). The RE was Ag|AgCl. The substrate material for the carbon electrode (Fig. 2.4a) is polyethylene terephthalate. For the platinum and gold electrodes (Fig. 2.4b and Fig 2.4c), the substrate is ceramic.
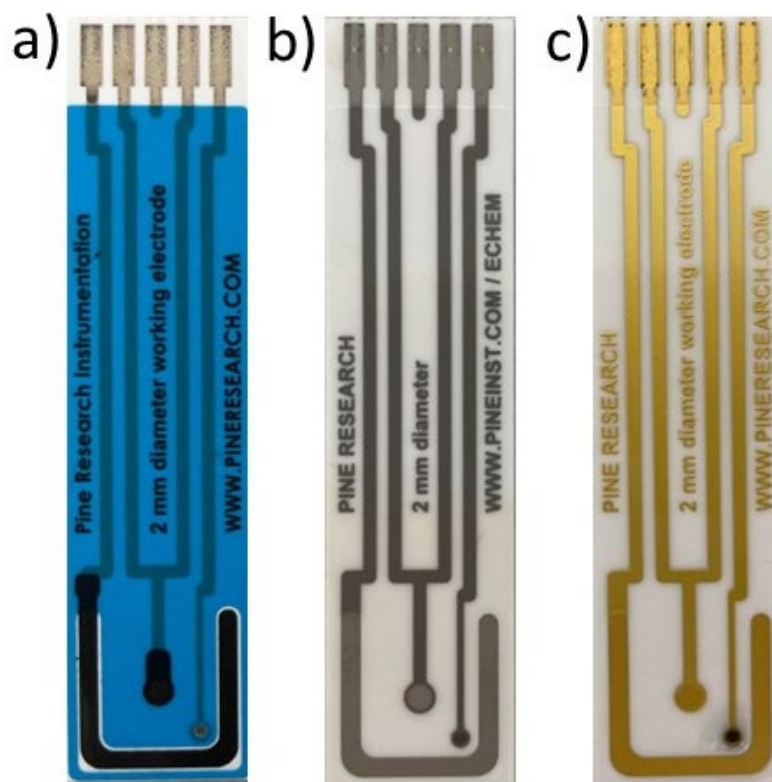


**Figure 2.4** Pine Research screen printed electrode assemblies with the WE and CE made of carbon (a), platinum (b), or gold (c). The RE printed is Ag|AgCl.

The electrochemical cell was assembled and filled with 15 mL of the sample solution. The potential step and sweep sequences are depicted in Figure 2.2. Briefly, the cell is held at a potential of -1.1 V for 180 seconds while the solution was stirring and for an additional 30 second without stirring. Next, the potential was swept from -1.1 V to +0.4 V at a rate of 100 mV/s; data for quantification is collected during this sweep. Finally, the cell potential was held at +0.4 V for 180 seconds to fully strip off the metals before beginning the next trial. For all solutions, ASV experiments were performed with the CE fritted and with the CE directly in the solution; ASV was collected in triplicate for each solution. Five experiments were conducted to compare the linearity of current peak height as a function of concentration as compiled in Table 2.1.

**Table 2.1 Anodic Stripping Voltammetry of Sample Solution Compositions**

| Experiment | Working Electrode | Analyte or Standard | Internal Standard | Mercury |
|---|---|---|---|---|
| 1 | Gold rod | Pb, 1 - 9 ppm | Cu, 0.1 ppm | Yes, 10 ppm |
| 2 | Gold rod | Pb, 1 - 9 ppm | None | Yes, 10 ppm |
| 3 | Gold rod | Pb, 1 - 9 ppm | None | None |
| 4 | Planar | Pb, 1 - 9 ppm | Cu, 0.1 ppm | Yes, 10 ppm |
| 5 | Planar | Pb, 1 - 9 ppm | None | None |

The solutions used during Experiment 1 contained three different metals: 10 ppm mercury, 0.1 pm lead, and 0.1 ppm copper. Mercury deposits onto the working electrode area to create a uniform area for copper and lead deposition. Lead is the metal of interest (the analyte). Copper acts as an internal standard. An ampergram of the

sweeping segment if shown in Figure 2.5, and the peak heights corresponding to oxidation of copper and lead were recorded. The peak height ration was calculated by diving the lead peak height by the copper peak height. For each experiment, the peak height of lead increased in magnitude with increasing lead concentration shown in Figure 2.5 inset. For experiments containing the internal standard of copper, the lead peak height was divided by the copper peak height to provide a peak height ratio.
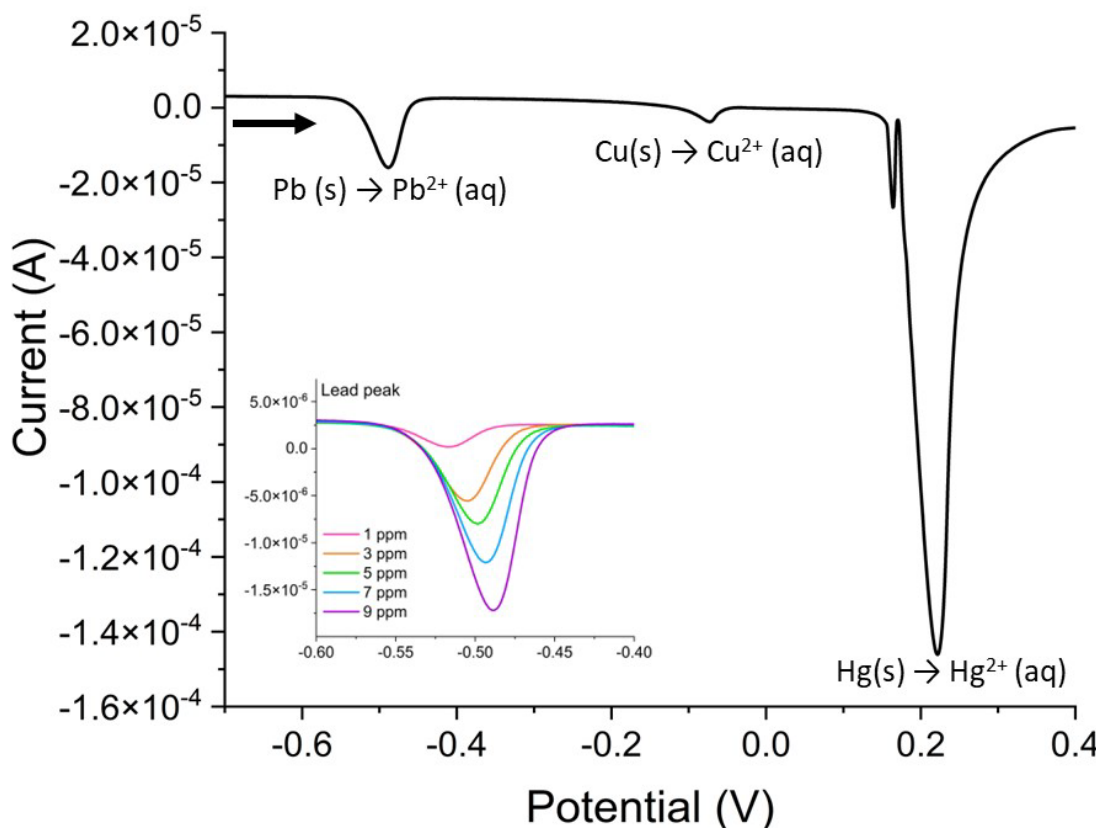


**Figure 2.5** Typical voltammogram collected during Experiment 1 contains peaks corresponding to the oxidation of 0.9 ppm lead (-0.51 V), 0.1 ppm copper (-0.03 V), and 10 ppm mercury (0.22 V). Lead peak current increased with increasing lead concentration (inset).

Our target system will not require calibration, so in Experient 2, copper was removed from the starting solution. In Experiment 3, copper and mercury were both removed from the solution. In Experiment 4, a planar screen-printed carbon electrode from PINE Research was used, with the presence of copper and mercury. In Experiment 5, a planar screen-printed carbon electrode from PINE Research was used, without the presence of copper or mercury.

Anodic Stripping Voltammetry for planar electrode evaluation

The target of the sensor is to detect arsenic. The planar electrodes evaluated with the interest of arsenic and not lead. The electrochemical cell was assembled and filled with 15 mL of the sample solution. For the Pine Research electrodes, the screen-printed counter electrode was used the CE, and the screen-printed RE was used, unless stated that a gel Ag|AgCl electrode was used. The planar electrodes from the University of Kentucky were used as the WE, the CE was a graphite rode, and the RE was a gel Ag|AgCl. The potential was held at -0.6 V for 180 s with stirring, then for an additional 30 seconds without stirring. The potential was swept from -0.6 V to +0.5 V at a scan rate of 100 mV/s. Finally, the cell potential was held at +0.5 V for 180 s to full strip off plated arsenic. Each ASV was collected in quintuplet. For each electrode, the current peak height was measured and plotted as a function of arsenic concentration.

## 2.2 Statistical Methods

In this work, the use of statistics was necessary to quantitatively compare the performance of the electrochemical cell as the electrode materials and configurations are varied in the presence of different redox-active species. Statistical data was used for quantitative comparison rather than to create a predictive model. The current

generated during a redox reaction is directly proportional to the amount of material present according to Faraday's Law (Eqn. 1.2), the relationship between peak current (or peak current ratio) and concentration is linear. For the statistical analyses, forms of linear regression were used to characterize the linear trend observed. In working to describe this data, several statistical models are used: a simple linear regression, a repeated measures ANOVA, and a linear mixed model. The limit of detection and linear dynamic range for the different sensor arrangements is also investigated using the simple linear model.

There are four assumptions of linear regression that must be met for the model to be useful. The first assumption is that there is a linear relationship between the independent and dependent variables. In this project, the peak current (or peak current ratio in Experiment 1) from the redox-active material has a linear relationship with the redox-active material's concentration. The peak current from the oxidation of lead is proportional to the concentration of lead. The other three assumptions involve the residuals. The residuals must be independent of each other, homoscedastic, and normally distributed. To define a residual, the least squares line must first be defined. In performing linear regression, a straight line is drawn through a data set that minimizes the sums of squares of the residuals, or residual sums of squares. This line is called the least squares regression line. It most accurately represents the pattern of the data points used to calculate it. Figure 2.6 shows an example of an accurate least squares regression line in red, and an inaccurate least squares regression line in blue.
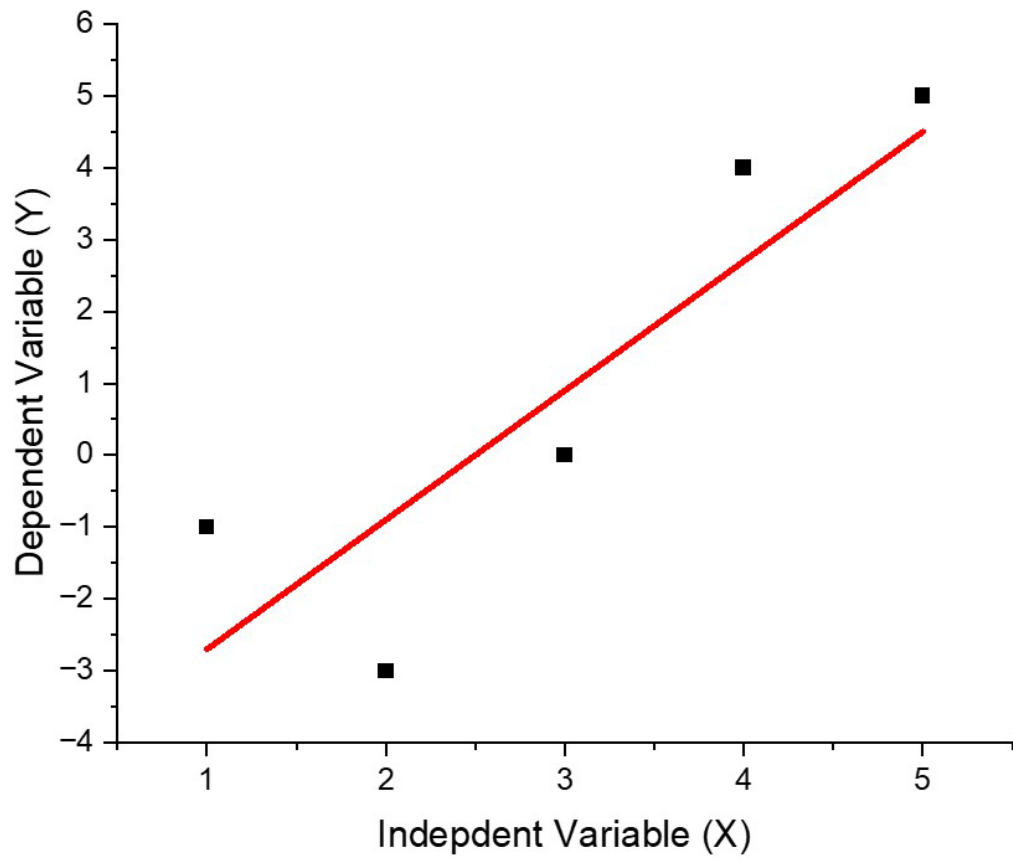
**Figure 2.6** A least squares regression line in shown in red through generic data plotted on a scatter plot.

An inaccurate least square line does not minimize the residuals, while the accurate one does. A residual is calculated from subtracting the actual value, $y$, from the predicted value, $\hat{y}$. Figure 2.7 illustrates the graphical approach to calculating a residual.
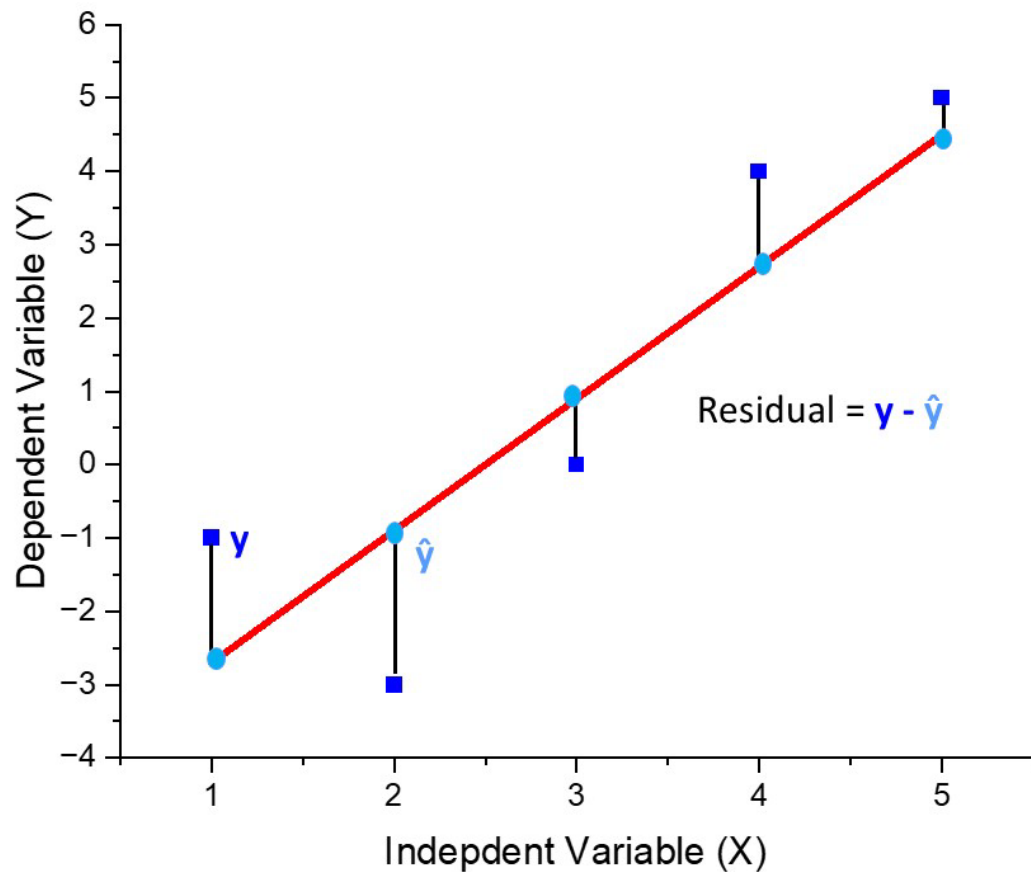


**Figure 2.7** Residual analysis of a least squares regression line for e a generic data set. A residual (black line) is calculated by subtracting the predicted value ($\hat{y}$; light blue dot) provided by the least squares regression line (red line) from the observed value (y; dark blue square).

Quantitively, the magnitude of the residuals is calculated with the residual sums of squares (RSS). The residual sums of squares, also known as sums of squares of the residuals, was calculated for each model, as shown in Equation 2.1, calculation.

(2.1)

$$RSS = \sum_{i=1}^{n} (y_i - \hat{y}_i)^2$$

where n is the number of sample points.

In this calculation, each residual is squared and then summed. Software is programed to calculate a least squares regression line that has the lowest RSS value. The coefficient of determination ($R^2$) is another statistic used to describe how well the least squares line fits the data. Equation 2.2 shows the calculation for the coefficient of determination.

(2.2)

$$R^2 = 1 - \frac{\sum_{i=1}^{n}(y_i - \hat{y}_i)^2}{\sum_{i=1}^{n}(y_i - \bar{y}_i)^2}$$

Where $\hat{y}$ is the predicted value of y from the regression model, $y$ is the actual value of y from the collected data, and $\bar{y}$ is the mean of the y values. $R^2$ explains how much of the variance in the dependent variable (peak current or peak current ratio) can be explained by the independent variable (concentration). Thus, the $R^2$ value can be used to describe how well the model fits the real-world data. There is not a formal statistical test to compare $R^2$ values, so they were directly compared. The closer $R^2$ is to 1, the more linear the data.

The Pearson's r value (r) is a more qualitative approach to evaluating the least squares regression line, shown in Equation 2.3.

(2.3)

$$r = \frac{\sum_{i=1}^{n}(x_i - \bar{x})(y_i - \bar{y})}{\sqrt{\sum_{i=1}^{n}(x_i - \bar{x})^2}\sqrt{\sum_{i=1}^{n}(y_i - \bar{y})^2}}$$

Where $x_i$ is the actual variable, $\bar{x}$ is the mean of the x variable, $y_i$ is the actual value of y variable from the collected data, and $\bar{y}$ is the mean of the y values. Pearson's r is most often used to state if the relationship has a positive or negative correlation. For these experiments, a positive, linear relationship is expected, so each r value should be positive.

The linear regression model assumptions are graphically tested for the data collected in this project. The independence of the residuals relates back to current peak height (or peak height ratio) collected in the experiment, meaning that if there is independence in the current peak height collected, then the residuals are also independent. Independence between the samples, and thus residuals, was evaluated through overlaying the oxidation peak from the stripping step of each trial at each concentration. The metal sample was plated onto the electrode then stripped off multiple times at each concentration, without changing the solution. Chemically, the electrode surface should be the same between each collection, so there should be no clear pattern nor trend as a function of number of trials between the oxidation peak magnitudes when overlayed. Additional stirring between each ASV ensured that the solution concentration nearest the working electrode surface was chemically the same for each trial. Figure 2.8 shows a representative overlay of three replicates showing the

37

lead and copper oxidation peaks from Experiment 1 without separation of the counter

electrode with a frit.
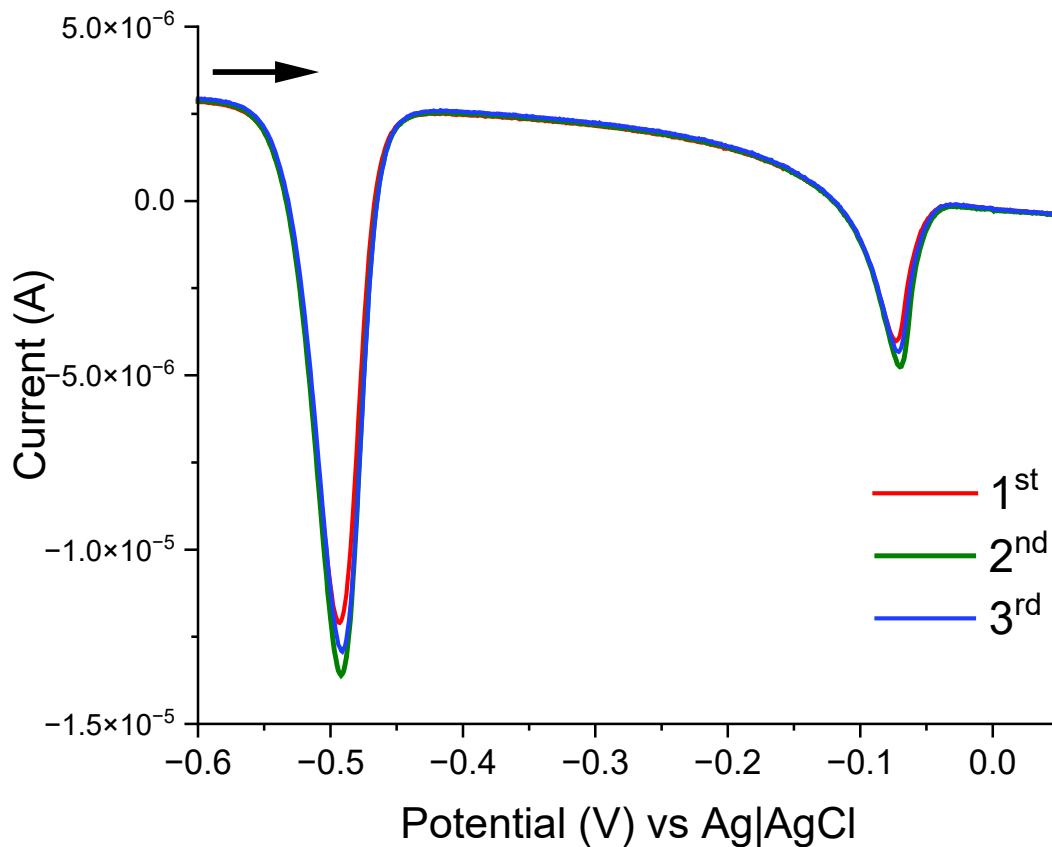


**Figure 2.8** Voltammograms of three replicates showing the lead (0.7 ppm) and copper (0.1 ppm) oxidation peaks from the Experiment 1; the CE was not separated via frit during these trials.

Differences in  first, second, and third current peak heights do not trend with

number of trials and appear to be random.

Next, the residuals should be homoscedastic; meaning that they should be

randomly distributed as the concentration increases. A plot of the residuals versus the

concentration shows if the residuals are randomly distributed. If the residuals are not

randomly distrusted a pattern such as coning would be visible. The residuals vs. lead

concentration for the simple linear regression without CE separation (red) and with CE

separation (blue) is shown in Figure 2.9.

In the simple linear model, the peak current ratios (Experiment 1 and 4), and
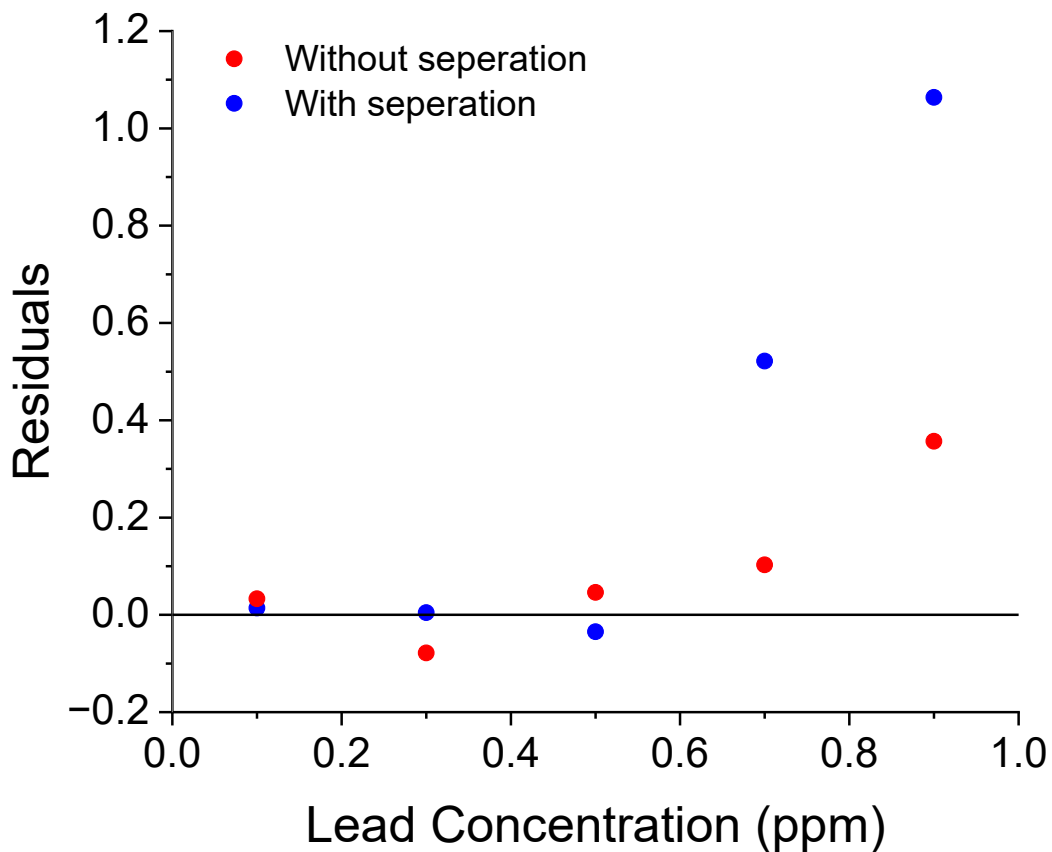


**Figure 2.9** Residuals versus lead concentration for the simple linear regression without separation (red) and with separation (blue).

peak currents (Experiment 2, 3, and 5) were averaged so that there is only one data

point for each concentration. In Figure 2.10, there is random scattering of the data

points along the x-axis for both electrode configurations at lower concentrations.

However, the residuals tend to increase at higher concentrations. The residuals vs. lead

concentration for the repeated measures ANOVA and linear mixed model regression

without separation (red) and with separation (blue) is shown in Figure 2.10. Since these models view the data the same way, the residuals are the same. For both electrode configurations, the residuals are randomly scattered around the x-axis for all the concentrations.
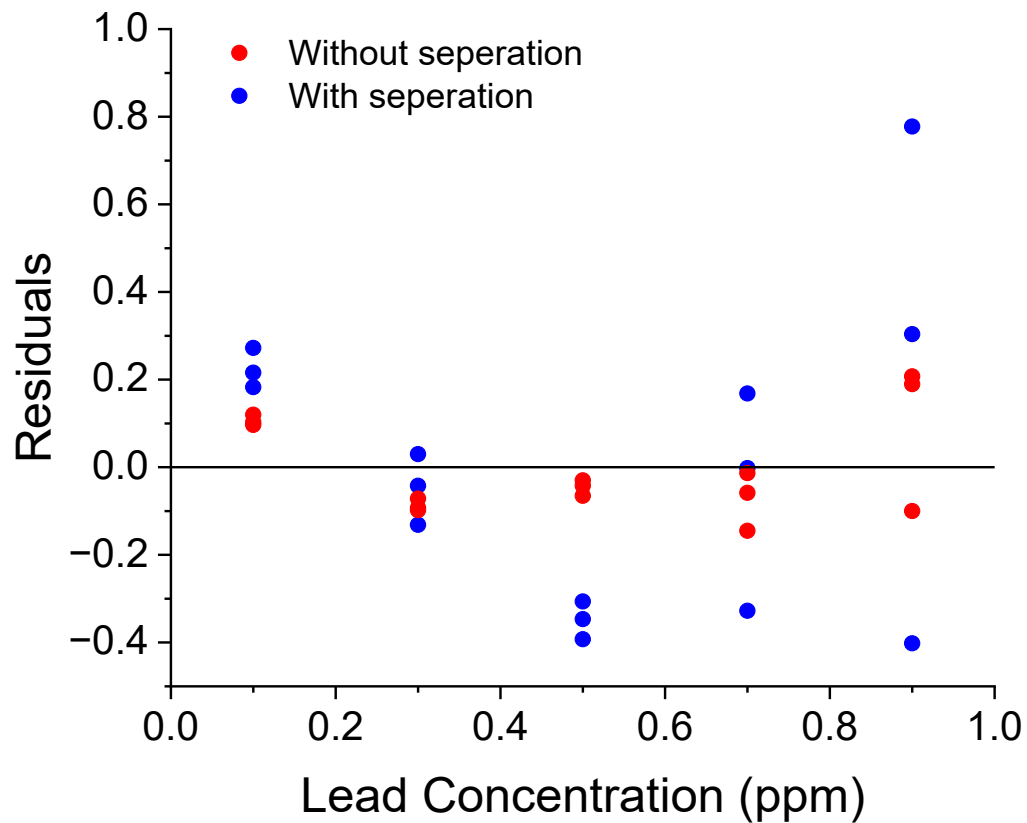


**Figure 2.10** Residuals versus lead concentration for the repeated measures ANOVA and linear mixed model without CE separation (red) and with CE separation (blue).

Lastly, the normality of the residuals was graphically validated through a probability-probability plot (p-p plot), which examines the distribution of the data.

Figure 2.11 shows the p-p plot from Experiment 1 without CE separation (red) and with

CE separation (blue) using the simple linear model.
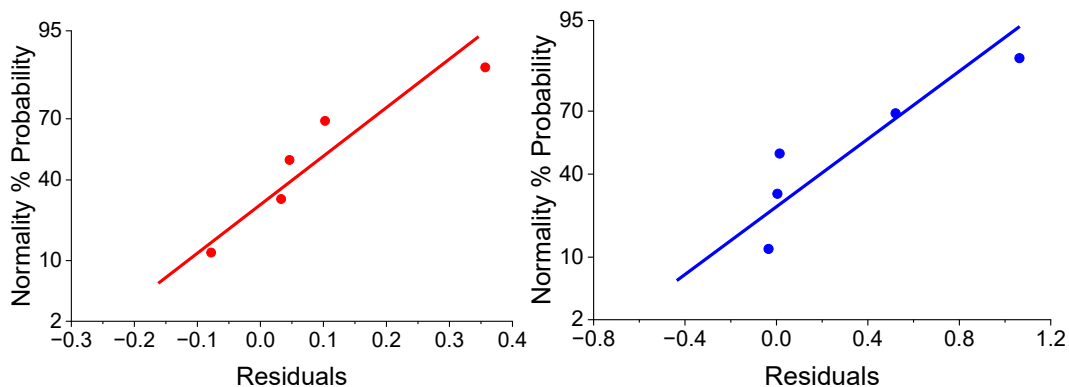


**Figure 2.11** Probability-Probability (p-p) plot of Experiment 1 without CE separation (red) and with CE separation (blue) using the simple linear model.

In this plot, the data would be considered normally distributed if it is perfectly

linear. Since this is only a graphical approach, near linear data is sufficient to conclude

that the residuals are normally distributed. If the residuals are not linear, this means

that they are not normally distributed, and so the model does not accurately represent

the data. In these experiments, this indicates that there is something chemically

occurring to cause the linear model to be ill fitting. Figure 2.11 shows the p-p plot from

Experiment 1 without CE separation (red) and with CE separation (blue) using the

repeated measures ANOVA and linear mixed model.
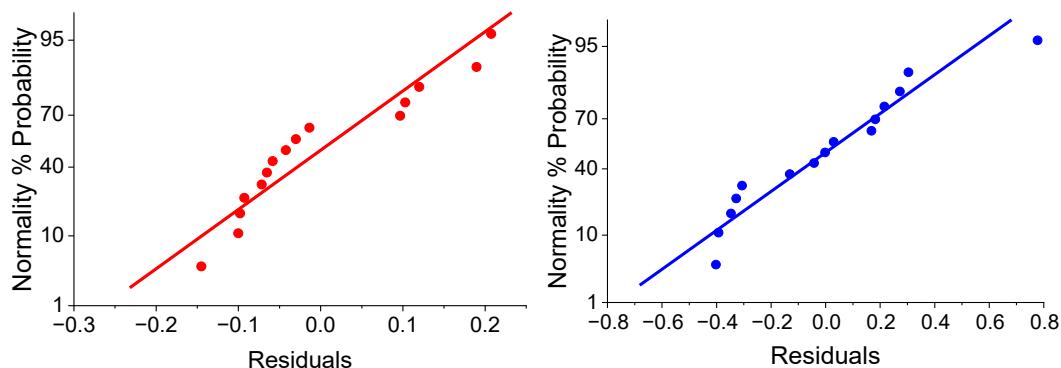
**Figure 2.12** Probability-Probability (p-p) plot of Experiment 1 without CE separation (red) and with CE separation (blue) using the repeated measures ANOVA and linear mixed model.

In Figure 2.12, both electrode configurations appear to have near linear data. For all three models, the assumptions have been verified, or otherwise noted. Because all necessary assumptions have been satisfied, the results of the regression models can be evaluated. First was a simple linear regression, where the peak current was averaged. In this model view, each data point is viewed as a single measurement at the corresponding concentration. In the analysis, we know that the singular data point represents an averaged value, but the model calculation does not. The interpretation of the simple linear regression results will only accurately describe averaged values, not the singular values. Since we are only using these models to compare linearity between different electrode configurations, the results and interpretation will still be useful.

In the repeated measures analysis of variance (ANOVA) and linear mixed model (LMM) the data is viewed as if it were a repeated measure on the same sample. A LMM is conceptually the same as an ANOVA, but some of the calculations are computed differently. Similarly, coefficient of determination ($R^2$), residual sums of squares (RSS),

and Pearson's r (r) will be the same value because they are representing the same data. However, in an ANOVA, the calculation for the degrees of freedom for the error term, a value needed to calculate a F-statistic and a p-value, is only approximated.[30] A package in R studio, lme4, offers the calculation of a LMM, where the degrees of freedom of the errors is acutely calculated.[30] The LMM model provides an F-statistic and a p-value, which more strongly supports the coefficient of determination ($R^2$), residual sums of squares (RSS), and Pearson's r (r) results of the model. The repeated measures ANOVA is more commonly understood than the LMM, so it has been included in the statistical results.

Evaluating the data from both viewpoints may provide chemical insight to the electrochemical cell that would have been overlooked otherwise. For each experiment, the coefficient of determination ($R^2$) was the primary statistic used for comparison. The residual sums of squares (RSS) and Pearson's r (r) were included in the statistical summaries for completion. The choice to use $R^2$ as the primary source for comparison between electrode configurations was based on the familiarity of the statistic and the ease of contextual meaning.

## 2.3 Results of Counter Electrode Comparison

The steps of analysis are outlined in Scheme 2.1. In general, the first step is pretreatment of the working electrode, if applicable to the electrode material. Second, analysis of redox-active species. Third, anodic stripping voltammetry (ASV) of lead solutions. Lastly, statistical analysis of the results using a simple linear model, repeated measures ANOVA, and a LMM.

**Scheme 2.1. Counter Electrode Analysis Outline**
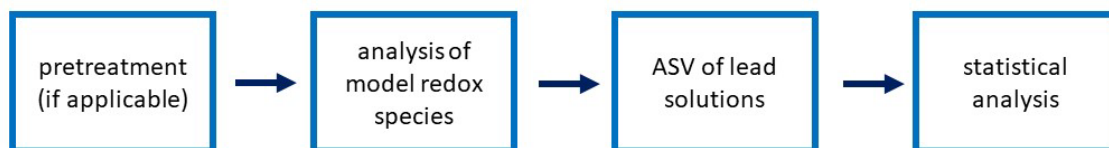
Analysis of a model redox-active species

Cyclic voltammograms of ferricyanide with the gold rod working electrode from

CHI and with the CE separated (blue) and without the CE separated (red) are shown in

Figure 2.13
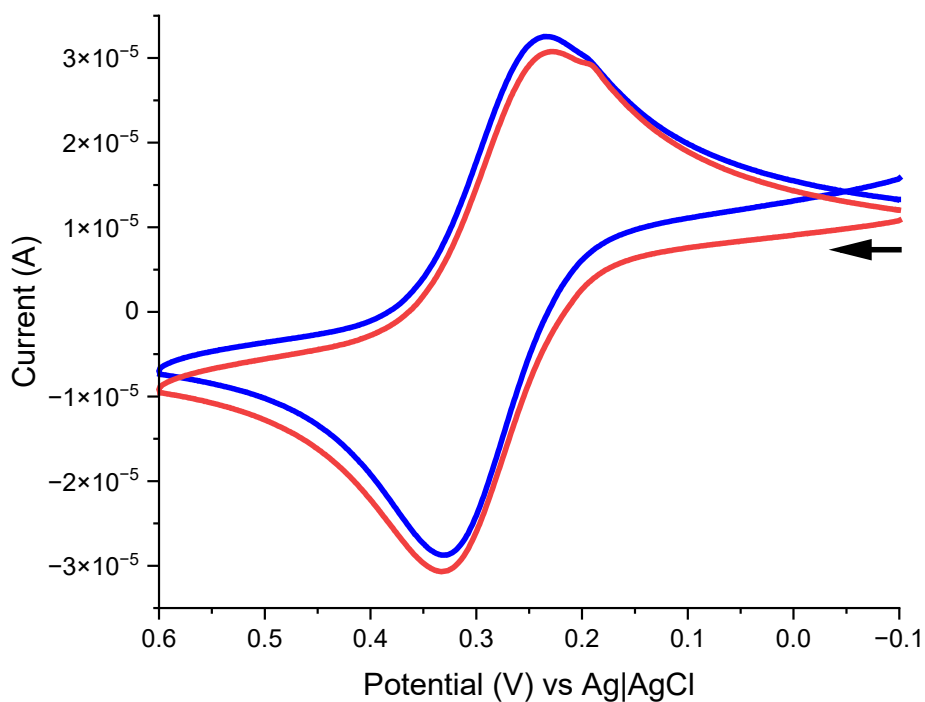


Figure 2.13. Cyclic voltammograms of 0.5 M ferricyanide using the gold rod as the working electrode with the CE fritted (red), and not fritted (blue).

Ferricyanide is commonly used to assess the electrochemical performance of

electrodes, modified electrodes, and electrode assemblies in aqueous systems.

Ferricyanide is reduced as the potential is swept from -0.1 V to +0.6 V, Equation 2.4a.

Then ferricyanide is oxidized as the potential is swept in the reverse, from +0.0 V to-0.8

V, Equation 2.4b.

(2.4a) $FCN^{3+} + e^- \rightarrow FCN^{4+}$

(2.4b) $FCN^{4+} \rightarrow FCN^{3+} + e^-$
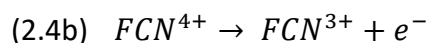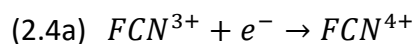
The peaks observed result from the diffusion of oxidized ferricyanide from the

bulk solution to the electrode surface as the potential is swept positively, and from

unoxidized ferricyanide moving away from the electrode surface as it is stripped off the

electrode.[25] In Figure 2.13, the ferricyanide voltammograms collected with the CE

separated (fritted) and not fritted have the same peak oxidation potential (0.337 V) and

reduction potential (0.228 V), and similar peak oxidation and reduction currents). There

is no change in peak splitting observed. In later experiments with the fabricated WE, the

shapes and splitting of the ferricyanide peaks will provide insight to the properties of

the gold WE.

The CV of gold in the presence of $H_2SO_4$, and the CV of ferricyanide will be used

to ascertain the quality and properties of fabricated gold electrodes. It is important to

note that the surface area of the gold rod working electrode is different than other

working electrodes used in later work. The current peak height is expected to vary

between working electrodes because of the surface area differences, but the shape of

the peaks should remain nearly identical.

Analyte analysis and generation of calibration curves

In these experiments, anodic stripping voltammetry (ASV) was utilized instead of

anodic stripping coulometry (ASC) due to the size of the sample chamber, which is too

large to practically allow exhaustive plating. With ASV, mercury is often added to the solution. Mercury is more easily reduced than many metal analytes; solution mercury plates onto the gold electrode and then the analytes are reduced onto the mercury thin film. This ensures that all analyte species experience an identical WE surface. However, the final design of the sensor will not include mercury, so the influence of mercury on quantification was evaluated while evaluating the counter electrode configurations.

An internal standard of copper was used in Experiment 1 and 4. An internal standard is a compound, different from the analyte that is added initially as a known amount.[15] Signal produced from the analyte is compared to the signal from the internal standard.[15] Internal standards are chosen so that they produce an analytical signal that is distinguishable from the analyte's signal.[15] In electrochemistry, the instrument response can vary slightly from run to run. The internal standard accounts for this variation. If the instrument causes variation in the internal standard's signal, the same degree of variation will be seen in the analyte's response.[15] So, when the internal standard and analyte's signal is compared, the variation will be accounted for. In these experiments, the lead signal is divided by the copper signal for comparison.

To understand the impacts of CE separation (or lack thereof) on quantification, we first analyzed standard solutions in the presence of Hg and the internal standard as a function of CE separation (Experiment 1). We then performed the same experiments with internal standard only (Experiment 2). Next, we analyzed the standard solutions without Hg and without an internal standard (Experiment 3). In Experiments 1-3, the WE were a gold rod. Experiment 4 and 5 used the same solution parameters as Experiment

3, but the WE was planar gold to more closely resemble our target electrode configuration.

This series of experiments allows for a comparison of the separated and not separated counter electrode. The statistical results from the simple linear regression model are summarized in Table 2.2, from the repeated measures ANOVA Table 2.3, and from the linear mixed model Table 2.4. The discussion of experimental results only discusses the coefficient of determination ($R^2$) from the linear mixed model. All raw data and additional analyses are found in the SI.

Analysis of Experiment 1 yielded an $R^2$ for the separated CE of 0.9658 ($F_{1,13}$=396.8, $p < 0.01$) and, without CE separation was 0.993 ($F_{1,13}$=2068, $p < 0.01$). We consider these coefficients to be sufficiently similar.

In Experiment 2, greater variation of peak current within the same concentration measurements was expected because we were comparing peak heights rather than peak height ratios as done in Experiment 1. The data do show greater variation among the same concentration measurements, however high coefficient of determinations were still achieved without the internal standard. With the LMM, the $R^2$ for the separated counter electrode was 1.0 ($F_{1,13}$= 1.157 x $10^{33}$, $p < 0.01$) and, without separation was 0.949 ($F_{1,13}$=263.2, $p < 0.01$). The $R^2$ was considered sufficiently high for both counter electrode configurations,

In Experiment 3, the absence of the mercury thin film allowed evaluation of lead quantification efforts on the gold surface. Variation within the same concentration measurements was expected and observed because the gold surface is through to be

less uniform than that of the mercury thin film. However high coefficients of determination were still observed. With the LMM, the $R^2$ for the separated counter electrode was 0.938, ($F_{1,13}$=213.6, p < 0.01), and without separation was 0.979, ($F_{1,13}$=642.6, p < 0.01). The $R^2$ was high for both counter electrode configurations. The $R^2$ are highest when the mercury thin film and copper internal standard are used, but these will not be used in later ASC evaluations of the manufactured electrodes, nor will they be present in the final electrochemical cell design.

In the analysis of Experiment 4 the peak height ratio of lead to copper and only the lead peak was evaluated. For the lead to copper peak height the $R^2$ was 0.970 ($F_{1,13}$= 454.4, p < 0.01) using the LMM. Analyzing only the lead peak yielded a $R^2$ of 0.966 ($F_{1,13}$= 396.7, p < 0.01), slightly lower than with the internal standard.

Analysis of Experiment 5 data yielded substantially different results than Experiments 1-4.The $R^2$ was very low at 0.830 ($F_{1,13}$= 69.57, p < 0.01). The statistical results for the simple linear regression model are summarized in Table 2.2, for the repeated measures ANOVA Table 2.3, and for the LMM Table 2.4.

**Table 2.2 Statistical results for all experiments using the simple linear regression model.**

| Experiment | Summary | Statistic | Result | |
|---|---|---|---|---|
| | | | With separation | Without separation |
| 1 | 10 ppm mercury, 0.1 ppm copper, 0.1 ppm lead with gold rod WE | $R^2$ | 0.990 | 0.992 |
| | | RSS | 8.246 | 52.496 |
| | | Pearson's r | 0.996 | 0.994 |
| 2 | 10 ppm mercury, 0.1 ppm copper, 0.1 ppm lead with gold rod WE | $R^2$ | 0.999 | 0.999 |
| | | RSS | 0.043 | 0.710 |
| | | Pearson's r | 0.999 | 0.999 |
| 3 | 0.1 ppm lead with gold rod WE | $R^2$ | 0.992 | 0.9971 |
| | | RSS | 2.191 | 3.625 |
| | | Pearson's r | 0.997 | 0.999 |

| | | | | |
|---|---|---|---|---|
| 4 | 10 ppm mercury, 0.1 ppm copper, 0.1 ppm lead with SPCE | $R^2$ | 0.956 | |
| | | RSS | 2.736 | |
| | | Pearson's r | 0.998 | |
| 5 | 0.1 ppm lead with SPCE | $R^2$ | 0.870 | |
| | | RSS | 4.031 | |
| | | Pearson's r | 0.950 | |

**Table 2.3 Statistical results for all experiments using the repeated measures ANOVA model.**

| Experiment | Summary | Statistic | Result | |
|---|---|---|---|---|
| | | | With separation | Without separation |
| 1 | 10 ppm mercury, 0.1 ppm copper, 0.1 ppm lead with gold rod WE | $R^2$ | 0.966 | 0.993 |
| | | RSS | 1.536 | 0.17 |
| | | Pearson's r | 0.984 | 0.997 |
| 2 | 10 ppm mercury, 0.1 ppm copper, 0.1 ppm lead with gold rod WE | $R^2$ | 0.941 | 0.949 |
| | | RSS | $2.5970 \times 10^{-11}$ | $2.0979 \times 10^{-11}$ |
| | | Pearson's r | 0.975 | 0.976 |
| 3 | 0.1 ppm lead with gold rod WE | $R^2$ | 0.938 | 0.979 |
| | | RSS | $4.343 \times 10^{-11}$ | $9.680 \times 10^{-12}$ |
| | | Pearson's r | 0.971 | 0.990 |
| 4 | 10 ppm mercury, 0.1 ppm copper, 0.1 ppm lead with SPCE | $R^2$ | 0.970 | |
| | | RSS | 0.361 | |
| | | Pearson's r | 0.986 | |
| 5 | 0.1 ppm lead with SPCE | $R^2$ | 0.830 | |
| | | RSS | $4.167 \times 10^{-11}$ | |
| | | Pearson's r | 0.918 | |

**Table 2.4 Statistical results for all experiments using the linear mixed model (LMM).**

| Experiment | Summary | Statistic | Result | |
|---|---|---|---|---|
| | | | With separation | Without separation |
| 1 | 10 ppm mercury, 0.1 ppm copper, 0.1 ppm lead with gold rod WE | $R^2$ | 0.966 | 0.993 |
| | | F-statistic | $F_{1,13} = 396.8$ | $F_{1,13} = 2068$ |
| | | p-value | $3.993 \times 10^{-11}$ | $1.022 \times 10^{-15}$ |
| 2 | 10 ppm mercury, 0.1 ppm copper, 0.1 ppm lead with gold rod WE | $R^2$ | 1.000 | 0.949 |
| | | F-statistic | $F_{1,13} = 1.157 \times 10^{33}$ | $F_{1,13} = 263.2$ |
| | | p-value | $2.2 \times 10^{-16}$ | $5.225 \times 10^{-10}$ |
| 3 | 0.1 ppm lead with gold rod WE | $R^2$ | 0.938 | 0.979 |
| | | F-statistic | $F_{1,13} = 213.6$ | $F_{1,13} = 642.6$ |
| | | p-value | $1.902 \times 10^{-9}$ | $1975 \times 10^{-12}$ |

49

| | | | |
|---|---|---|---|
| 4 | 10 ppm mercury, 0.1 ppm copper, 0.1 ppm lead with SPCE | $R^2$ <br> F-statistic <br> p-value | 0.970 <br> $F_{1,13} = 454.4$ <br> $1.697 \times 10^{-11}$ |
| 5 | 0.1 ppm lead with SPCE | $R^2$ <br> F-statistic <br> p-value | 0.830 <br> $F_{1,13} = 69.57$ <br> $1.412 \times 10^{-6}$ |

Not surprisingly, the results indicate that the addition of mercury for the thin film mercury electrode and use of the internal standard of copper yield more linear measurements of analyte concentration. Still, in all three experiments with the gold rod WE, high coefficients of determination, above 0.9, were observed regardless of the CE configuration. These results suggest that the counter electrode may not need to be separated from the bulk solution.

## 2.4 Comparison of the gold rod WE and the PINE screen-printed electrode assemblies using arsenic

Simplification of the electrochemical cell could include use of custom planar electrodes, so our next analyses compared the performance of a commercially available gold rod WE with the performance of a commercially planar electrode assemblies. While we anticipate using a gold, WE in the final device, other electrode materials were briefly analyzed to see if a cheaper electrode material might yield sufficient quantification results. PINE Research produces a screen-printed gold electrode on a ceramic substrate, along with screen-printed carbon electrode on polyethylene terephthalate, and screen-printed platinum electrode on ceramic as shown in Figure 2.4. The planar Pine electrode assemblies and the gold rod from CHI were used for method development, and to set a baseline as reference for all other electrodes. With the CHI gold rod working electrode, a graphite rod was used as the counter electrode, and a Ag|AgCl gel electrode was the

reference electrode. In the planar Pine electrode assembly, the counter electrode is graphite, and the reference electrode was a Ag|AgCl gel electrode.

Anodic Stripping Voltammetry for Arsenic Calibration Reference

Arsenic stripping current was measured at increasing concentrations of 1 ppb, 2 ppb, 3 ppb, 4 ppb, 5 ppb and 10 ppb using ASV. Each solution was measured in quintolet. A potential of -0.6 V was applied for 180 seconds while the solution was stirring and for an additional 30 second without stirring. The potential was swept from -0.6 V to +0.5 V at a rate of 100 mV/s, and then held at +0.5 V for 180 seconds to fully strip off arsenic before beginning the next trial.

Evaluation of PINE Research screen-printed carbon electrode (CSPE) on polyethylene terephthalate

There is not a pretreatment step for the CSPE provided by PINE Research. This planar electrode is designed to be used immediately, without any treatment. Arsenic was plated and stripped from the carbon electrode using the ASV procedure described previously. Repeated measurements on the same arsenic concentration showed an increase in the stripping peak current with each measurement. This may result from one or a combination of incomplete stripping of arsenic between measurements, changes in the electrode area, or a pretreatment of the electrode is required.

To determine if incomplete stripping contributed to the trends in peak current, 100 ppb arsenic was plated onto the working electrode at a potential of -0.6 V was for 180 seconds while the solution was stirring and for an additional 30 second without stirring. The electrode was removed from the arsenic solution and placed into the electrolyte

solution (10 mM NaCl and 10 mM HNO$_3$ in water). A linear sweep from -0.6 V to +0.5 V

was collected five times, shown in Figure 2.14a. Then a cyclic voltammogram, where the

cell potential was cycled from -0.6 V to + 0.5 V was collected before the third, fourth,

and fifth, shown in Figure 2.14b. A third, fourth and fifth linear sweep was collected,

with a CV of the same parameters collected before the fourth in fifth sweep.
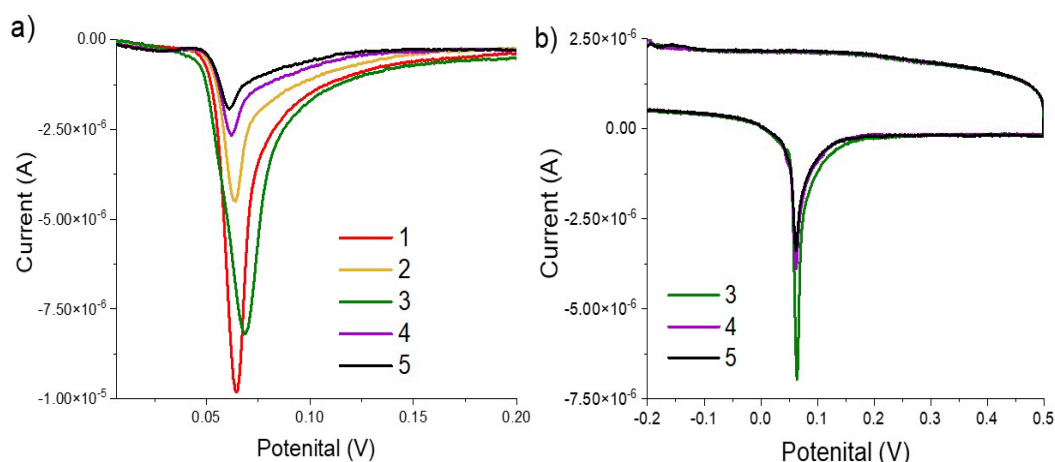


**Figure 2.14** Linear sweep voltammogram (LSV, a) from -0.6 V to +0.5 V after arsenic plating (PINE Research carbon screen-printed electrode; electrolyte of 10 mM NaCl and 10 mM HNO$_3$ in water). Cyclic voltammogram (b) from -0.6 V to + 0.5 V before third, fourth, and fifth LSV. Multiple LSV's demonstrate retained arsenic on carbon SPE.

As expected, the first peak corresponding to oxidation of arsenic in the LSV

collected after the plating step has the largest current magnitude. Additional liner

sweeps show the presence of arsenic on the electrode, despite initial striping sweep.

While the fifth linear sweep does show a large decrease in the arsenic oxidation peak

current, detection of arsenic was not expected beyond the initial stripping step. The

oxidation peaks from the cyclic voltammograms (fig 2.14inset) also show decreases in

the amount of arsenic present after multiple stripping steps. Together, these results

indicate that arsenic is being retained within the carbon electrode (incomplete stripping). As such, the determined arsenic concentration from a sample will be inaccurate, eliminating carbon as a choice for electrode material in the final device.

*Evaluation of PINE Research screen-printed platinum electrode (PSPE) on ceramic*

The platinum electrode was pretreated by cycling the electrode assembly in 0.5 mM sulfuric acid from -0.3 V to 1.7 V until the platinum peaks were reproducible. A representative cyclic voltammogram showing platinum redox activity is shown in Figure 2.15 using a Ag|AgCl gel reference electrode.
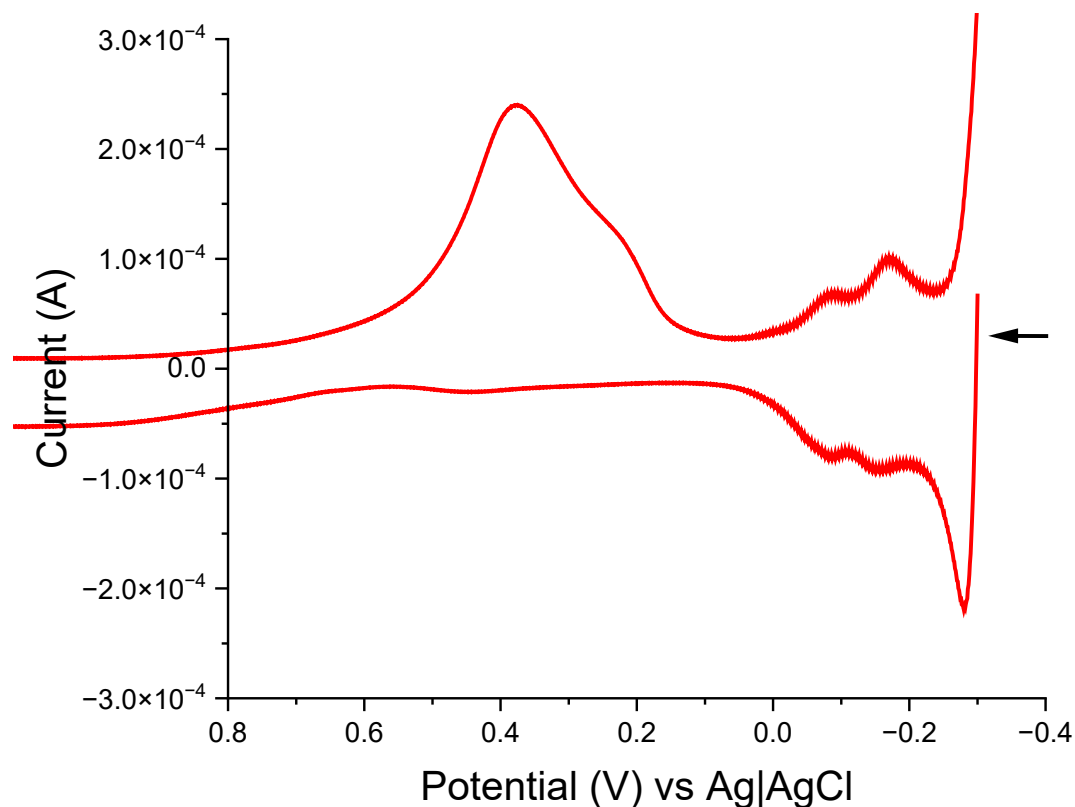


**Figure 2.15** Cyclic voltammogram of PINE Research platinum screen-printed electrode using an external Ag|AgCl gel reference electrode in 0.5 mM sulfuric acid. (Cycled from -0.3 V to +1.7 V at 100 mV/s).

The planar reference electrode on the screen-printed PINE electrode was evaluated. Cyclic voltammograms of electrolyte (10 mM NaCl and 10 mM $HNO_3$ in water) cycled from -0.6 V to + 0.5 V were collected with the PINE Research platinum screen-printed electrode using the screen-printed planar reference (blue) and Ag|AgCl gel electrode (red), shown in Figure 2.16.
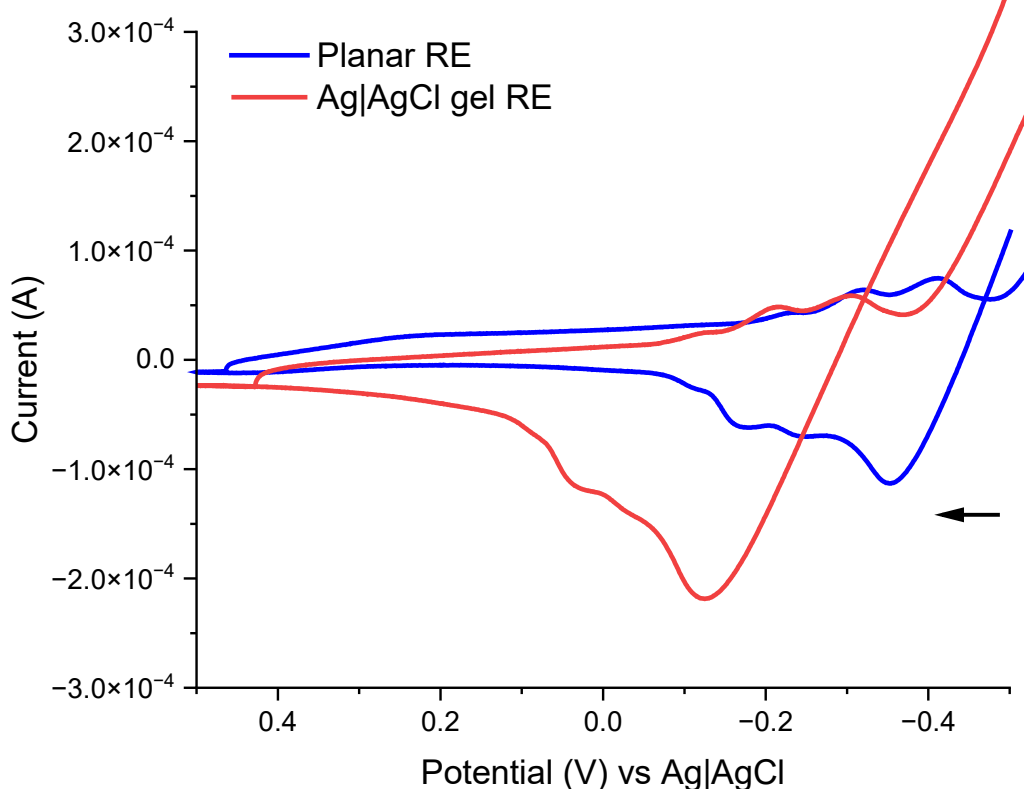


**Figure 2.16.** Cyclic voltammograms of electrolyte (10 mM NaCl and 10 mM $HNO_3$ in water) from -0.6 V to + 0.5 V with the PINE Research platinum screen-printed electrode using the screen-printed planar reference (blue) and a Ag|AgCl gel reference electrode (red) at 100 mV/s.

The peaks observed here result from platinum redox activity. The peak shapes are similar. There are multiple oxidation and reduction peaks observed for the planer reference electrode and the Ag|AgCl gel reference electrode. The peak potentials and

peak magnitudes differ. The peak potentials shift more positively for the oxidation and reduction sweeps with the Ag|AgCl gel reference electrode. These differences between the reference electrode configurations suggest that the internal reference electrode is failing. To further support this conclusion, 0.5 mM ferricyanide was cycled from -0.8 V to +0.0 V using the internal and external reference electrode, shown in Figure 2.17.
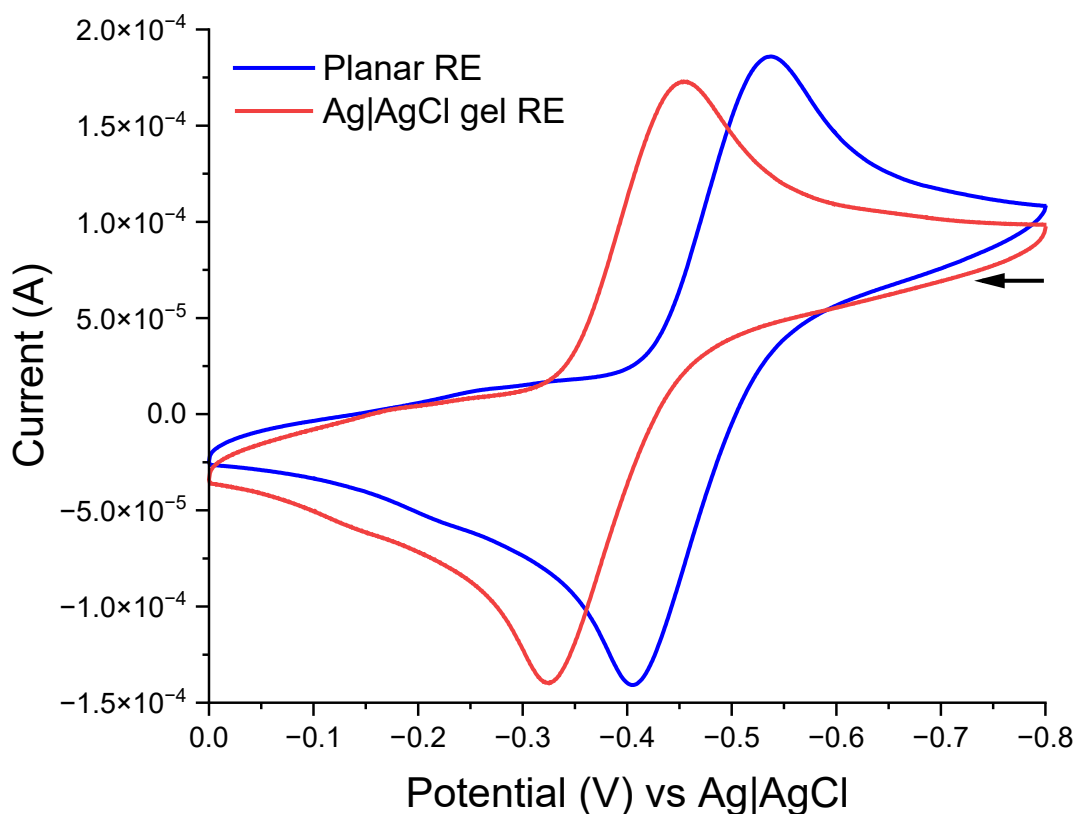


Figure 2.17. Cyclic voltammograms of 0.5 mM ferricyanide in water from -0.6 V to +0.0 V with the PINE Research platinum screen-printed electrode using the screen-printed internal reference (blue) and an external Ag|AgCl gel reference electrode (red) at 100 mV/s.

The peak shape observed here results from the chemical composition of ferricyanide, as expected, the peak shapes are very similar. There is a change in the peak potentials with the screen-printed planar electrode and the Ag|AgCl gel electrode. The

peak potentials for the oxidation and reduction peaks shift more positively from  when the Ag|AgCl gel reference electrode was used, as previously observed. These differences between the reference electrode configurations suggest that the internal reference electrode is failing. Next, excess arsenic, 205 ppm arsenic in electrolyte was cycled from -0.6 V to + 0.5 V with the carbon screen-printed electrode using the external reference electrode. This voltammogram (blue) is overlaid in Figure  with the voltammogram of platinum only using the external reference electrode (red) from Figure 2.18.
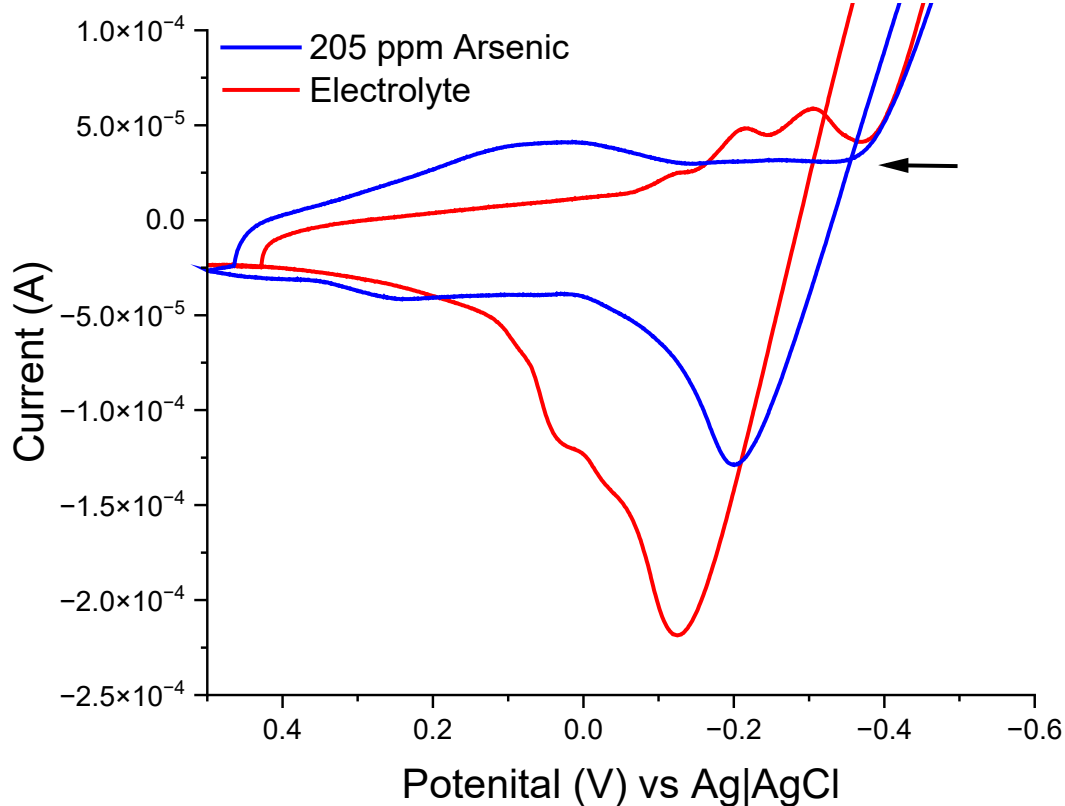


Figure 2.18. Cyclic voltammograms of 205 ppm arsenic in electrolyte (blue) and electrolyte (red) cycled from -0.6 V to + 0.5 V with the PINE Research platinum screen-printed electrode using the screen-printed with an external Ag/AgCl gel reference electrode at 100 mV/s.

Platinum oxidation occurs at the same potential as arsenic oxidation (near -0.15 V). As such, platinum is not a suitable as the working electrode material for quantification of arsenic, as signal from platinum oxidation will infer with signal from arsenic oxidation.

Evaluation of PINE Research screen-printed gold electrode (GSPE) on ceramic

An Ag|AgCl gel reference electrode was used in these trials instead of the screen-printed reference electrode because of the finding from the platinum screen-printed electrode. The gold electrode was pretreated by cycling 0.5 M sulfuric acid from -0.375 V to + 1.7 V for 10 cycles, or until the redox peaks were reproducible. A cyclic voltammograms of this pretreatment is shown in Figure 2.19.
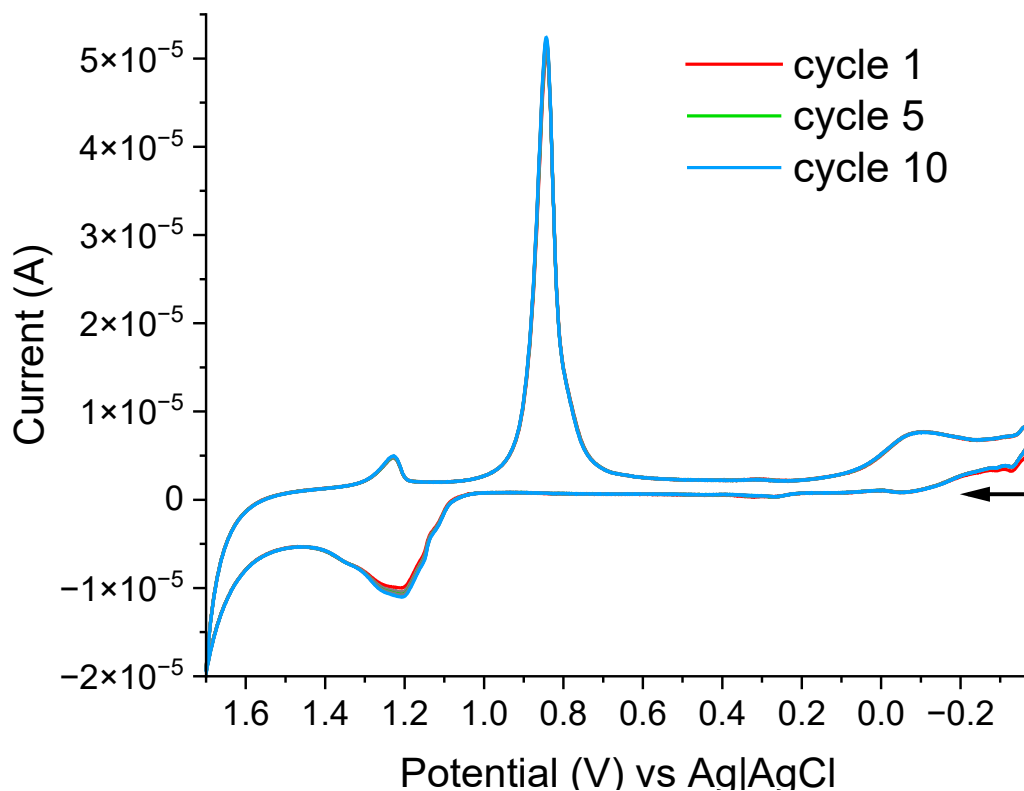
**Figure 2.19** Pretreatment cyclic voltammogram of PINE Research gold screen-printed electrode cycling in 50 mM sulfuric acid from -0.375 V to + 1.7 V at at 100 mV/s. Shown in red is cycle 1, in green cycle 5, and in blue cycle 10. Cycles 2, 3, 4, 6, 7, 8, and 9 are shown in gray.

An arsenic calibration curve using the ASV procedure outlined previously was attempted. Repeated measurements on the same concentration showed an apparent increase in the stripping peak current with each measurement. At the end of the day, discoloration of the electrode was noted, shown in Figure 2.20b next to an unused GSPE electrode Figure 2.20a.
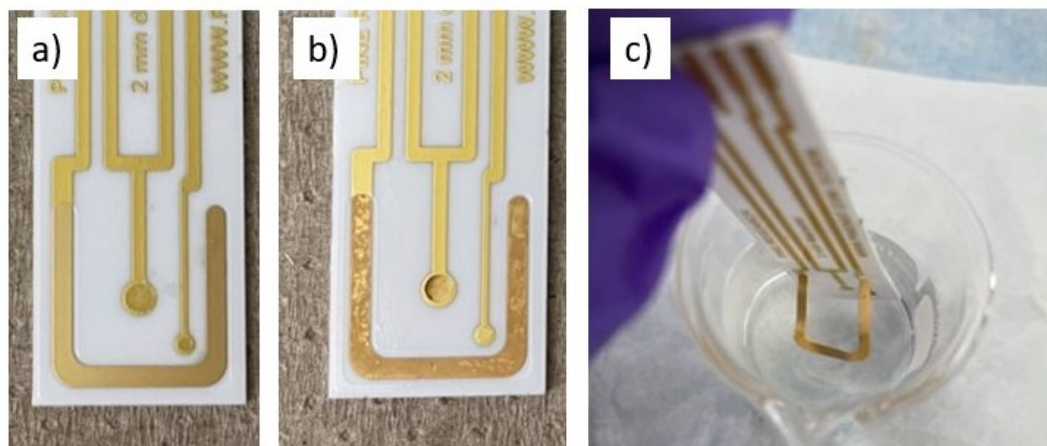
**Figure 2.20** PINE Research gold screen-printed electrodes unused (a), after extensive use (b), and showing delamination of counter electrode (c).

Macroscopic discoloration could indicate undesirable changes to the physical and chemical structure of the electrode. The next day, a pretreatment cyclic voltammogram was collected to clean the electrode surface. Then 50 mM ferricyanide in 0.1 M KCl in water solution was cycled from -0.6 V to +0.5 V for 10 cycles three times, for a total of 30 cycles, with a pretreatment CV collected in between each. A final pretreatment CV was collected on this electrode to evaluate changes in gold redox activity, shown in Figure 2.21 (blue), overlaid with the initial pretreatment CV, before any heavy metal was introduced.
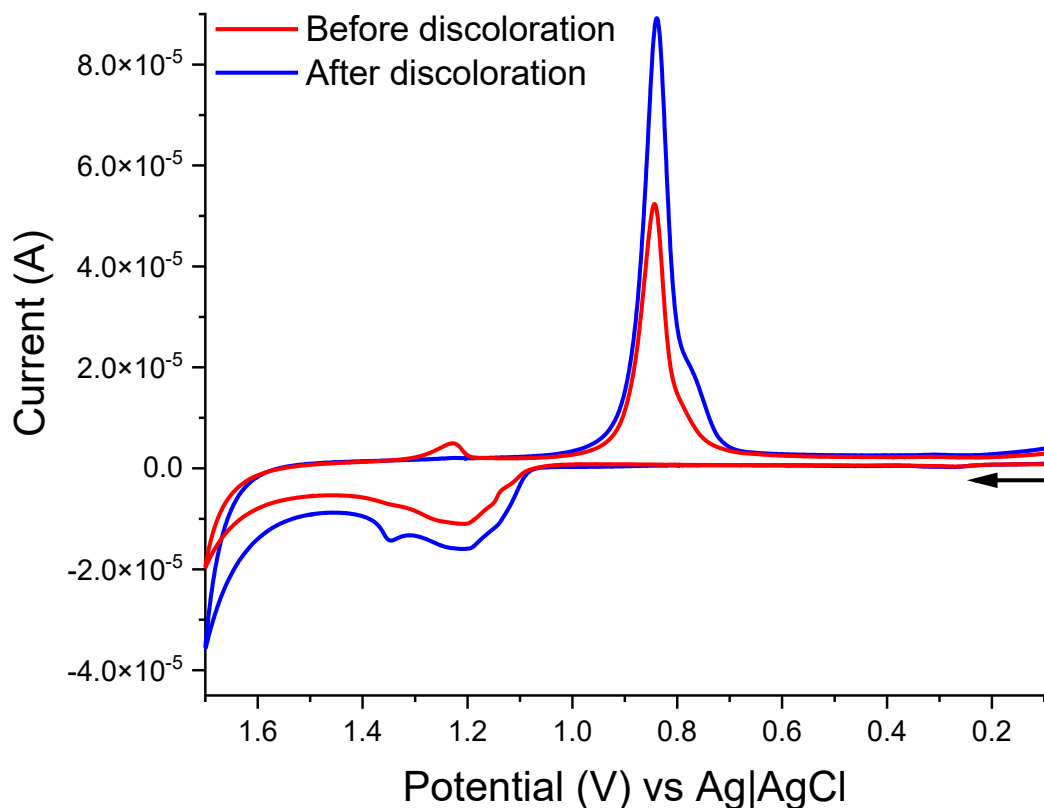
**Figure 2.21** Cyclic voltammogram of gold redox activity I the presence of 0.5 mM sulfuric acid cycled from -0.375 V to 1.8 V on the PINE Research gold screen-printed electrode using an external Ag|AgCl gel reference electrode before heavy metal analysis (blue), and after discoloration and ferricyanide experiments (red) at 100 mV/s.

There is an increase in the peak currents at +1.4 V, +1.2 V, and +0.8 V after discoloration of the electrode, suggesting an increase in the working electrode surface area.

Cyclic voltammograms of 50 mM ferricyanide in 0.1 M KCl in water from exhaustively using the gold screen-printed electrode are shown in Figure 2.22.
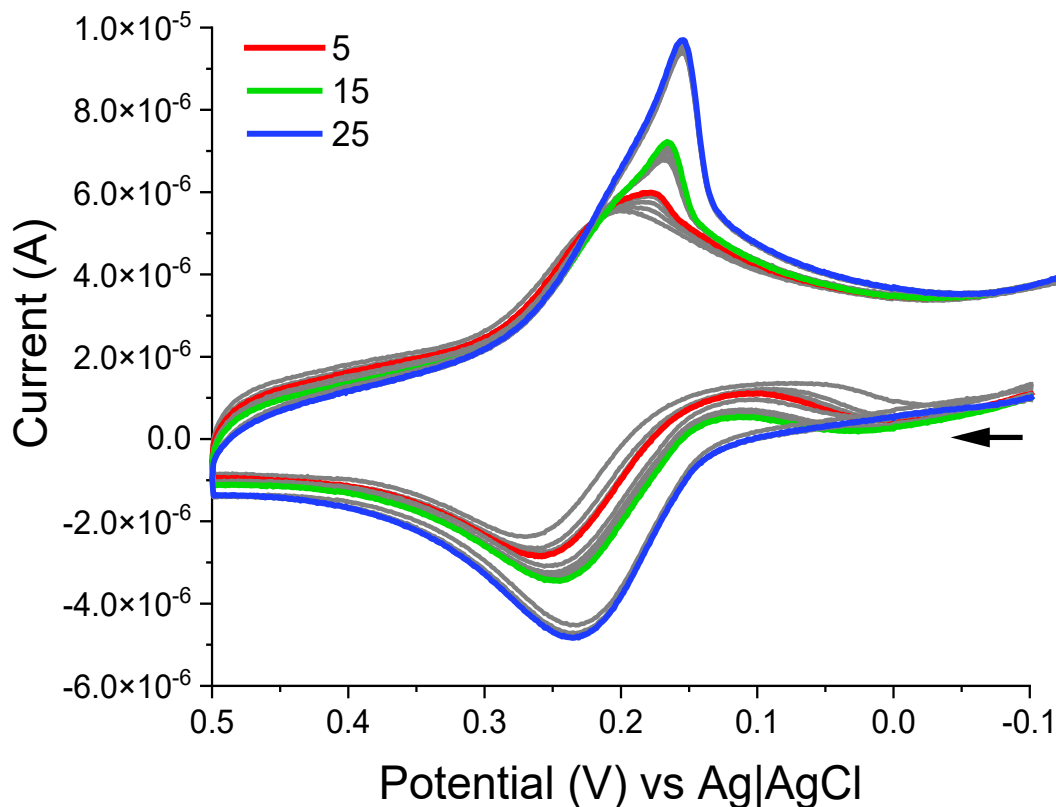
**Figure 2.22**. Cyclic voltammograms of 50 mM ferricyanide in 0.1 M KCl cycled from -0.6 V to + 0.5 V for 30 cycles at 100 mV/s using the Pine Research gold screen printed elctrode . Cycle 5 (red), 15 (green), and 25 (blue), are shown in color, and the other cycles in grey.

The reduction and oxidation of ferricyanide is seen near +0.2 V. The magnitude of the peak currents increases after each cycle. Further, the reduction peak shape is not the same as the oxidation peak shape. The peak shape begins very broad, becoming very sharp with consecutive cycles. The reduction peak of cycle 5 has a width of 0.13, cycle 15 of 0.10 V, while cycle 25 has a much smaller width of 0.06 V. Together, the changes in reduction peak shape and decreases in peak splitting suggest analyte is physically trapped within or behind the WE. This is consistent with the delamination observed (Fig 2.20), as the backside of the delaminated surface is also gold, providing the additional electrode area.

Evaluation of the CHI, Inc gold rod working electrode

In this electrochemical cell, the WE was a fixed disc, non-rotating, 2 mm diameter gold rod from CHI, Inc. The counter electrode was a graphite rod. The reference electrode was an Ag|AgCl gel electrode. The ASV procedure outlined at the beginning of this chapter was used with an additional step. Between concentration increases, the WE and CE were soaked in 25% $HNO_3$ for 2 minutes, and then dipped into a stock of 1 ppb arsenic. Without the additional soaking in acid, the measurements were not independent of each other; each sample showed a decrease in peak current as repeated measurements were taken. Representative voltammograms of arsenic oxidation peak from the first ASV of each concentration: 0 ppb, 1 ppb, 2 ppb, 3 ppb, 4 ppb, 5 ppb, and 10 ppb using the fixed disc, non-rotating, 2 mm diameter gold rod from CH Instruments, Inc as the working electrode are shown in Figure 2.23.
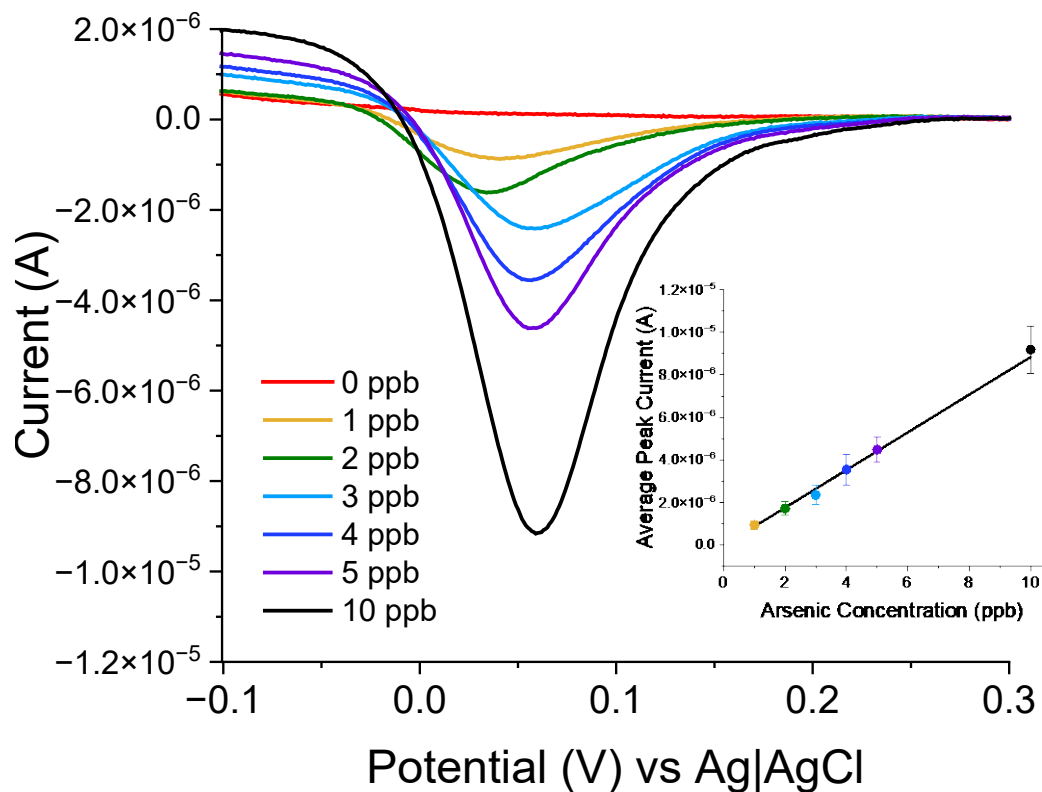
**Figure 2.23** Representative stripping voltammograms of arsenic oxidation peak from the first ASV of each concentration: 0 ppb, 1 ppb, 2 ppb, 3 ppb, 4 ppb, 5 ppb, and 10 ppb using the fixed disc, non-rotating, 2 mm diameter gold rod from CHI Instruments, Inc as the working electrode at 100 mV/s.

The expected linear relationship between arsenic concentration and peak current is observed. As the arsenic concentration increases, the magnitude of the peak current also increases. Repeated measurements of each concentration are shown in the appendix. There is no clear pattern of peak current magnitude within repeated measures of the same concentration indicating that each repeated measurement is independent of each other. The residuals versus arsenic concentration are shown in Fig 2.24a, and the probability-probability plot (p-p plot) in Fig 2.24b for the simple linear regression model.

63
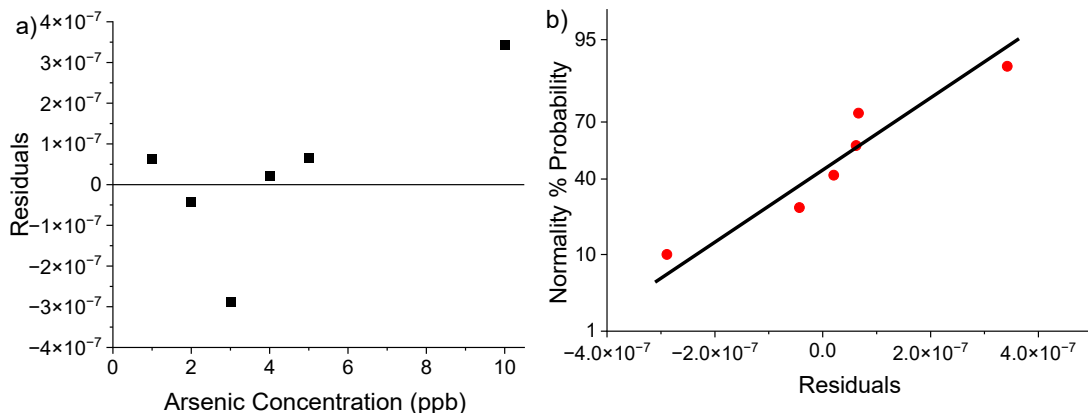
**Figure 2.24** The residuals versus arsenic concentration (a), and the probability-probability plot (p-p plot) (b) for the simple linear regression model.

The simple linear regression model residuals appear to be homoscedastic because they are randomly distributed around the x-axis. The p-p plot of the simple linear regression model residuals indicate that the residuals are also normally distributed. The least squares regression line with standard deviation bars for the simple linear regression is shown in Figure 2.23inset.

The residuals versus arsenic concentration are shown in Fig 2.25a, and the probability-probability plot (p-p plot) in Fig 2.25b for the repeated measures ANOVA and linear mixed model.
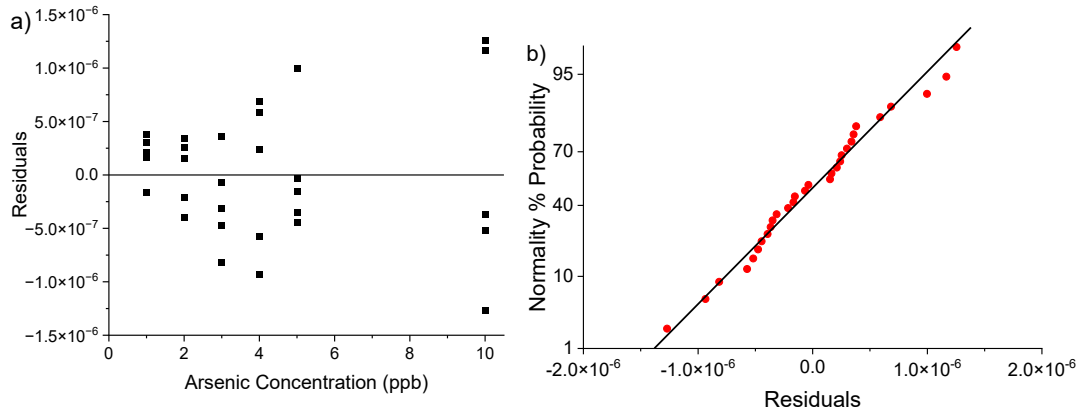
**Figure 2.25** The residuals versus arsenic concentration (a), and the probability-probability plot (p-p plot) (b) for the repeated measures ANOVA and linear mixed model.

The residuals from the ANOVA model are heteroscedastic because they show a clear coning pattern, the spread of the residuals across the x-axis increases as concentration increases. This indicates that the measurement is not as repeatable as the arsenic concentration increases. The p-p plot of the ANOVA residuals shown in Figure 2.25b indicate that the residuals are normally distributed. The least squares regression line with the repeated measures ANOVA and linear mixed model regression is shown in Figure 2.26.
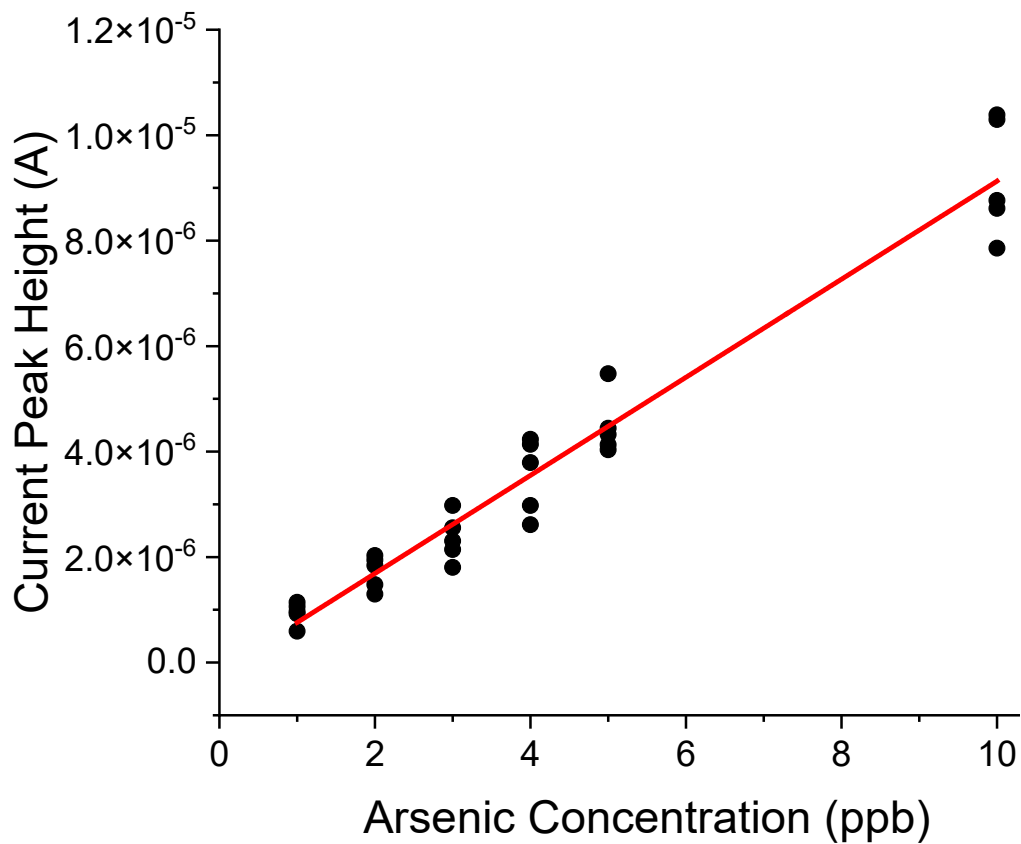
**Figure 2.26** The least squares regression line with the repeated measures ANOVA and linear mixed model regression

The statistical results from the three regression models are shown in Table 2.5. All three regression models show a high $R^2$ value, above 0.95.

**Table 2.5 Summary Statistics for Arsenic Calibration Curve with Gold Fixed Disc Electrode**

| Model | Statistic | Result |
|---|---|---|
| Simple linear regression | $R^2$ | 1.000 |
| | RSS | $4.134 \times 10^{-35}$ |
| | Pearson's R | 1.000 |
| Oneway Repeated measures ANOVA | $R^2$ | 0.954 |
| | RSS | $1.023 \times 10^{-11}$ |
| | Pearson's R | 0.976 |

| | | |
|---|---|---|
| Linear mixed model in RStudio | $R^2$ | 0.954 |
| | F-statistic | $F_{1,28} = 599$ |
| | p-value | $2.2 \times 10^{-16}$ |

## III. Investigation of Prototype Electrodes from Collaborators

### 3.1 Materials

*Reagents:* potassium chloride from Fischer Chemical, potassium ferricyanide from Fischer Chemical, concentrated sulfuric acid from Fischer Chemical, 18 MΩ water.

*Gold Electrodes from Collaborators:* Gold electrodes were inkjet printed onto various substrates using commercial inks and other inks in development. Our collaborators at the University of Kentucky (Md. Tawabur Rahman and Aron Huckaba) performed all electrode printing. Metalon JG-125 gold ink from Novacentrix was used. Diethylene glycol, glycerol, and water are the solvents in this ink. The general process is described here by Nayak *et al*. Full descriptions of the inkjet printing procedures are beyond the scope of this work, but details will be noted when relevant to the experimental design. All polymer substrates were 3D printed by our collaborator at the University of Louisville (Tommy Roussel) using commercially available PLA (grey, green) and PETG (black) filaments. All PLA substrates were printed at 212°C. PETG substrates were printed at 244°C with a Creality Ender 6 SE on a flexible polyetheride surface.

*Instrumentation:* All electrochemical measurements were performed in a 3-electrode electrochemical cell using a CHI 760E potentiostat. A 3-electrode electrochemical cell, which consists of a WE, CE, and RE, was used for the electrochemical studies described here. The reference electrode was an Ag|AgCl gel electrode. The counter electrode was a graphite rod for the CHI gold rod WE and inkjet printed gold WE. A planar gold counter

electrode was used for the Pine Research screen printed electrode. All scanning electron

microscopy images were collected using a Hitachi flexiSEM 100.

## 3.2 Inkjet Printed Working Electrodes

Printed electrodes are shown in Figure 3.1. The gold for Electrode 1 was inkjet printed

onto a glass substrate and then thermally annealed. For thermal annealing, the

substrate was heated on a hot plate at 100 °C for 10 minutes, then 450 °C for 20 minutes.

The gold for Electrode 2 was inkjet printed onto a glass substrate and then photonically

annealed with visible light using a UV lamp. UV light was used at 350 V for 50 msec with

an energy of 6.94 J/cm$^2$ repeated 25 times. Gold for Electrode 3 was inkjet printed onto

a 3D printed polylactic acid (PLA) substrate and then photonically annealed with visible

light. A UV lamp was used with 350 V for 30 msec with 3.06 J/cm$^2$, with no repetition.

Electrodes 4 – 37 were photonically annealed with IR light. After evaluation of these,

thirty-four more electrodes were printed from our collaborators. Efforts were made to

print two electrodes per substrate, with 1 or more layers of printed gold and in multiple

patterns to create different electrode areas. The electrodes have up to four layers of

gold, and shapes vary from two lines, three lines, fours and closed for the bottom square

shape. Each electrode was annealed only once at the conclusion of the printing of all

layers. These electrodes are shown in Figure 3.1 number 4 – 37 and summarized in Table

3.1.
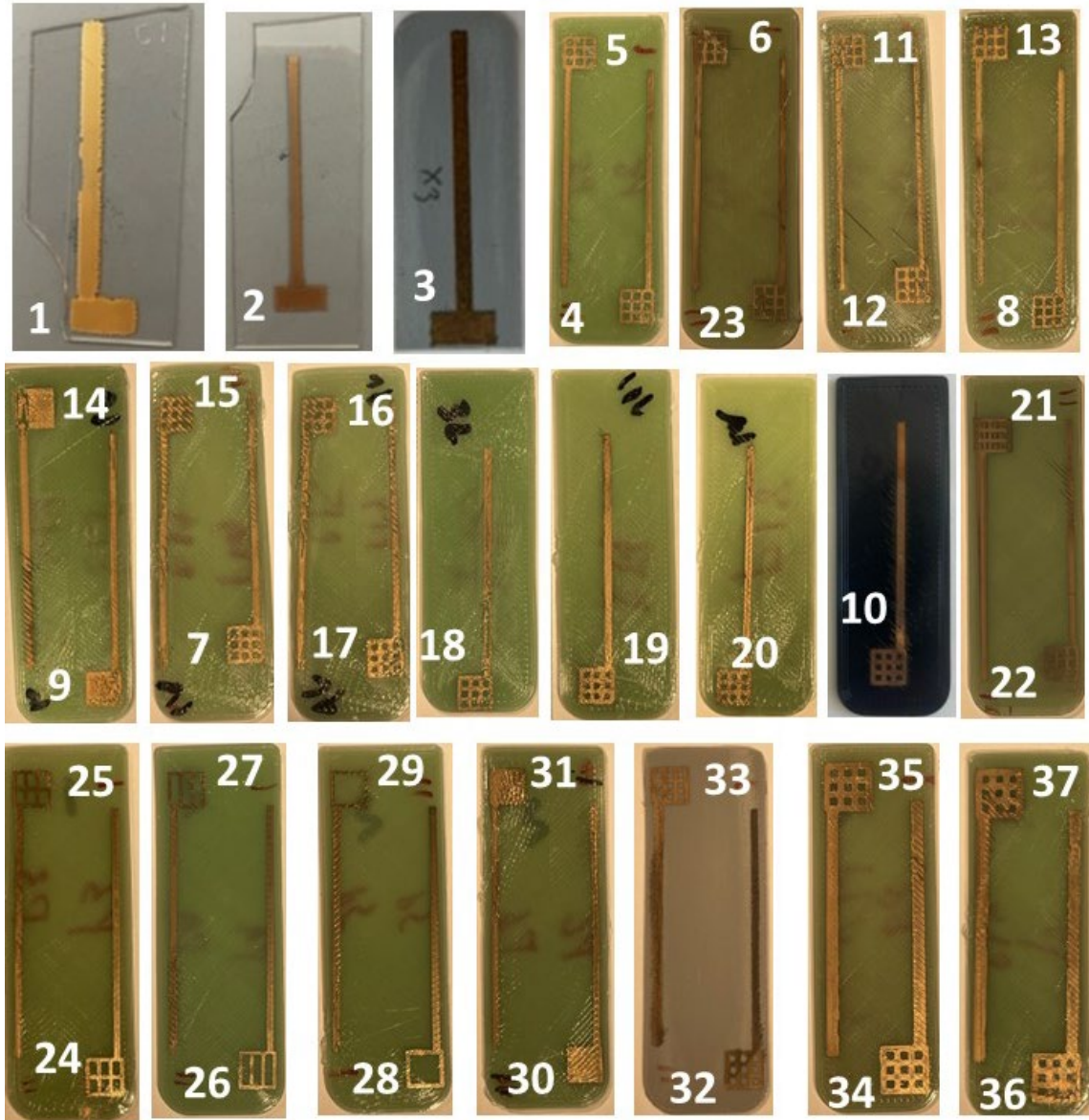
**Figure 3.1.** Gold inkjet printed electrodes on glass substrates (1, 2), PLA substrates (3 – 37). Electrodes 9 and 14 are closed shaped. Electrodes 28 and 29 are open shaped. Electrodes 26 and 27 are two lined. Electrodes 24 and 25 are three lined. Electrodes 7 and 15 represent the four lines.

Sheet resistance was measured for some of the electrodes using a 4-point probe at the

locations indicated in Figure 3.2. The sheet resistance is summarized in Table 3.1.

**Figure 3.2**.Four-point sheet resistance measurement locations on electrodes. Diagram created by the University of Kentucky collaborators.

**Table 3.1 Summary of printed electrode substrate, shapes, layers, and annealing parameters**

| Electrode | Substrate | Shape | Layers | Annealing parameters | Place 1 (ohm/sq) | Place 2 (ohm/sq) | Place 3 (ohm/sq) |
|---|---|---|---|---|---|---|---|
| 1 | Glass | Closed | | Thermal | NA | NA | NA |
| 2 | Glass | Closed | | Visible | NA | NA | NA |
| 3 | PLA - gray | closed | | Visible | NA | NA | NA |
| 4 | PLA | 4 lines | 1 | IR | 11.48 | 100 | $10^5$ |
| 5 | PLA | 4 lines | 2 | IR | 201.6 | 5.84 | 57.70 |
| 6 | PLA | 4 lines | 2 | IR | 565 | 77.7 | 58.7 |
| 7 | PLA | 4 lines | 3 | IR | 3.4 | 3.1 | 4.9 |
| 8 | PLA | 4 lines | 3 | IR | 1.8 | 1.8 | 50.55 |
| 9 | PLA | closed | 4 | IR | - | - | - |
| 10 | PETG | 4 lines | 4 | IR | 100 | 1000 | $10^9$ |
| 11 | PLA | 4 lines | 4 | IR | 1.6 | 0.8 | - |
| 12 | PLA | 4 lines | 4 | IR | 1.4 | 1.6 | 7.95 |
| 13 | PLA | 4 lines | 2 | IR | 5.75 | NA | 210.5 |
| 14 | PLA | 4 lines | 3 | IR | - | - | - |
| 15 | PLA | 4 lines | 4 | IR | - | - | - |
| 16 | PLA | 4 lines | 4 | IR | - | - | - |
| 17 | PLA | 4 lines | 4 | IR | - | - | - |
| 18 | PLA | 4 lines | 3 | IR | 4.4 | 2.8 | 3.4 |
| 19 | PLA | 4 lines | 4 | IR | 298 | NA | 2.9 |
| 20 | PLA | 4 lines | 4 | IR | 298 | NA | 2.9 |
| 21 | PLA | 4 lines | 1 | IR | - | - | - |
| 22 | PLA | 4 lines | 2 | IR | 115.5 | 1000 | - |
| 23 | PLA | 4 lines | 1 | IR | 115.5 | 1000 | - |
| 24 | PLA | 3 lines | 1 | IR | 532 | 345 | 102 |
| 25 | PLA | 3 lines | 2 | IR | 33 | 5.5 | 79.8 |
| 26 | PLA | 2 lines | 1 | IR | 173.3 | 308 | 510 |
| 27 | PLA | 2 lines | 2 | IR | 22 | 4.3 | 32.3 |
| 28 | PLA | Open | 1 | IR | 60.8 | 220 | - |
| 29 | PLA | Open | 2 | IR | 47.5 | 69.55 | 159.4 |
| 30 | PLA | Closed | 1 | IR | 69.2 | 12.5 | 20.85 |
| 31 | PLA | Closed | 2 | IR | 6.3 | 5.7 | 1.33 |

| 32 | Old PLA | 4 lines | 1 | IR | - | - | - |
|----|---------|---------|---|----|-----|-----|-----|
| 33 | Old PLA | 4 lines | 2 | IR | 7.1 | 5.4 | 6.9 |
| 34 | PLA | Large 4 lines | 1 | IR | 151.5 | 120 | 818 |
| 35 | PLA | Large 4 lines | 2 | IR | 9.9 | 3.7 | 7.1 |
| 36 | PLA | Large 4 lines | 1 | IR | 119.5 | 124.3 | 2.2 |
| 37 | PLA | Large 4 lines | 2 | IR | 3.0 |  | 24.6 |

Electrodes 4, 5, 7, and 9 served as representative samples of 1, 2, 3, and 4 layers of gold respectively; these electrodes were analyzed electrochemically. All these electrodes have a four-line shape except for Electrode 9 which has a closed shape. The PETG substrate, Electrode 10, with four layers was also characterized. Figure 3.3 shows a more detailed photograph of the electrodes.
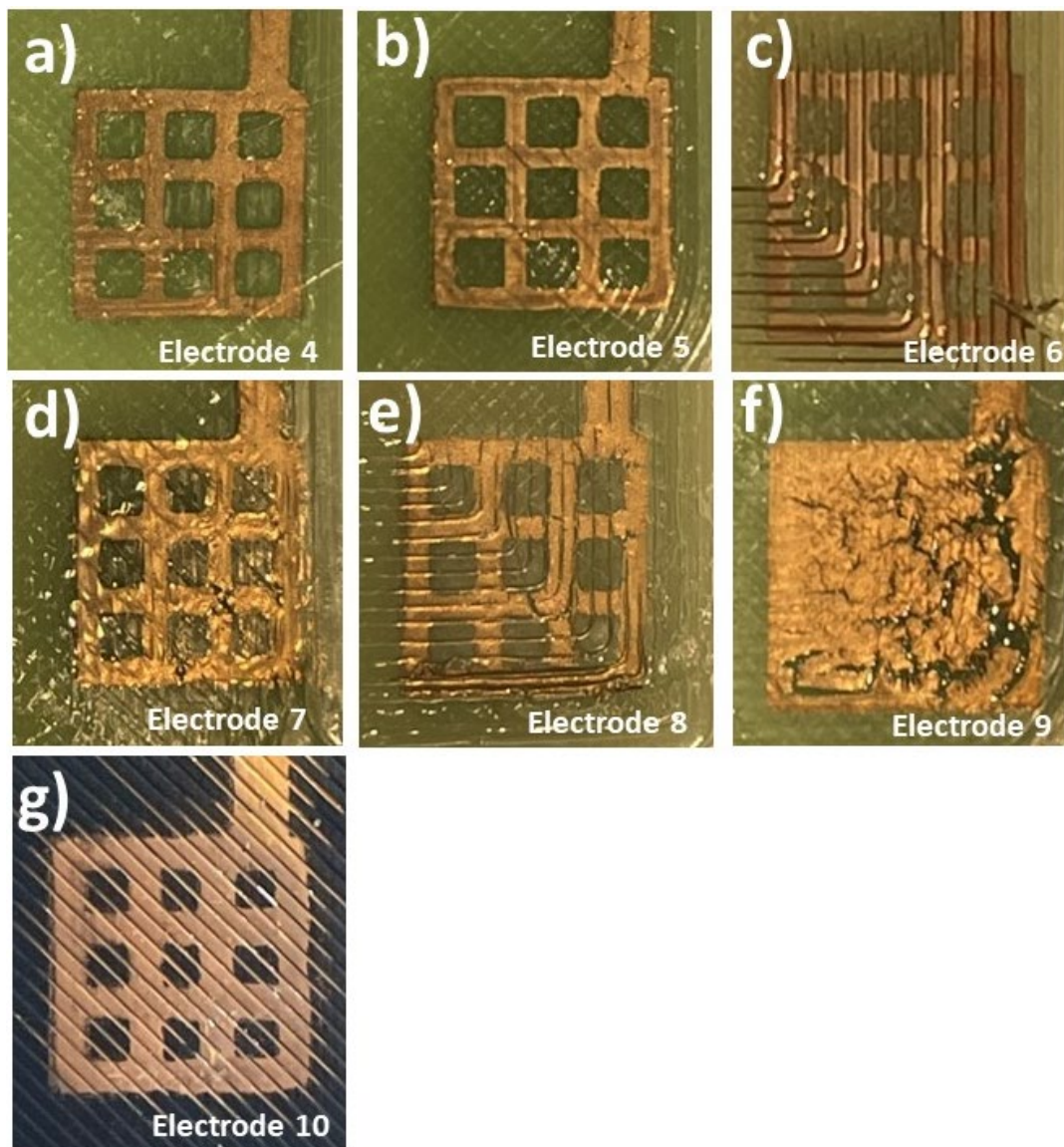
**Figure 3.3** Detailed images of gold inkjet printed electrodes with increasing layers of gold characterized with electrochemical experiments and SEM imaging. Electrode 4 (a) has one layer. Electrode 5 (b) and electrode 6 (c) have two layers. Electrode 7 (d) and electrode 8 (e) have three layers. Electrode 9 (f) and electrode 10 (g) have four layers.

It is important to note that some of these electrodes appear to be flakey, have cracks in the gold, and have ink running into the grooves of the substrate. The electrodes chosen for further characterization showed the most uniform coverage of gold at the square area and appeared to be connected at the junction of the rectangle to the square (place

2). A glass piece was used to flatten the substrates after annealing because they began

melting. The flattening process is apparent in the gold pattern for several electrodes

creating cracks in the gold. For electrode 10, on PETG, evidence of capillary action is

observed. The gold moves into the pattern of the PETG substrate such that the gold

thickness is not known, and the surface area of the working electrode is difficult to

determine accurately. There are inconsistent patterns of the measured sheet resistance,

likely due to the non-uniform coverage of gold ink on the plastic. This morphology will

cause intermittent contact of the gold surface in the electrochemical cell, at the

potentiostat connection and to the solution.

## 3.3 Methods

*Electrochemical Characterization.* The electrochemical cell consisted of the printed gold

electrode as the working electrode, the counter electrode was a graphite rod, and the

reference electrode was a gel Ag|AgCl, all placed in a beaker. To ensure the same area

of WE remained submerged in different solutions over the course of the experiment, a

knife blade was used to mark submersion depth on each substrate. The electrode was

first cycled in 0.5 M $H_2SO_4$ between $-0.375$ V and $+1.800$ V for a total of 10 cycles, or

until reproducible peaks were observed. The goal of cycling $H_2SO_4$ on the gold working

electrode is to chemically clean the electrode surface so that it is chemically uniform for

electrochemical measurements. Then a cyclic voltammograms of ferricyanide in 0.1 M

sodium chloride were collected between -0.1 V and $+0.6$ V vs. Ag|AgCl for a range of

analyte concentrations (1 mm $-$ 10 mM) and at a range of scan rates (10 mV/s $-$ 500

mV/s) were collected.

Finally, anodic stripping voltammetry (ASV) of increasing arsenic concentrations were

collected. Between each concentration increase, a cyclic voltammogram of electrolyte

only was collected from + 0 V to + 0.8 V for 10 cycles between arsenic concentration

increases.


### 3.4 Theoretical treatment of electrochemical data

A representative cyclic voltammogram of ferricyanide/ferrocyanide is shown in Figure

3.4.
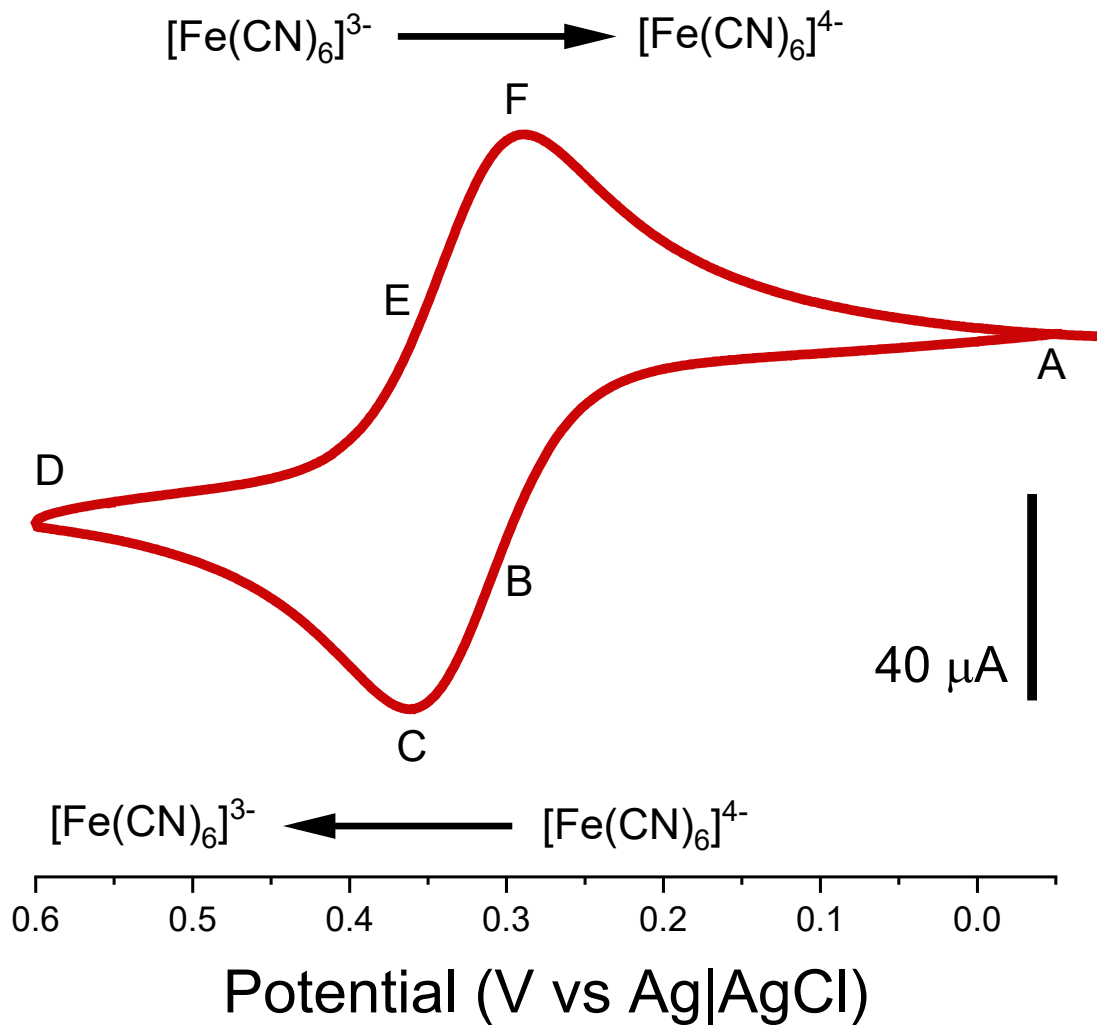
**Figure 3.4.** Cyclic voltammogram of ferricyanide cycled between -0.1 V and +0.6 V at 100 mV/s with the Pine research screen printed gold electrode as the WE and CE, and an Ag|AgCl as the RE. This cyclic voltammagram illustrates the initial potential (A), the oxidative formal potential $E_{1/2}$ (b), the oxidation peak current (C), the potential switching (D), the reduction formal potential $E_{1/2}$ (e), the reduction peak potential (F), and back to the initial potential (A). The potential is swept positively from A to D, oxidizing ferrocyanide to ferricyanide through a one electron transfer. Then the potential is swept negative from D to A reducing ferricyanide back to ferrocyanide.

During the oxidation sweep, moving from point A to point D, ferrocyanide is oxidized to

ferricyanide at the working electrode surface. An increase in current is observed,

76

corresponding to the electrons generated from the oxidation of ferricyanide at the working electrode surface, In the solution nearest the electrode surface, there is a higher concentration of ferrocyanide relative to the bulk solution.[25] At point D, the potential switches, moving towards a lower potential, point A. Ferricyanide is reduced to ferrocyanide. At points B and E, [ferrocyanide] and [ferricyanide] are at equilibrium with each other. This is referred to as the $E_{1/2}$ value, which is used to estimate the formal potential.[25] At point C, the oxidation peak, the most abundant species at the working electrode is ferricyanide.[25] At point F, the most abundant species is ferrocyanide. The Nernst equation, Equation 3.1a, describes how the redox potential of a given analyte changes with changes in concentrations of the oxidized species near the electrode surface.[25]

(Eq 3.1a)      $E = E^0 + \frac{RT}{nF} \ln \frac{(oxidized)}{(reduced)}$

Where E is the cell potential (V), $E^0$ is the standard potential (V), R is the real gas constant (J $K^{-1}$ $mol^{-1}$), T is the temperature (K), n is the number of electrons exchanged, F is Faraday's Constant (C $mol^{-1}$). For ferricyanide Equation 3.1 can be rewritten as Equation 3.1b.[25]

(Eq 3.1b)      $E = E^{0,} + \frac{RT}{F} \ln \frac{[Fe(CN)_6]^{4+}}{[Fe(CN)_6]^{3+}}$

Where n becomes 1 because only one electron is exchanged, and $E^0$ becomes $E^{0,}$, the standard cell potential. The $E^{0,}$ is estimated from the $E_{1/2}$ value. The Nernst Equation is also expressed as Equation 3.1c.[25]

(Eq 3.1b)      $E = E^{0,} + 0.059V \ln \frac{[Fe(CN)_6]^{4+}}{[Fe(CN)_6]^{3+}}$

When the oxidized and reduced species are freely diffusing in solution, peaks are observed, as the changes in concentrations of the oxidized and reduced species are limited by the rate(s) of diffusion of these species.[25,26] When a molecule behaves ideally, it is referred to as a Nernstian system, and deviations from the ideal Nernstian behavior provide insight to the electronic and structural properties of the molecule. When Nernstian behavior is observed, the peak separation, $\Delta E_p$, potential difference between point C and point F, should be 59 mV for a 1-electron system.[25,26] Further, as described by Faraday's the current corresponding to a Faradaic process is proportional to the amount of analyte present.[26,31] When the oxidized and reduced analyte species are freely diffusing and the redox processes are chemically reversible, the ratio of oxidation peak current to reduction peak current should be 1.[31] The current produced during the reduction process corresponds to the number of molecules reduced at the working electrode. During oxidation, the same number of molecules are expected to be oxidized at the working electrode, so the current should be equal in magnitude but opposite in sign. For all cyclic voltammograms of ferricyanide discussed in this work, Ep, ipR, and ipO were tabulated and $\Delta E_p$ was calculated. Because the same analyte and electrolyte are used throughout, the diffusion coefficient is expected to be the same for each experiment.

Redox reactions are classified into three categories: electrochemically reversible, electrochemically irreversible, and quasireversible.[25,26,31] Electrochemical reversibility is different than chemical reversibility. In a chemically reversible reaction, the reactants and products are never fully consumed, they are constantly being produced.[15] The rate

of the forward reaction is equal to the rate of the reverse reaction.[15] In a chemically

irreversible reaction, the reactants are completely consumed to products, and cannot

convert back to reactants.[15] The reaction rate of the forward reaction is much larger

than the reverse reaction rate. Electrochemical reversibility refers to the rate of the

electron transfer, whereas chemical reversibility refers to the conversion of reactants to

products. For an electrochemically reversible system which is a Nernstian system, the

current is only limited by mass transport of the redox species from the bulk solution to

the electrode surface.[26,31] As the scan rate increases, peak potential, $E_p$ and peak

separation, $\Delta E_p$ are not expected to change.[25] Increases in peak current are described

by the Randles-Sevcik equation, Equation 3.2a.

(Eq 3.2a)     $i_p = 0.4463 n F A C^0 \left( \dfrac{nF\nu D}{RT} \right)^{1/2}$

Where $i_p$ is the peak current (A), $n$ is the number of electrons, A is the electrode surface

area ($cm^2$), $C^0$ is the analyte concentration, $\nu$ is the scan rate (V/s), $D$ is the diffusion

coefficient ($cm^2 s^{-1}$), F is Faraday's constant ($9.65 \times 10^{-4}$ C $mol^{-1}$), R is the gas constant

($8.314$ J $K^{-1}$ $mol^{-1}$), T is the temperature (K). A faster scan rate means that the applied

potential changes faster than at lower scan rates, so the size of the diffusion layer is

smaller at higher scan rates, resulting in higher currents.[25] For an electrochemically

irreversible system, the current is limited by slow charge-transfer kinetics; the rate of

mass transport is fast relative to the rate of the electron transfer.[25,31] In an

electrochemically irreversible system, $\Delta E_p$ is expected to increase and $E_p$ will shift to

extreme potentials as the scan rate increases.[26,31] A quasireversible system describes

systems in between reversible and irreversible, influenced by both charge-transfer kinetics and diffusional mass transport.[26,31]

The Randles-Sevcik equation describes the relationship between peak current and scan rate in an electrochemically reversible system; peak current is proportional to the square root of the scan rate.[25,31] Eqn. 3.2a can be rearranged to yield Equation 3.2b, emphasizing this relationship.

(Eq 3.2b) $$i_p = \left[ 0.4463nFAC^0 \left( \frac{nFD}{RT} \right)^{1/2} \right] v^{1/2}$$

The plot of the peak current versus the square root of the scan rate is linear for Nernstian, electrochemically reversible systems. Deviations from linearity suggest that the reaction is influenced by other factors than diffusion of the analyte.[31] The slope of this line can be used to calculate the diffusion coefficient, in a further rearranged expression of Eqn. 3.2a.

(Eq 3.2c) $$slope = \left[ 0.4463nFAC^0 \left( \frac{nFD}{RT} \right)^{1/2} \right]$$

(Eq 3.2d) $$D = \left( \frac{slope}{0.4463nFAC^0} \right)^2 \frac{RT}{nF}$$

The diffusion coefficient of ferricyanide in 0.1 M potassium chloride at 25 °C was found to be 0.726 x $10^{-5}$ cm$^{-1}$/sec in the literature.[32] The slope of peak current as a function of $v^{1/2}$ was used to calculated the diffusion coefficient of ferricyanide for Electrode 3. The peak-to-peak separation, which can also be used to assess uncompensated resistance in the electrochemical cell, was evaluated through a trumpet plot.[25] Here, the peak potentials minus the $E_{1/2}$ values are plotted as a function of the log of the scan rate (log(v)). This calculation is shown in Equation 3.3 for the oxidation peak potential.

(Eq 3.3) $$E_{P,o} - E_{\frac{1}{2}} = E_p$$

A plot of Ep versus log(v) is expected to show consistent peak separation between the oxidation and reduction peak if uncompensated resistance is low; the resulting data in the trumpet plot is linear with a slope near zero. If there is an increase in peak separation with increased scan rate, and all other variables are constant, uncompensated resistance is high and a trumpet shape is observed in the data.[25,31]

Resistance is directly related to current and voltage in Ohm's law, Equation 3.4.

(Eq. 3.4) $$i = \frac{V}{R}$$

Where $i$ is the current (A), V is the potential (V), and R is the resistance (Ω). When the resistance changes, the current is directly impacted. The electrochemical cell's geometry and solution composition controls the solution resistance.[26,31] The solution resistance is made of compensated resistance and uncompensated resistance.[31] In a three-electrode cell, the counter electrode acts as an electron sink as current flows between the working electrode and counter electrode, lowering the resistance in cell, but does not rid the cell of resistance.[31] Compensated resistance is lowered by placing the reference electrode in close proximity to the working electrode.[31] Uncompensated resistance is not accounted for by the electrode geometry. In these experiments, only the WE are changed, so changes in uncompensated resistance are due to the different WE used.

## 3.5 Electrochemical Characterization of Inkjet Printed Working Electrodes – Results and Discussion

CV in sulfuric acid

The CHI gold rod and Pine Research electrode were cycled in 0.5 M sulfuric acid between

-0.375 V and +1.800 V at 100 mV/s until the gold redox peaks were reproducible, as

shown in Figure 3.5.
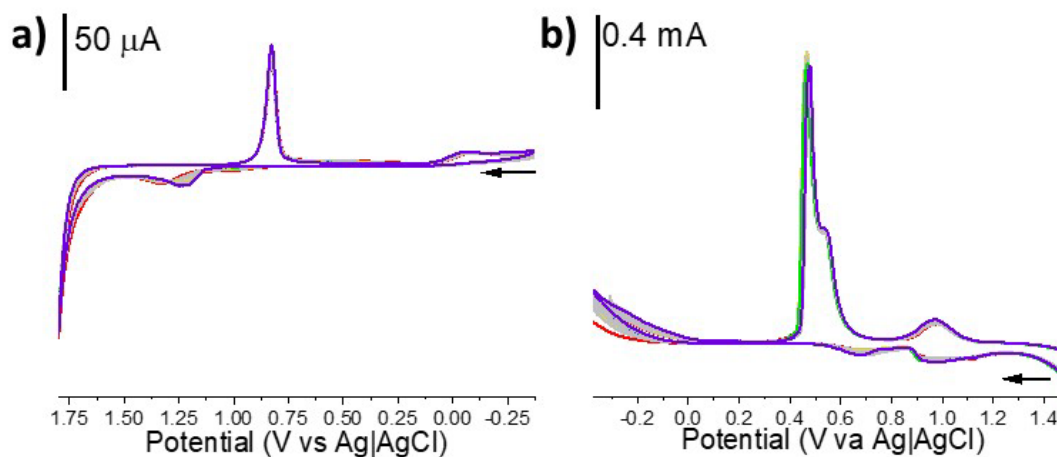


**Figure 3.5** Cyclic voltammograms of CHI Instruments gold rod (a) and Pine Research screen printed gold electrode in 0.5 M $H_2SO_4$, cycled from – 0.375 V to +1.800 V for 20 cycles at 100 mV/s. The inkjet CHI Instrument gold rod functioned as the working electrode, graphite rod as the CE, and gel Ag|AgCl as the RE. The Pine Research screen printed gold electrode functioned as the working electrode, planar screen printed counter elctrode as the CE, and gel Ag|AgCl as the RE.

Inkjet jet printed electrodes 1, 3, 5, 7, 9 and 10 were cycled in 0.5 M sulfuric acid

between -0.375 V and +1.800 V at 100 mV/s until the gold redox peaks were

reproducible, as shown in Figure 3.6.
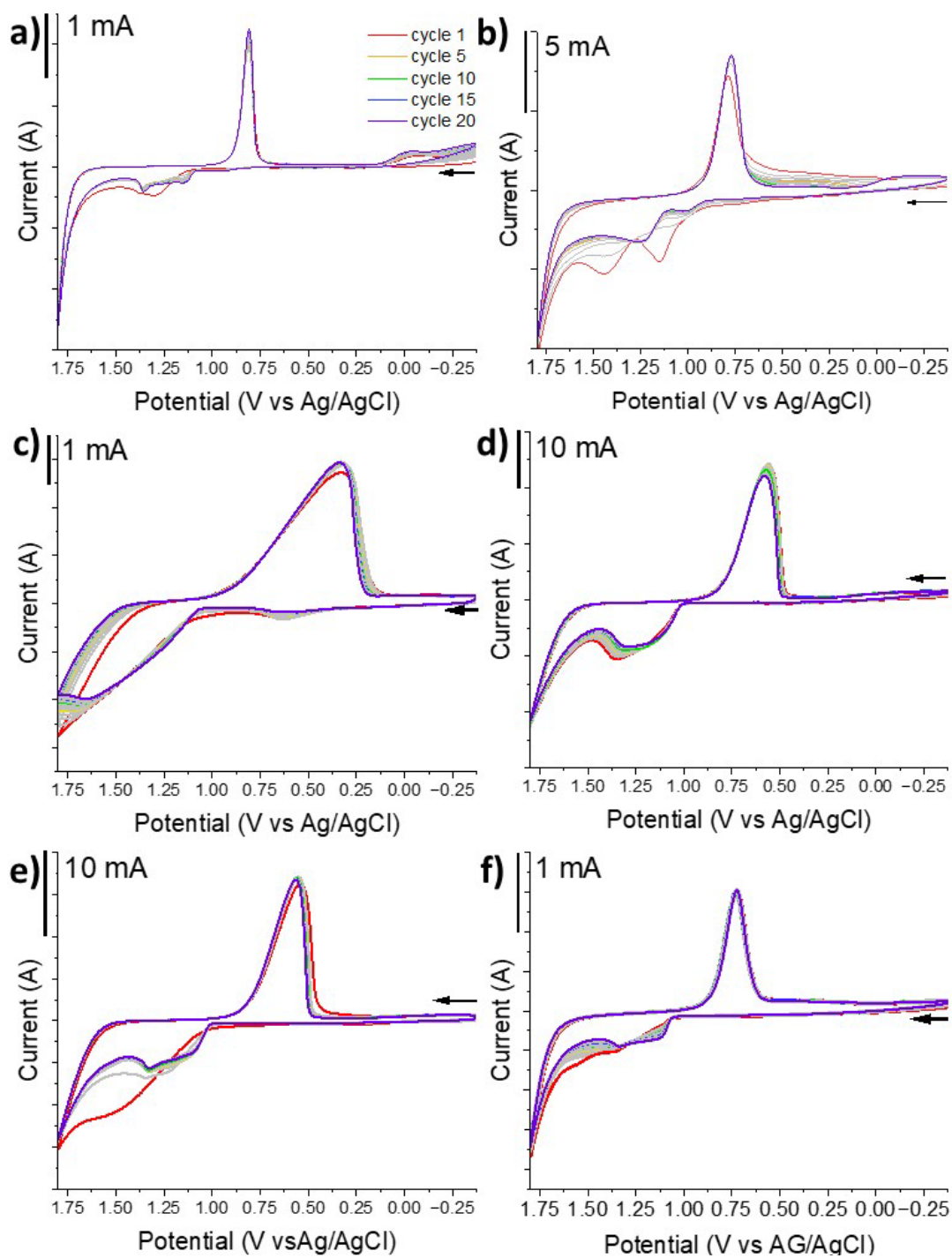
**Figure 3.6.** Cyclic voltammograms of Electrode 1 (a), Electrode 3 (b), Electrode 5 (c), Electrode 7 (d), Electrode 9 (e), and Electrode 10 (f) in 0.5 M $H_2SO_4$, cycled from −0.375 V to +1.800 V for 20 cycles at 100 mV/s. The inkjet printed electrode functioned as the working electrode, graphite rod as the CE, and gel Ag|AgCl as the RE.

The peaks in these cyclic voltammograms are from monolayer gold oxide formation and removal on the electrode surface. The oxidation peaks near +1.00 V and + 1.25 V are consistent with the potential values and peak shape seen with the gold rod working electrode and screen-printed gold PINE Research electrode. Similarly, the broad asymmetric peak from + 0.6 V to +1.0 V are also consistent with the baseline gold electrodes. The peaks are much broader than the gold rod working electrode and screen-printed gold PINE Research electrode for all of the inkjet printed electrodes. This broadening is particularly pronounced for Electrode 5 (Fig 3.6c), Electrode 7 (Fig. 5.6d), and Electrode 9 (Fig 3.6e). In Fig 3.3b, Electrode 5 appears to have unformal coverage of PLA by the gold ink, but only has 2 layers of gold which may not provide uniform coverage of the PLA by the gold ink microscopically. In Fig 3.3d and Figure 3.3f, Electrodes 7 and 9 have apparent discontinuous coverage of PLA by the gold ink. The nonhomogeneous gold coverage creates defects in the gold electrode, minimizing the conductivity and increasing resistance. Electrode 1, Electrode 3, and Electrode 10 have a much sharper reduction peak, at + 0.9 V, + 0.8 V, and + 0.75 V respectively, than the other inkjet printed electrodes. Electrode 9 and 10 both have four layers of gold, but Electrode 10 has more pronounced gold redox peaks. In Figure 3.3f and Figure 3.3g, Electrode 10 has significantly more uniform coverage of PLA by the gold ink than Electrode 9 contributing to a more chemically uniform gold. Electrode 1 and Electrode 3 have different annealing parameters. Electrode 1, printed on glass, is visually much smoother with uniform gold coverage than all other electrodes. Electrode 3, printed on

very rough PLA has visually uniform gold coverage, but the gold ink appears much

rougher.

CV ferricyanide as a function of ferricyanide concentration

Cyclic voltammograms with increasing concentrations of ferricyanide were collected

using the CHI gold rod, Pine Research screen printed gold planar electrode shown in

Figure 3.7.
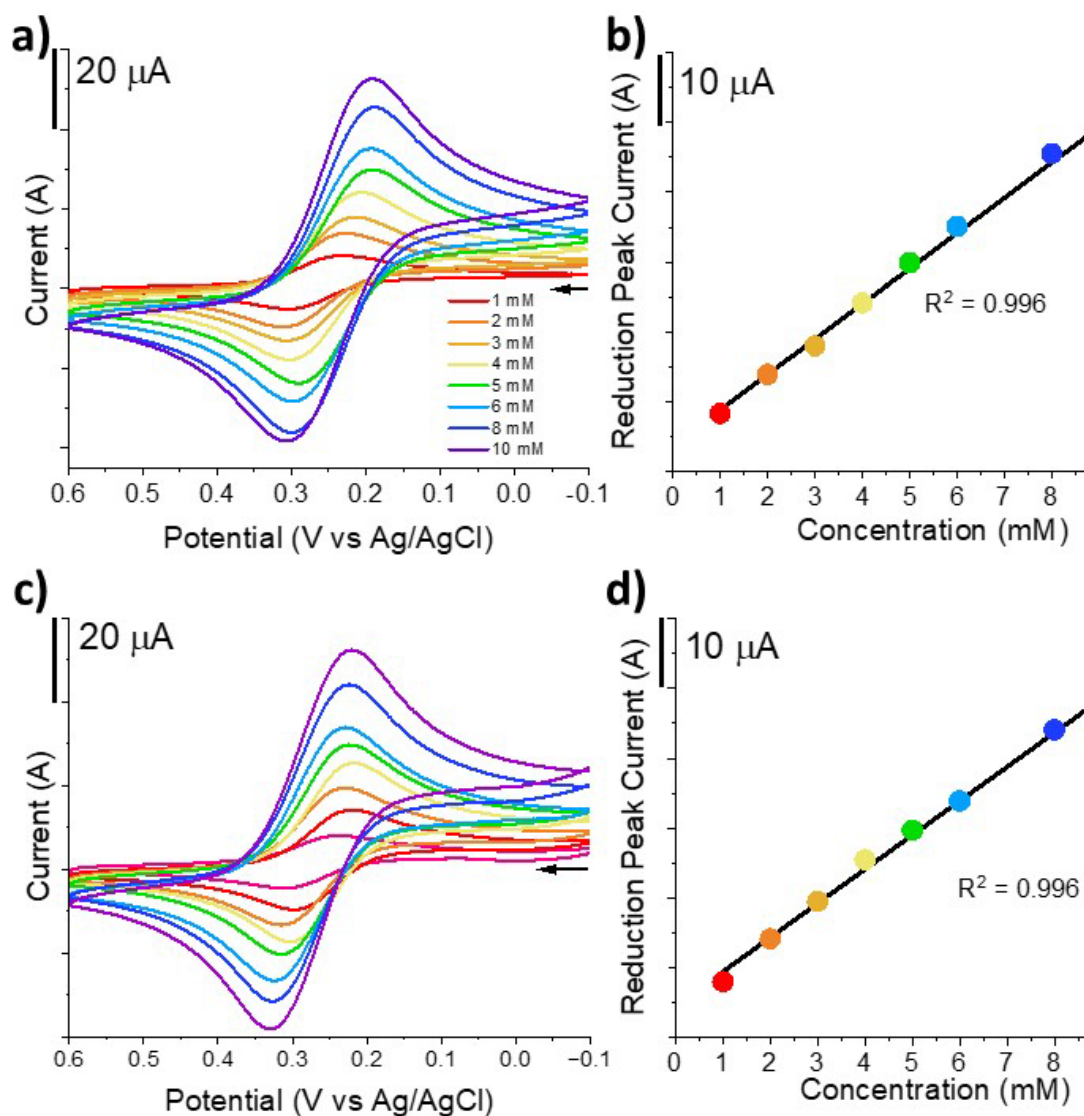
**Figure 3.7.** Cyclic voltammogram of ferricyanide at increasing concentrations of (1 mM to 10 mM) at a scan rate of 100 mV/s using CHI instruments gold rod WE (a) and the Pine research gold electrode (c). Corresponding calibration curve of reduction peak height versus ferricyanide concentration for CHI instruments gold rod WE (b), Pine research gold electrode (d). An Ag/AgCl gel reference electrode was used for both, and a graphite rod counter electrode was used with the CH Instruments gold rod.

The electrochemical data for the CHI gold rod and Pine Research gold screen printed electrode is summarized in Table 3.2.

**Table 3.2 Electrochemical Data for CHI Gold Rod Working Electrode and Pine Research Gold Screen Printed Electrode**

| Electrode | Analyte | v | $E_{p,o}$ (V) | $E_{p,r}$ (V) | $\Delta E$ (V) | $I_{p,o}$ (µA) | $I_{p,r}$ (µA) | $I_{p,o}/I_{p,r}$ |
|---|---|---|---|---|---|---|---|---|
| CHI Rod | 1 mM FCN | 100 | 0.305 | 0.305 | 0.072 | -5.19 | 8.39 | 0.618 |
| CHI Rod | 2 mM FCN | 100 | 0.311 | 0.311 | 0.085 | -9.35 | 14.0 | 0.666 |
| CHI Rod | 3 mM FCN | 100 | 0.306 | 0.306 | 0.092 | -13.3 | 18.0 | 0.721 |
| CHI Rod | 4 mM FCN | 100 | 0.303 | 0.303 | 0.097 | -17.8 | 24.5 | 0.727 |
| CHI Rod | 5 mM FCN | 100 | 0.290 | 0.290 | 0.098 | -23.6 | 30.1 | 0.784 |
| CHI Rod | 6 mM FCN | 100 | 0.298 | 0.298 | 0.104 | -28.2 | 35.2 | 0.801 |
| CHI Rod | 8 mM FCN | 100 | 0.299 | 0.299 | 0.110 | -35.8 | 45.5 | 0.788 |
| CHI Rod | 10 mM FCN | 100 | 0.307 | 0.307 | 0.116 | -38.2 | 52.6 | 0.725 |
| CHI Rod | 5 mM FCN | 10 | 0.302 | - | - | -8.96 | 15.1 | 0.618 |
| CHI Rod | 5 mM FCN | 25 | 0.312 | - | - | -16.1 | 22.1 | 0.723 |
| CHI Rod | 5 mM FCN | 50 | 0.326 | 0.262 | 0.064 | -24.0 | 30.0 | 0.799 |
| CHI Rod | 5 mM FCN | 100 | 0.350 | 0.279 | 0.071 | -33.2 | 39.8 | 0.835 |
| CHI Rod | 5 mM FCN | 250 | 0.328 | 0.266 | 0.062 | -72.1 | 65.7 | 1.098 |
| CHI Rod | 5 mM FCN | 500 | 0.375 | 0.292 | 0.083 | -10.0 | 88.3 | 1.178 |
| Pine | 1 mM FCN | 100 | 0.310 | 0.238 | 0.071 | -4.63 | 8.02 | 0.578 |
| Pine | 2 mM FCN | 100 | 0.295 | 0.223 | 0.072 | -9.67 | 14.3 | 0.676 |
| Pine | 3 mM FCN | 100 | 0.312 | 0.230 | 0.083 | -13.5 | 19.4 | 0.695 |
| Pine | 4 mM FCN | 100 | 0.302 | 0.219 | 0.083 | -17.6 | 25.4 | 0.692 |
| Pine | 5 mM FCN | 100 | 0.313 | 0.222 | 0.091 | -20.4 | 29.3 | 0.685 |
| Pine | 6 mM FCN | 100 | 0.325 | 0.229 | 0.096 | -26.6 | 33.9 | 0.784 |
| Pine | 8 mM FCN | 100 | 0.327 | 0.224 | 0.103 | -31.3 | 44.0 | 0.711 |
| Pine | 10 mM FCN | 100 | 0.330 | 0.221 | 0.109 | -38.4 | 52.3 | 0.734 |
| Pine | 5 mM FCN | 10 | 0.334 | 0.266 | 0.068 | -4.37 | 13.0 | 0.337 |
| Pine | 5 mM FCN | 25 | 0.339 | 0.271 | 0.068 | -9.63 | 19.2 | 0.503 |
| Pine | 5 mM FCN | 50 | 0.349 | 0.279 | 0.07 | -15.4 | 26.0 | 0.592 |
| Pine | 5 mM FCN | 100 | 0.362 | 0.29 | 0.072 | -23.6 | 33.0 | 0.722 |
| Pine | 5 mM FCN | 250 | 0.385 | 0.303 | 0.082 | -32.6 | 39.8 | 0.819 |
| Pine | 5 mM FCN | 500 | 0.395 | 0.303 | 0.092 | -51.8 | 53.1 | 0.976 |

Here, the CHI gold rod and the Pine screen printed electrode array serve as controls or benchmarks to which the electrochemical behavior of the inkjet printed electrodes are compared. Faraday's law says that current is proportional to concentration, and thus predicts that as the concentration of ferricyanide increases the peal current should

increase linearly. For the CHI gold rod, the relationship of reduction peak current to ferricyanide concentration is very linear, $R^2$ = 0.996. For the Pine Research electrode, the relationship of reduction peak current to ferricyanide concentration is very linear, $R^2$ = 0.996. For both electrodes, there is an increase in the ΔE as the concentration increases.  The change in peak potential should not change as concentration increases. The peak separation, ΔE, increases slightly for both the CHI rod and Pine Research electrode. The ΔE increases by 0.054 V for the CHI  rod, at 1 mM the ΔE is 0.072 V and at 10 mM the ΔE is 0.116 V. The ΔE increases by 0.038 V for the CHI rod, at 1 mM the ΔE is 0.071 V and at 10 mM the ΔE is 0.109 V. The oxidation/reduction peak current ratios for the CHI gold rod ranges from 0.618 to 0.801, and for the Pine Research electrode ranges from 0.578 and 0.734. The reduction peak current is slightly larger than the oxidation peak current. The peak ratio is expected to be 1 for electrochemically reversible systems. The smaller oxidation peak suggests that not all the ferricyanide is removed during the oxidative sweep.

Electrode 1 delaminated when placed into the ferricyanide solution, shown in Figure 3.8. The gold inkjet printed onto glass substrate electrodes, 1 and 2, were not further characterized with electrochemistry. Since the final sensor design will not use glass as the substrate for the electrodes, work with inkjet printed gold onto glass substrates was not continued.
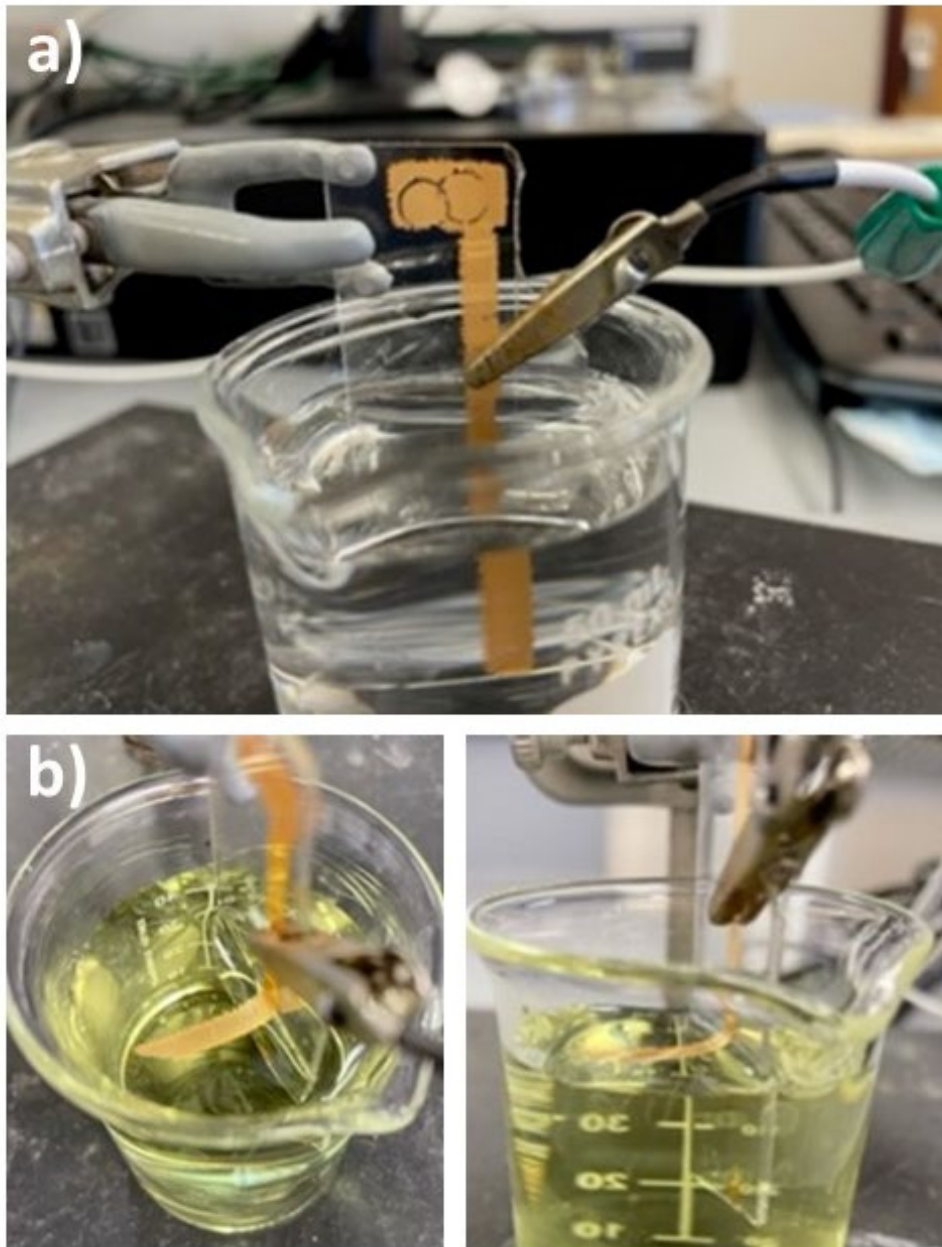
**Figure 3.8**. Electrode 1 in a beaker with $H_2SO_4$ (a), and in 0.5 M ferricyanide (b and C).

Cyclic voltammograms with increasing concentrations of ferricyanide were collected using Electrode 3, shown in Figure 3.9. Here Electrode 3was the working electrode, a graphite rod served as the counter electrode, and an Ag|AgCl gel reference electrode.
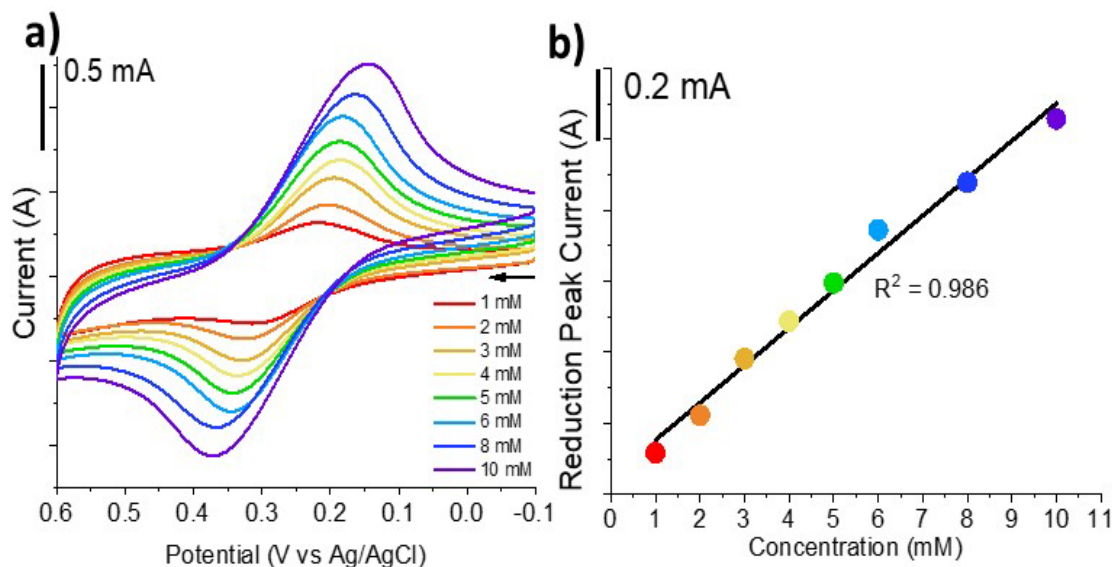
**Figure 3.9.** Cyclic voltammogram of ferricyanide at increasing concentrations (1 mM – 10 mM) at a scan rate of 100 mV/s using Electrode 3 (a), and reduction peak current versus concentration (b). An Ag|AgCl gel electrode was used as the reference electrode and a graphite rod for the counter electrode.

Electrochemical data for Electrode 3 is summarized in Table 3.3, with the other inkjet printed electrodes. There is a slightly less linear relationship between reduction peak current and ferricyanide concentration for Electrode 3 than the control electrodes, however, the $R^2$ value is still high, $R^2$ = 0.986. Compared to the CHI rod and Pine research electrode, the peaks in the cyclic voltammogram of electrode 3 are much broader. The peak width half max of 10 mM is 0.185 V, larger than the Pine Research electrode which is 0156 V. The ΔE also increases as concentration of ferricyanide increases by 0.139 V, at 1 mM ferricyanide ΔE = 0.090 V, and at 10 mM ferricyanide ΔE = 0.229. The increase in ΔE is almost twice as large as the commercially available electrodes. The differences observed in the CV relative to the controls are a result of the working electrode since the only difference between the electrochemical cells is the working electrode. Further,

there is an increase in current in the non-faradaic regions of the CV. From +0.45 V to +0.6 V, the current is generated from non-faradaic processes. This increase in current in this region and the increase in peak broadness suggests an increase in ohmic drop, or low conductivity in the working electrode. Visually, the gold on Electrode 3 is not very shiny, even after several electrochemical experiments compared to the CHI rod and Pine Research electrode. The dullness of the gold suggests impurities within it, increasing the resistance. The gold ink contains carbohydrate ligands and could still be present if they did not fully degrade during the annealing process.

Cyclic voltammograms of increasing ferricyanide concentration were not collected on Electrodes 5, 7, 9, and 10 because they began flaking off the PLA substrate after other electrochemical characterizations. Placement of the alligator clip from the potentiostat leads onto the electrode led to scrapping of the gold off the PLA substrate, so the alligator clip could not be placed again without extreme maneuvering.

CV ferricyanide as a function of scan rate

Cyclic voltammograms of 0.5 M ferricyanide were collected with increasing with increasing scan rates using the CHI gold rod and the Pine Research screen printed gold electrode shown in Figure 3.9a and Figure 3.9c respectively. The oxidation and reduction peak current is plotted versus the square root of the scan rate in Figure 3.10b and Figure 3.10d.
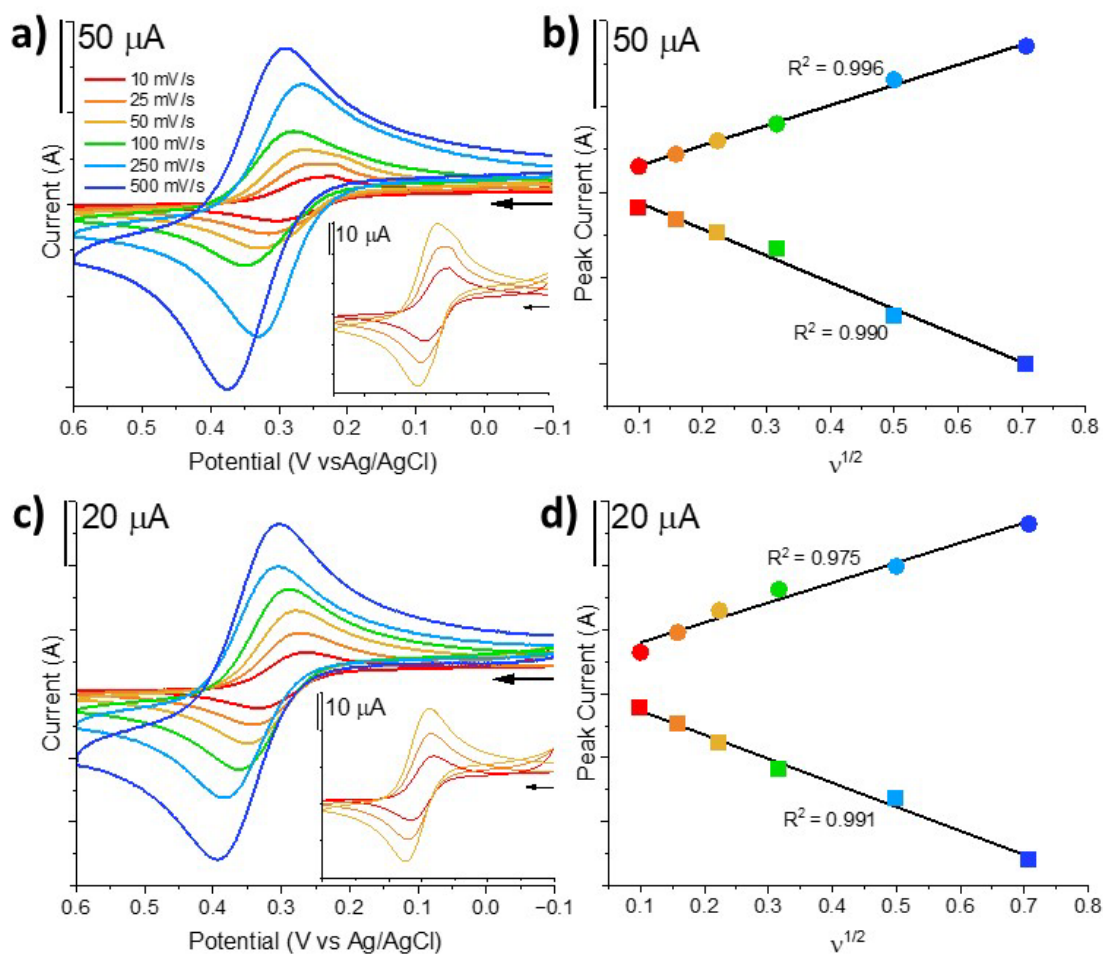
**Figure 3.10.** Cyclic voltammogram of 5 mM ferricyanide in 0.1 M KCl in water with increasing scan rates of 10 mV/s, 25 mV/s, 50 mV/s, 100 mV/s, 250 mV/s, and 500 mV/s using a gold rod from CHI instruments as the WE (a), Pine Research screen-printed gold working electrode (c). The 10 mV/s, 25 mV/s, and 50 mV/s are enlarged to show detail for CHI instruments gold rod (inset) and Pine Research screen-printed gold working electrode (inset). Reduction (circle) and oxidation (square) peak height versus $v^{1/2}$ for gold rod (b) and Pine gold electrode (d).

The peak width half max was calculated for the CHI and Pine Research gold rod for the reduction peak at a scan rate of 250 mV/s.  For the CHI gold rod, the peak width is 0.171 V, and for the Pine research electrode it is 0.156 V.

The Randles-Sevcik equation predicts a linear relationship between peak current and $v^{1/2}$. The oxidation peak current versus $v^{1/2}$ for the CHI gold rod has a $R^2$ of 0.990, and the reduction peak current versus $v^{1/2}$ has a $R^2$ value of 0.996, both highly linear. In Figure 3.9a inset, the CHI rod at the 10 mV/s, 25 mV/s, and  50 mV/s scan rate, a second reduction peak is observed.  This second peak is not seen in the Pine Research electrode Oxidation and reduction of ferricyanide is a one electron process, so there should only be one oxidation and one reduction peak. The second peak observed here could be due to surface confinement or ligand dissociation of ferricyanide. The $\Delta E$ does increase for both commercially available electrodes as the scan rate increases. The peak separation of the CHI gold rod increases by 0.019 V, $\Delta E$ = 0.064 V at 100 mV/s to $\Delta E$ = 0.083 V at 500 mV/s. The peak separation of Pine Research electrode increases by 0.022 V, $\Delta E$ = 0.070 V at 100 mV/s to $\Delta E$ = 0.092 V at 500 mV/s. The oxidation/reduction peak current ratios for the CHI gold rod ranges from 0.618 to 1.178, and for the Pine Research electrode ranges from 0.337 and 0.976.

The peak potential minus the $E_{1/2}$ was plotted for the oxidation and reduction peak potential versus the log of the scan rate to create a trumpet plot for the CHI rod and Pine Research electrode, shown in Figure 3.11.
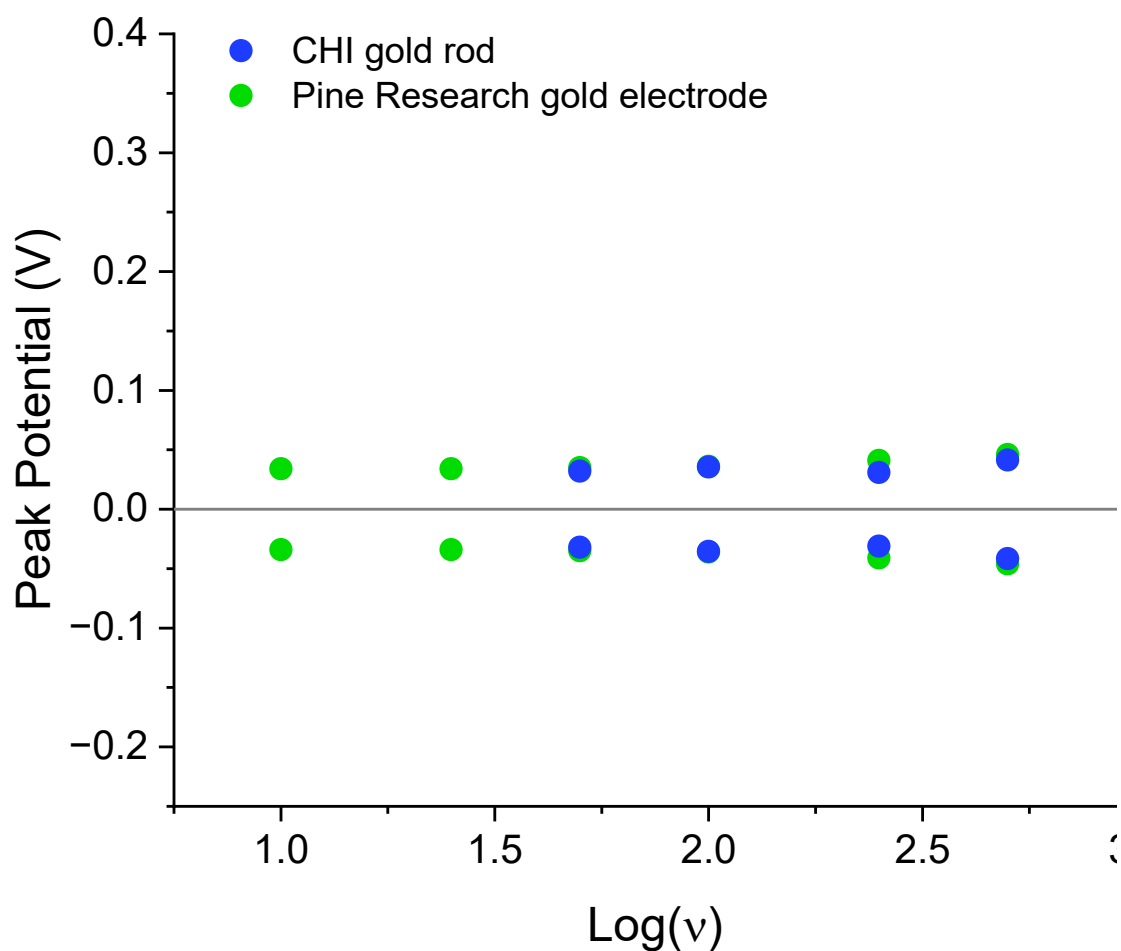
**Figure 3.11.** Plot of peak potential versus log(ν) for CHI gold rod (blue) and Pine Research screen printed electrode (green).

The peak separation increases very slightly for both electrodes as scan rate increases. For the CHI gold rod, the peak separation is 0.062 V at 250 mV/s and increases by 0.021 V to 0.083 V at 500 mV/s. For the Pine Research electrode, the peak separation is 0.082 V at 250 mV/s, and increases by 0.010 V to 0.092 V at 50 mV/s. These increases are small compared to the inkjet printed electrodes (Fig 3.14). The CHI gold rod and Pine Research electrode are commercially available model electrodes and therefore conductive as expected, so uncompensated resistance is low. These data also demonstrate that the

electrolyte is sufficient to minimize Ohmic drop in solution, and electrolyte does not largely contribute to the uncompensated resistance observed in the inkjet printed electrodes.

Cyclic voltammograms of 0.5 mM ferricyanide were collected as the scan rate was increased for Electrodes 3, 5, 7, 9, and 10 in Figure 3.12.
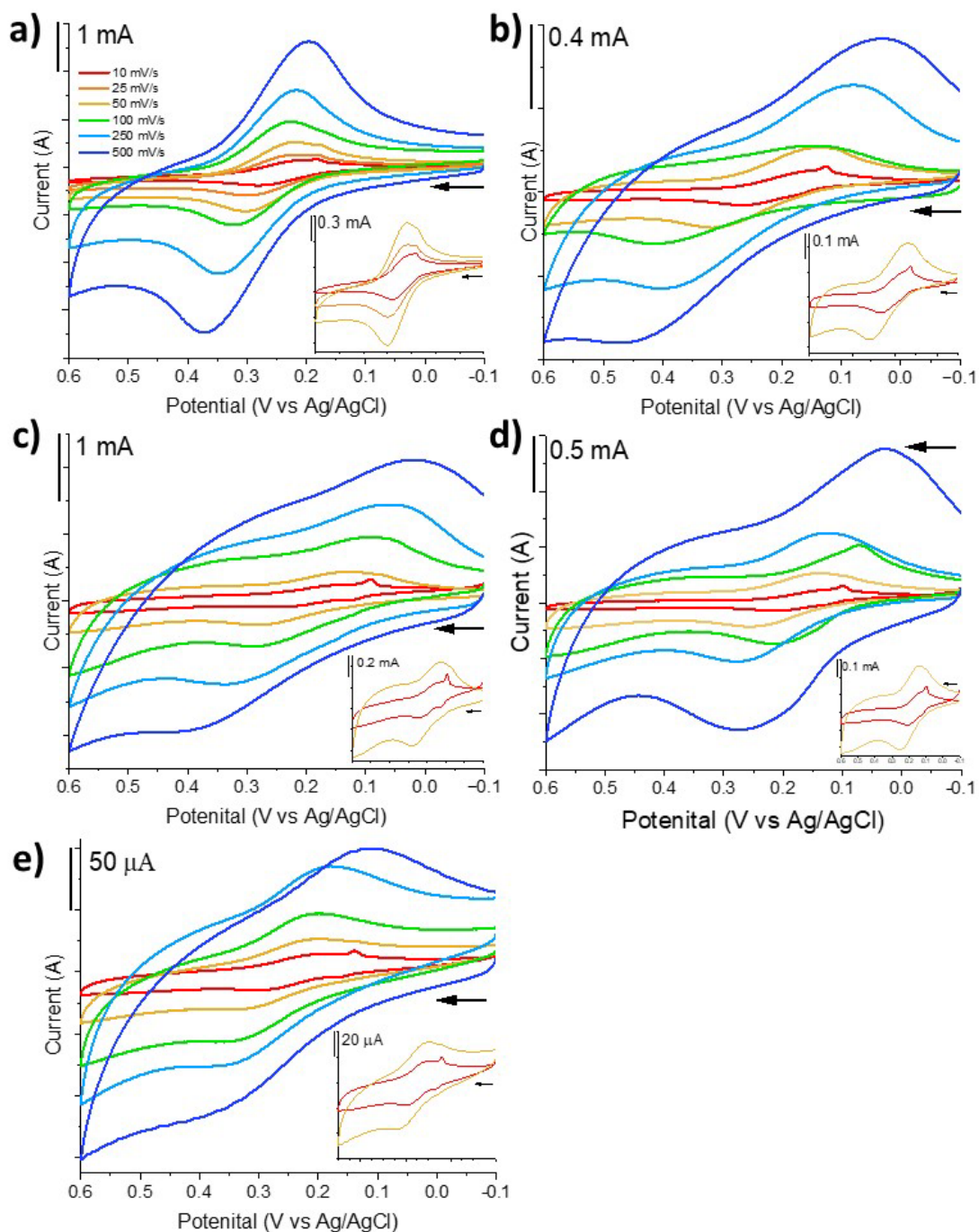
**Figure 3.12.** Cyclic voltammogram of 5 mM ferricyanide in 0.1 M KCl in water with increasing scan rates of 10 mV/s, 25 mV/s, 50 mV/s, 100 mV/s, 250 mV/s, and 500 mV/s with Electrode 3 (a), Electrode 5 (b), Electrode 7 (c), Electrode 9 (d) and Electrode 10 (e).

Table 3.3 the electrochemical data for Electrodes 3, 5, 7, 9, and 10. All voltammograms display large peak broadening compared to the CHI gold rod and Pine Research electrode. The peak width half max was calculated for each electrode for the reduction peak at a scan rate of 250 mV/s. Electrode 3 has a width of 0.141 V, Electrode 5 is 0.195 V, Electrode 7 is 0.194 V, Electrode 9 is 0.214 V, and Electrode 10 is 0.190 V. Electrode 3 has the smallest peak width, and closest to the CHI gold rod and Pine Research electrode. There is a large amount of non-Faradaic current observed in all electrodes from +0.4 V to +0.6 V. The increase in current in this region and the increase in peak broadness suggests an increase in resistance, or low conductivity from the working electrode.

Peak separation greatly increases in Electrode 3, 5, 9 and 10 from 100 mV/s to 500 mV/s. Peak separation for Electrode 7 was not compared because the reduction peak at 100 mV/s is inconsistently shifted negatively and does not trend as expected. The peak separation of the Electrode 3 increases by 0.079 V, $\Delta E = 0.099$ V at 100 mV/s to $\Delta E = 0.175$ V at 500 mV/s. The peak separation of Electrode 5 increases by 0.174 V, $\Delta E = 0.271$ V at 100 mV/s to $\Delta E = 445$ V at 500 mV/s. The peak separation of the Electrode 9 increases by 0.189 V, $\Delta E = 0.188$ V at 100 mV/s to $\Delta E = 0.377$ V at 500 mV/s. The peak separation of Electrode 10 increases by 0.102 V, $\Delta E = 0.154$ V at 100 mV/s to $\Delta E = 0.256$ V at 500 mV/s. The peak separation for Electrodes 3, 5, 9, and 10 are much greater than the commercially available electrodes. The large increase in peak separation would suggest an electrochemically irreversible system. However, ferricyanide is known to be

an electrochemically reversible molecule, so the apparent irreversibility comes from the WE, not the solution.

The oxidation/reduction peak current for Electrode 3 ranges from 1.314 to 2.406, for Electrode 5 the range is 0.888 to 1.103, for Electrode 7 the range is 1.209 to 1.385, for Electrode 9 the range is 0.701 to 0.916, and for Electrode 10 the range is 0.881 to 1.192. The peak current ratio range is similar the commercially available electrode ranges observed with the scan rate cyclic voltammograms.

At slower scan rates, a second peak is seen in the inkjet printed electrodes and CHI gold rod. The peak current was not recorded at these scan rates if the second peak was present. This second peak is likely caused by surface confinement of ferricyanide. This second peak is very sharp, and mimics the peak shape observed in Figure 2.22, where the Pine Research electrode has delaminated from the ceramic surface. The delamination caused ferricyanide to be trapped underneath it. The electrochemical data for Electrodes 3, 5, 7, 9, and 10 are summarized in Table 3.3.

The oxidation and reduction peak current were plotted versus the square root of the

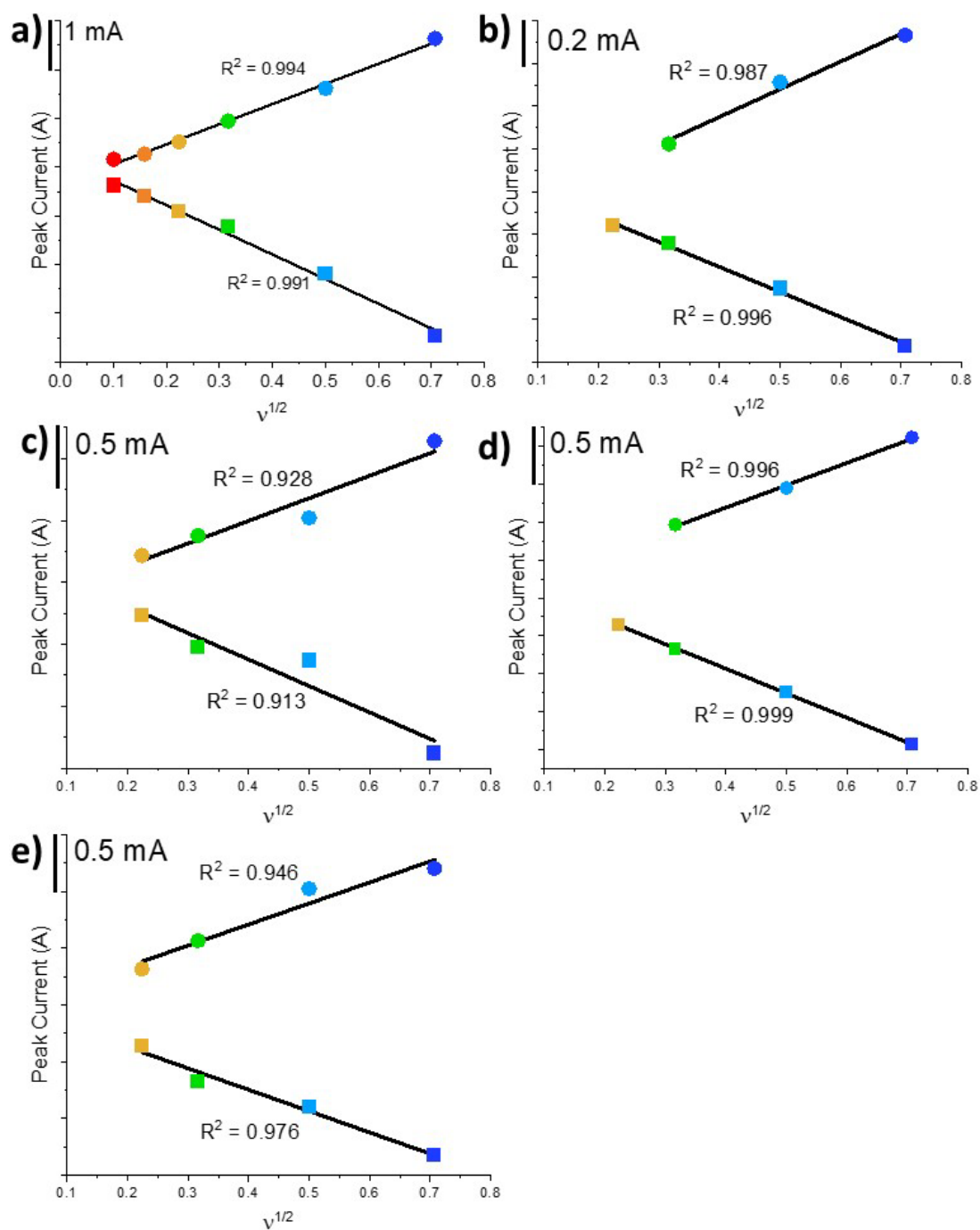scan rate for Electrodes 3, 5, 7, 9, and 10 in Figure 3.13



**Figure 3.13.** Reduction (circle) and oxidation (square) peak height versus $v^{1/2}$ for Electrode 3 (a), Electrode 5 (b), Electrode 7 (c), Electrode 9 (d) and Electrode 10 (e).

In Figure 3.13, the peak currents increase linearly as scan rate increases, as predicted by the Randles-Sevcik equation. The oxidation peak current was compared for these electrodes because the secondary peak was not observed at 50 mV/s in the oxidative sweep. For Electrode 3, the $R^2$ was 0.991, Electrode 5 was 0.996, Electrode 7 was 0.913, Electrode 9 was 0.999, and Electrode 10 was 0.976. The linearity of the inkjet printed electrodes is similar to the linearity of the commercially available electrodes. The Randles-Sevcik equation was used to calculate the diffusion coefficient of ferricyanide for the CH Instrument gold rod, Pine Research screen printed electrode, and Electrode 3. The working electrode area for the CH Instruments rod and Pine research electrode is 0.02 $cm^2$, and for Electrode 3 the area submerged in solution was 0.5 $cm^2$. The area of the working electrode must be known for this calculation and the flakiness and cracking of Electrodes 5, 7, and 9 make this value unknown. Electrode 10 has apparent capillary action, increasing the size of the working electrode. The diffusion coefficient of ferricyanide was 1.25 x $10^{-9}$ $cm^2$/s for the CH Instrument rod and Pine Research electrode. For Electrode 3 the diffusion coefficient of ferricyanide was 2.01 x $10^{-12}$ $cm^2$/s. The experimentally determined diffusion coefficient of ferricyanide is smaller than the literature value.
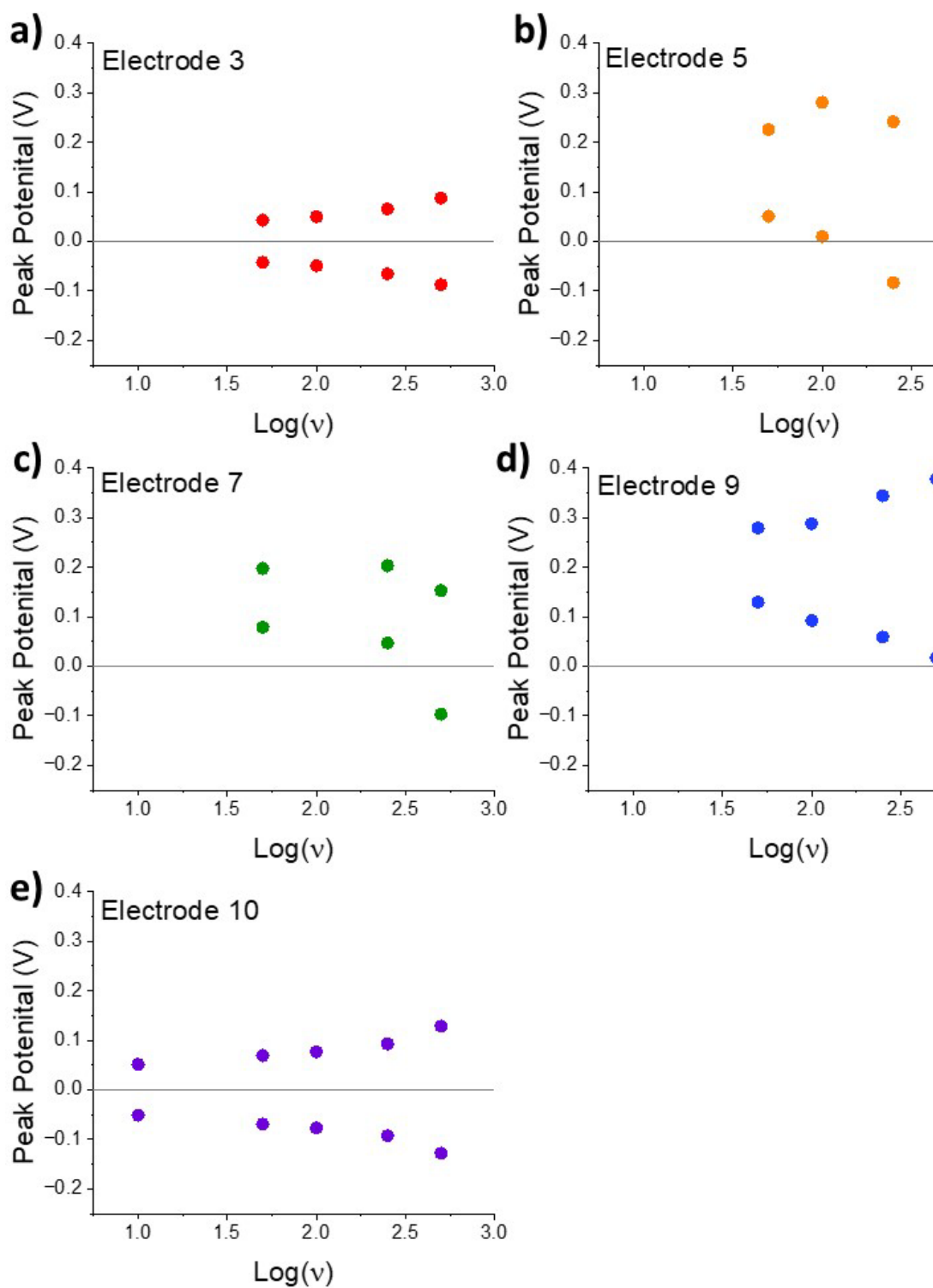
**Figure 3.14.** Plot of peak potential versus log(v) for Electrode 3 (a), Electrode 5 (b), Electrode 7 (c), Electrode 9 (d), and Electrode 10 (e).

A trumpet plot was created for Electrodes 3, 5, 7, 9, and 10, shown in Figure 3.14.

In Figure 3.14, there is an inconsistent peak separation for Electrodes 3, 5, 7, 9, and 10. Electrodes 3, 9 and 10 show an increase in the peak separation as scan rate increases, but generally a trumpet shape is observed.

For Electrodes 5, 7, and 9, the peak potentials are not centered around the x-axis that is expected and observed for the CHI gold rod and Pine Research electrodes, nor is a consistent pattern of increase observed. The trumpeting pattern results from high uncompensated resistance in the electrochemical cell. Inconsistencies in the trumpeting pattern result from the flakiness and breakage seen in Figure 3.3 shows the area of the electrode used as the working electrode.

The differences in electrode layer and shape do not tend to improve the electrode performance. Electrodes 3 and 10 performed best in comparison to Electrodes 5, 7, and 9. The peak shape of the gold redox activity in Figure 3.5b and Figure 3.5f are most similar to the commercially available electrodes. High resistance is observed in the cyclic voltammograms of ferricyanide with Electrode 3 and 10, but the peak shape is more defined than Electrodes 5, 7, and 9. Electrode 9 and 10 both have four layers of gold, but Electrode 10 provided results more similar to the commercially available electrodes. The gold ink on Electrode 10 is visually more uniform, whereas there is extremely nonhomogeneous coverage of Electrode 9.

**Table 3.3 Electrochemical Data for Electrodes 5, 3, 5, 9, and 10.**

| Electrode | Analyte | v | $E_{p,o}$ (V) | $E_{p,r}$ (V) | $\Delta E$ (V) | $I_{p,o}$ (mA) | $I_{p,r}$ (mA) | $I_{p,o}/I_{p,r}$ |
|-----------|---------|-----|-------|-------|-------|--------|-------|-------|
| 3 | 1 mM FCN | 100 | 0.218 | 0.308 | 0.090 | -0.282 | 0.316 | 0.892 |
| 3 | 2 mM FCN | 100 | 0.205 | 0.326 | 0.122 | -0.374 | 0.422 | 0.885 |
| 3 | 3 mM FCN | 100 | 0.195 | 0.329 | 0.134 | -0.505 | 0.582 | 0.867 |
| 3 | 4 mM FCN | 100 | 0.185 | 0.335 | 0.150 | -0.591 | 0.688 | 0.860 |

| | | | | | | | | |
|---|---|---|---|---|---|---|---|---|
| 3 | 5 mM FCN | 100 | 0.187 | 0.343 | 0.156 | -0.647 | 0.796 | 0.814 |
| 3 | 6 mM FCN | 100 | 0.182 | 0.345 | 0.163 | -0.802 | 0.946 | 0.848 |
| 3 | 8 mM FCN | 100 | 0.164 | 0.368 | 0.204 | -0.898 | 1.08 | 0.831 |
| 3 | 10 mM FCN | 100 | 0.145 | 0.374 | 0.229 | -1.07 | 1.26 | 0.847 |
| 3 | 5 mM FCN | 10 | 0.283 | - | - | -0.383 | 0.159 | 2.406 |
| 3 | 5 mM FCN | 25 | 0.301 | - | - | -0.592 | 0.263 | 2.252 |
| 3 | 5 mM FCN | 50 | 0.302 | 0.217 | 0.085 | -0.926 | 0.517 | 1.791 |
| 3 | 5 mM FCN | 100 | 0.324 | 0.225 | 0.099 | -1.22 | 0.946 | 1.290 |
| 3 | 5 mM FCN | 250 | 0.347 | 0.216 | 0.131 | -2.20 | 1.61 | 1.366 |
| 3 | 5 mM FCN | 500 | 0.371 | 0.196 | 0.175 | -3.47 | 2.64 | 1.314 |
| 5 | 5 mM FCN | 10 | 0.267 | - | - | - | - | - |
| 5 | 5 mM FCN | 50 | 0.313 | 0.138 | 0.175 | -0.163 | - | - |
| 5 | 5 mM FCN | 100 | 0.416 | 0.145 | 0.271 | -0.246 | 0.223 | 1.103 |
| 5 | 5 mM FCN | 250 | 0.404 | 0.079 | 0.325 | -0.456 | 0.513 | 0.888 |
| 5 | 5 mM FCN | 500 | 0.475 | 0.030 | 0.445 | -0.726 | 0.733 | 0.991 |
| 7 | 5 mM FCN | 10 | 0.216 | - | - | - | - | - |
| 7 | 5 mM FCN | 50 | 0.256 | 0.138 | 0.118 | -0.271 | 0.216 | 1.251 |
| 7 | 5 mM FCN | 100 | 0.214 | - | - | -0.522 | 0.377 | 1.385 |
| 7 | 5 mM FCN | 250 | 0.281 | 0.125 | 0.156 | -0.631 | 0.52 | 1.214 |
| 7 | 5 mM FCN | 500 | 0.277 | 0.028 | 0.249 | -1.38 | 1.14 | 1.209 |
| 9 | 5 mM FCN | 10 | - | - | - | - | - | - |
| 9 | 5 mM FCN | 50 | 0.272 | - | - | -0.361 | - | - |
| 9 | 5 mM FCN | 100 | 0.277 | 0.089 | 0.188 | -6.76 | 0.965 | 0.701 |
| 9 | 5 mM FCN | 250 | 0.334 | 0.061 | 0.273 | -1.24 | 1.45 | 0.860 |
| 9 | 5 mM FCN | 500 | 0.397 | 0.020 | 0.377 | -1.94 | 2.12 | 0.916 |
| 10 | 5 mM FCN | 10 | 0.302 | 0.199 | 0.103 | - | - | - |
| 10 | 5 mM FCN | 50 | 0.339 | 0.201 | 0.138 | -0.00360 | 0.00317 | 1.136 |
| 10 | 5 mM FCN | 100 | 0.353 | 0.199 | 0.154 | -0.00677 | 0.00568 | 1.192 |
| 10 | 5 mM FCN | 250 | 0.361 | 0.175 | 0.186 | -0.00903 | 0.103 | 0.881 |
| 10 | 5 mM FCN | 500 | 0.371 | 0.114 | 0.256 | -0.133 | 0.120 | 1.104 |

Anodic Stripping Voltammetry with Electrode 3

Anodic stripping voltammetry of arsenic was preformed using Electrode 3 as the WE, a graphite rod as the CE, and an Ag|AgCl gel RE. Arsenic stripping current was measured at increasing concentrations of 1 ppb, 2 ppb, 3 ppb, 4 ppb, 5 ppb and 10 ppb using ASV. A potential of -0.6 V was applied for 180 seconds while the solution was stirring and for an additional 30 second without stirring. The potential was swept from

-0.6 V to +0.5 V at a rate of 100 mV/s, and then held at +0.5 V for 180 seconds to fully

strip off arsenic before beginning the next trial. The oxidation peak current from ASV is
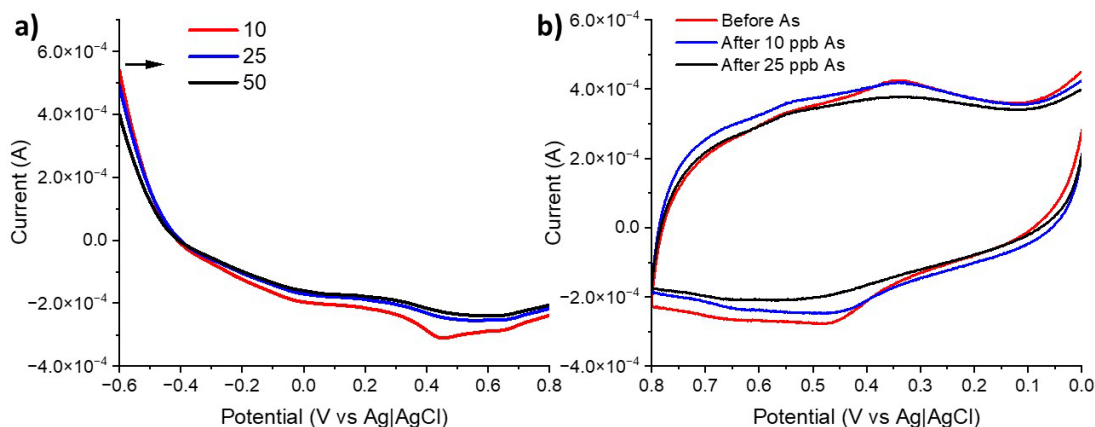
shown in Figure 3.14.



**Figure 3.15** Stripping of arsenic at 10 ppb, 25 ppb, and 50 ppb (a) using Electrode 3 as the WE, a graphite rod as the CE, and an Ag|AgCl gel RE. Cyclic voltammograms of electrolyte after increases in arsenic concentration (b) between +0.0 V and +0.8 v at 100 mV/s.

An oxidation peak is seen near +0.41 V at 10 ppb arsenic, but this peak does not increase

as concentration of arsenic increases, suggesting that arsenic is being retained. The peak

seen at +0.41 V may be caused by oxidation of gold, not arsenic. Arsenic is known to

form alloys with gold, so alloy formation might be occurring. Cyclic voltammograms of

only electrolyte reveal similar results. After no addition of arsenic, an oxidation peak

near +0.45 V is seen. After arsenic is added, this oxidation peak decreases, and

eventually goes away. As arsenic alloys with gold, the chemical environment changes,

so different potentials are needed to reduce and oxidize the alloyed area instead of only

gold or only arsenic.

### 3.6 Characterization of Inkjet Printed Working Electrodes with Scanning Electron Microscopy (SEM) – Results and Discussion

Electrochemical characterization provides information about the electronic properties and physical stability of the electrode. Scanning electron microscopy (SEM) provides additional information about the inkjet printed gold electrode morphology. Scanning electron microscopy was performed on Electrodes 1, 2, 3, 4, 6, and 8.

Scanning electron microscopy is an imaging technique using interactions between the sample and an electron beam to generate images. Electrons are emitted from a filament, and several lenses are used to columnate the beam and focus it onto the sample under vacuum.[33] This is also referred to as the incident electron beam. As the electron beam interacts with the sample, several different processes occur leading to scattered or emitted electrons and photons, shown in Figure 3.16, taken from ref 33.
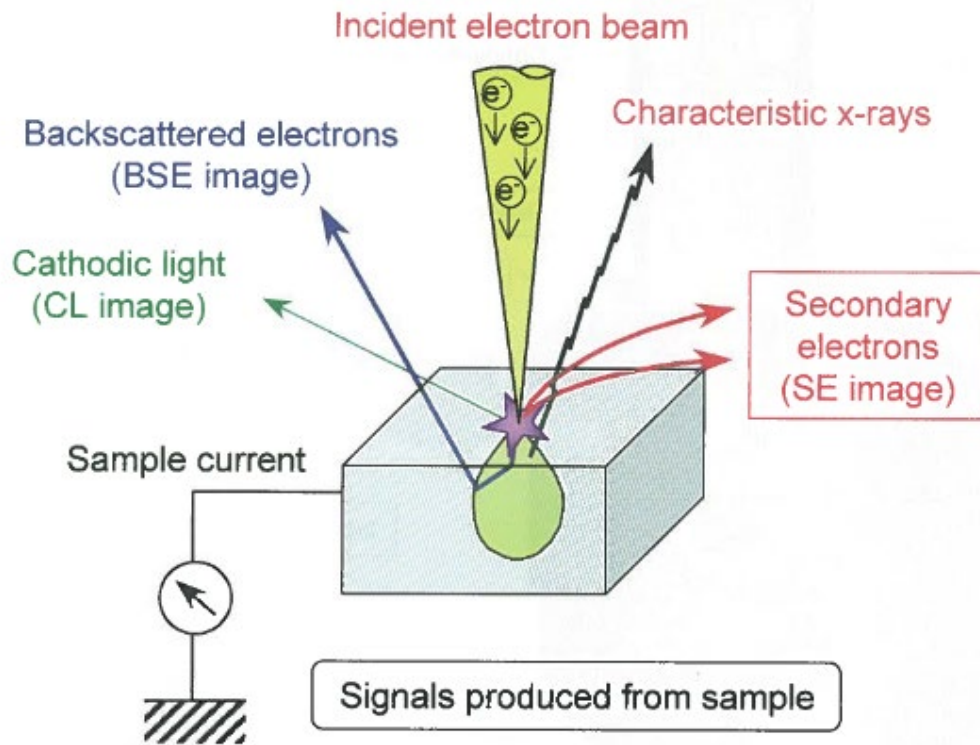
**Figure 3.16.** Incident electron beam hitting sample to produce backscattered electrons, secondary electrons, photons, and X-rays during scanning electron microscopy imaging. Image taken from Ref. 33

X-rays are also generated from the interaction of the incident electron beam and the sample but were not used for characterization in this work. Images collected in this work utilize backscattered electrons (BE) and secondary electrons (SE). Electrons are very small relative to the atoms in the sample, which allows them to interact with the sample through scattering.[33] Backscattered electrons come from deep within the sample, illustrated in Figure 3.16, as the blue arrow comes from within the sample.[33] These electrons interact with the sample and are scattered back into the vacuum, with high energy.[33] They interact strongly with the sample and provide compositional information.[33] Secondary electrons come from near the surface of the material,

illustrated in Figure 3.16, as the red arrows come from the surface of the sample. As secondary electrons enter the sample, electrostatic forces pull the electron in, and lose energy before moving back into the vacuum.[33] Secondary electrons provide information about the composition of the sample.[33] Detectors inside the SEM detect the backscattered electrons and secondary electrons. SEM images are collected through rastering. In SEM the incident electron beam is scanned across the sample, collecting an image in small areas to form a larger image.[33] Scanning electron microscopy (SEM) images were collected for Electrode 1, Electrode 2, and Electrode 3, Figure 3.17.
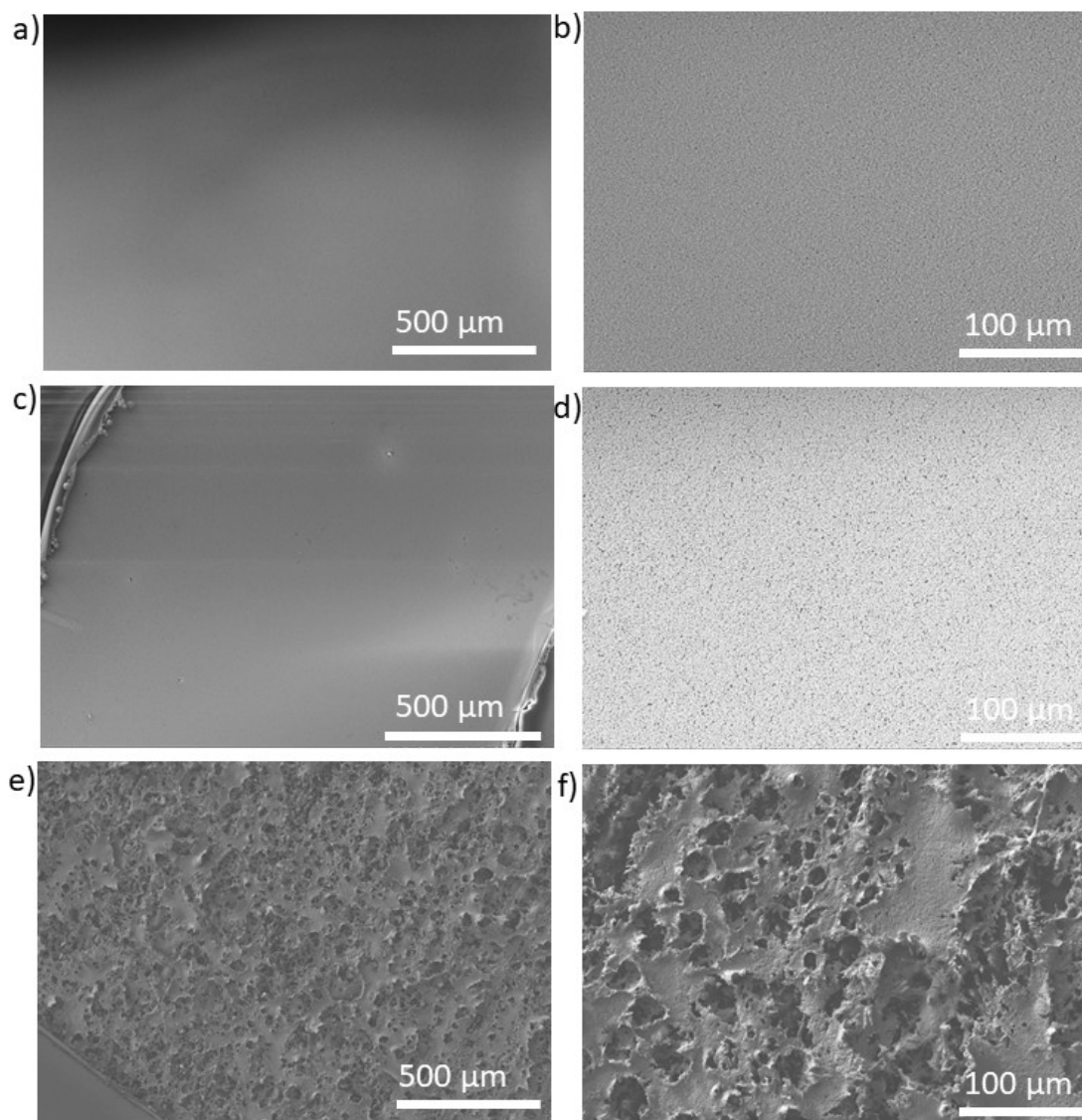
**Figure 3.17** Scanning electron microscopy images of Electrode 1 (a) and (b), Electrode 2 (c) and (d), and Electrode 3 (e) and (f); all images were generated from secondary electrons.

Copper tape was used to connect the electrode to the sample holder and is visible in the corner of Figure 3.16e. Electrode 3, with PLA substrate (Fig. 3.17 e, f), is rough relative to Electrodes 1 and 2 (Fig. 3.17 a-d; gold on glass electrodes). The observed morphology of Electrode 3 supports observed electrode behavior including broader peak in cyclic

voltammograms, Figure 3.8a and 3.11a. The porous holes may cause different chemical environments of gold. The cyclic voltammogram of gold redox activity of Electrode 3 showed broader oxidation peaks than the commercially available electrode. The increase in peak separation as scan rate increases, Figure 3.17a is also explained by the surface roughness. The differences in chemical environment cause ferricyanide to experience applied potential inconsistently. Thus, ferricyanide oxidizes and reduces over a wider potential range. Smaller morphological differences are observed as a function of annealing parameters when the substrate was glass. The photonically annealed gold on glass substrate, Electrode 1 appears smoother than thermally annealed gold on glass, Electrode 2.  However, both glass substrates have a smoother and more uniform coverage of gold than other inkjet printed electrodes. Scanning electron microscopy (SEM) images were collected for Electrodes 4, 6, and 8 in Figure 3.17.
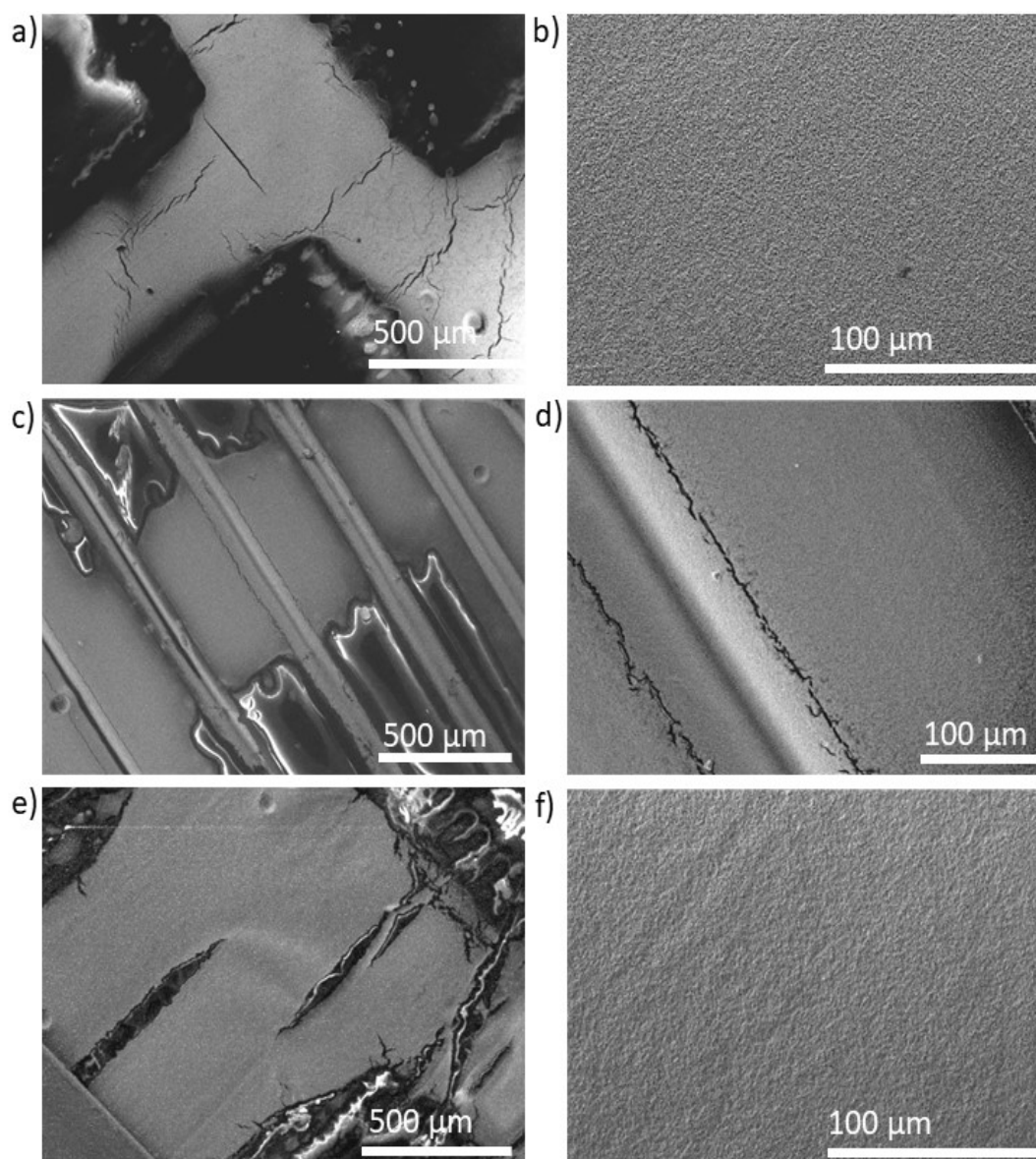
**Figure 3.18** Scanning electron microscopy images of Electrode 4 (a) and (b), Electrode 6 (c) and (d), and Electrode 8 (e) and (f). All images generated using secondary electrons.

Copper tape was used to connect the electrode to the sample holder and is visible in Figure 3.18e. Very bright regions visible at 500 µm are attributed to charging current on the PLA substrate, as PLA is not conductive. This phenomenon is referred to as charge up, as negative current from the incident electron beam builds up on the nonconductive

110

sample area.[33] At larger magnitudes, the gold coverage of Electrode 4 (Fig 3.18b), Electrode 6 (Fig 3.18d), and Electrode 8 (Fig 3.18f) appears to be smoother than Electrode 3. The coverage is more similar to the Pine Research electrode and Electrodes 1 and 2. At larger magnitudes, gold coverage is not consistent for Electrode 4 (Fig 3.18a), Electrode 6(Fig 3.18e), Electrode 8 (Fig 3.18e). Electrode 4 shows many cracks of the gold at 500 µm, but smooth, uniform coverage of PLA at 100 µm. Electrode 6 shows wicking of gold into the PLA grooved pattern at 500 µm (Fig 3.18c). Electrode 6 also shows cracking of gold on the PLA grooves at 100 µm (Fig 3.18d). Electrode 10 showed visible wicking of gold ink into the PETG substrate. The wicking and cracking could contribute to the uncompensated seen in the trumpet of Electrode 10 in Fig 3.18e. Electrode 9 and 10 both have four layers, represented by Electrode 8 (Fig 3.18e and Fig 3.18f).  There is extreme breakage of the gold and minor delamination of Electrode 8 at 500 µm (Fig 3.18e), but a smooth surface is observed at 100 µm (Fig 3.18d). The increase in gold layers does not appear to improve smoothness at observed 100 µm, or gold coverage of PLA observed at 500 µm. Further, there were not significant differences in electrochemical performance of the various layered electrodes. In general, cracking and flaking of an electrode contributes to resistance in the electrochemical cell. These features also contribute to heterogenous chemical environments, similarly to the surface roughness of Electrode 3. Together, these features contribute to added uncompensated resistance observed in Figure 3.14, where peak separation increased as scan rate increased for inkjet printed electrodes. They also contribute to peak broadening observed in cyclic voltammograms of gold redox activity (Fig 3.7) and

ferricyanide (Fig 3.11). The porosity and flaking also supports possible surface confinement of ferricyanide. The secondary reduction peak seen at slow scan rates could be due to ferricyanide becoming trapped between the gold electrode and PLA at the cracks and flaking of the gold.

Smaller morphological differences are observed as a function of annealing parameters on the PLA substrates. Electrode 3 was photonically annealed with visible light, and electrodes 4, 6, and 8 were annealed with visible light. Electrodes 4, 6, and 8 appear to be smoother, similar to the gold inkjet printed onto the glass substrates, Electrodes 1 and 2. Electrode 3 is much rougher than Electrodes on glass substrates and Electrodes photonically annealed with IR light.

## Chapter 2 Conclusions

Separation of the counter electrodes was concluded to not be necessary. Several experiments where the counter electrode was separated from the bulk solution with a glass fritted tube showed no significant difference in electrochemical cell performance. Cell performance was evaluated by plotting the oxidation peak current of lead (or ratio of lead peak current to copper peak current) after anodic stripping voltammetry as a function of lead concentration. In these experiments copper was used as an internal standard and mercury as a working electrode. As these were removed, high linearity of the lead peak current sustained regardless of counter electrode separation. The linearity was evaluated with three different approaches, a simple linear regression model, repeated measures ANOVA model, and linear mixed model. A planar screen-printed carbon electrode from Pine Research was used to evaluate cell performance when all three electrodes are in a planar configuration. High linearity was also observed here.

Alternative working electrode materials were evaluated with commercially available working electrodes. Here, arsenic, the heavy metal of interest, was plated and stripped with anodic stripping voltammetry. The oxidation peak current of arsenic was plotted as a function of arsenic concentration. The CH Instrument gold rod working electrode was used to create a linearity baseline to compare these electrodes to, as well as inkjet printed electrodes from our collaborators. A platinum screen printed electrode from Pine Research was used to evaluate platinum material as the working electrode. Platinum was shown to be electrochemcially active in the oxidation and reduction potentials of arsenic. A carbon screen printed electrode from Pine Research was used

to evaluate carbon as the working electrode material. Electrochemical characterization showed absorption of arsenic into the carbon electrode. Neither platinum nor carbon are proper alternatives to gold as the working electrode material. A gold screen printed electrode from pine research was used to evaluate cell performance of gold when in a planar configuration. Delamination and discoloration of the gold was observed after extensive use. Arsenic is known to form alloys with gold resulting in this observation. The formation of gold-arsenic alloys will need to be extensively evaluated in the electrodes provided by the collaborators.

## Chapter 3 Conclusions

The gold inkjet printed onto glass, Electrode 1, was electrochemically active, and showed reproducible gold redox activity. Scanning electron microscopy images of electrode 1 and 2 showed a smooth, uniform coverage of the glass substrate. However, after a short time, a few hours in solution, the gold delaminated from the glass substrate. Glass substrates were no longer considered as substrate material since the final sensor design will not be made of glass.

Gold inkjet printed on PLA electrodes were electrochemically active. The gold did not delaminate after extensive exposure to solution. Electrode 3, 5, 7, and 9 showed increases in peak broadness and peak separation as scan rate increased in cyclic voltammograms of ferricyanide compared to commercially available electrodes, the CHI gold rod and Pine Research screen printed gold electrode. These features indicate high uncompensated resistance. Scanning electron microscopy images revealed cracking of the gold on the PLA substrate. The gold did not uniformly cover and tended to bleed out of the desired shape when annealed photonically with IR light on the new PLA substrate.

114

Gold inkjet printed onto the green PLA was made with varying layers of gold, however the number of layers did not seem to trend with gold coverage. The heterogenous pattern of the green PLA appeared to dominate how well the gold ink covered. For example, gold coverage of PLA was more uniform when grooves were not present. Gold inkjet printed on the grey PLA was uniformly covered. The grey PLA did not have grooves or patterns but was very rough. Gold inkjet printed onto PETG, electrode 10, was electrochemically active, and did not delaminate after exposure to solution. High uncompensated resistance was observed in the cyclic voltammograms of ferricyanide in the peak broadness and increase in peak separation as scan rate increases. Electrode 3 and 10 performed better than the other inkjet printed electrodes. The peak broadness and separation was still present, but not as significant as Electrode 5, 7, and 9.

Scanning electron microscopy explained observed electrochemical behavior of the inkjet printed electrodes. Gold inkjet printed onto glass was homogenous and smooth regardless of annealing parameters. Gold inkjet printed onto grey PLA was very rough and porous, but the gold covered the PLA and did not crack or flake. The rough morphology supports the high resistance and possible surface confinement of ferricyanide during electrochemical characterizations. Gold inkjet printed onto green PLA was smoother than the grey PLA but was cracking and flaking. The gold ink did not want to cover the green PLA as well as the grey PLA. This could be due to the PLA surface morphology, full of grooves and patterns, or the differences in annealing, IR versus visible photonic annealing. The gold inkjet printed onto green PLA substrates, Electrode 5, 7, and 9 also showed high resistance and possible surface confinement of ferricyanide

regardless of the number of layers of gold printed. Gold inkjet printed onto to the PETG substrate was not evaluated with SEM, but electrochemical data shows high resistance and possible surface confinement of ferricyanide, however these features were not as significant as the gold on green PLA electrodes. The cracking and flaking of gold were not apparent visually, but wicking of gold ink into the grooves of the PETG was.

## Future Directions

The membrane separating the counter electrode membrane from the working electrode membrane was found to not be necessary in the electrochemical sensor design. The focus on our collaborative work is now evaluating the performance of gold inkjet printed onto 3-D printed plastic substrate. Thus far, gold inkjet printed on to grey PLA has uniform coverage, and functions as a working electrode during electrochemical characterization. Gold inkjet printed onto green PLA and PETG have inconsistent patterns from the 3-D printing process, which impacted the gold ink coverage of them. The gold ink is visually seen bleeding into the pattern on the plastic, and the gold area is inconsistent because of the grooves. The collaborators at the University of Louisville have printed new plastic electrodes that are smoother and some with intentional, and consistent patterning. These substrates are more homogenous in morphology.  At the University of Kentucky, the collaborators will inkjet print onto these new substrates. Their focus will be examining the relationship between the number of layers and electrochemical behavior and impacts of annealing parameters on electrochemical behavior.

References

(1) Babar, N.-U.-A.; Joya, K.; Tayyab, M.; Ashiq, M.; Sohail, M. Highly Sensitive and Selective Detection of Arsenic Using Electrogenerated Nanotextured Gold Assemblage. *ACS Omega* **2019**, *4* (9).

(2) Agency for Toxic Substances and Diseases Registry. Toxicological Profile for Arsenic, 2007. http://www.atsdr.cdc.gov/toxprofiles/tp2.pdf (accessed 2022-01-14).

(3) A. K. Singh. Chemistry of Arsenic in Groundwater of Ganges-Brahmaputra River Basen. *Curr. Sci.* **2006**, *91* (5).

(4) Hong, Y.-S.; Song, K.-H.; Chung, J.-Y. Health Effects of Chronic Arsenic Exposure. *J Prev Med Public Health* **2014**, *47* (5). https://doi.org/10.3961/jpmph.14.035.

(5) Hughes, M.; Beck, B.; Chen, Y.; Lewis, A.; Thomas, D. Arsenic Exposure and Toxicology: A Historical Perspective. *Toxical Sci* **2011**, *132* (2). https://doi.org/10.1093/toxsci/kfr184.

(6) Marei, M. M.; Kaht, K. L.; Roussel, T. J.; Keynton, R. S.; Baldwin, R. P. Measurement of As(III) with in Situ Subtraction of Background and Interferent Signals by Double Potential Step-Anodic Stripping Coulometry. *Sens. Actuators B Chem.* **2019**, *301*.

(7) Ghosh, A. Evaluation of Chronic Arsenic Poisoning Due to Consumption of Contaminated Ground Water in West Bengal, India. *Int. J. Prev. Med.* **2013**, *4* (8).

(8) Rahman, M.; Sengupta, M.; Ahamed, S.; Lodh, D.; Das, B.; Hossain, M. A.; Nayak, B.; Mukherjee, A.; Chakraborti, D. Murshidabd-One of the Nine Groundwater Arsenic-Affected Districts of West Bengal, India. Part 1: Magnitude of Contamination and Population at Risk. *Clin. Toxicol.* **2005**, *43*.

(9) Podgorski, J.; Berg, M. Global Threats of Arsenic in Ground Water. *Science* **2020**, *368* (6493).

(10) Phillips, A.; Hung, Y.-T.; Bosela, P. A. Love Canal Tragedy. *J. Perform. Constr. Facil.* **2007**.

(11) Bullitt County History Museum. Valley of Drums. bullitcountyhistory.org May 31, 2022.

(12) National Priorities List and Superfund Alternative Approach Sites. https://www.epa.gov/superfund/search-superfund-sites-where-you-live (accessed 2023-04-08).

(13) Armbruster, D.; Pry, T. Limit of Blank, Limit of Detection, and Limit of Quantification. *Clin Biochem Rev* **2008**, *29* (1).

(14) Jia, X.; Gong, D.; Wang, J.; Huang, F.; Duan, T.; Zhang, X. Arsenic Speciation in Environmental Waters by a New Specific Phosphine Modified Polymer Microsphere Preconcentration and HPLC-ICP-MS Determination. *Talanta* **2016**, *160*, 437–443.

(15) Harris, D. C. *Quantitative Chemical Analysis*, ninth.; W. H. Freeman & Company, 2016.

(16) Lindemann, T.; Hamester, M.; Hinrichs, J.; Wills, J. High Sensitivity Arsenic Speciation: HPLC Sector Field ICP-MS.

(17) United States Department of Agriculture Food Safety and Inspection Service, Office of Public Health Service. Determination of Arsenic by Atomic Absorption Spectroscopy, 2016.

(18) Martin, T. D.; Brockhoff, C. A.; Creed, J. T. Determination of Metals and Trace Elements in Water and Wastes by Inductively Coupled Plasma-Atomic Emission Spectrometry.

(19) Jia, X.; Gong, D.; Wang, J.; Huang, F.; Duan, T.; Zhang, X. Arsenic Speciation in Environmental Waters by a New Specific Phosphine Modified Polymer Microsphere Preconcentration and HPLC-ICP-MS Determination. *Talanta* **2016**, *160*, 437–443.

(20) Shrivas, K.; Shanker, R.; Dewangan, K. Gold Nanoparticles as a Localized Surface Plasmon Resonance Based Chemical Sensor for On-Site Colorimetric Detection of Arsenic in Water Samples. *Sens. Actuators B Chem.* **2015**, *220*.

(21) Hach Arsenic Test Kit.

(22) Kelsey Khat. An Electrochemical Instrument for the Analysis of Heavy Metals in Water Via Anodic Stripping Coulometry for Applications in Remote Sensing, 2019.

(23) Kolya, H.; Hashitsume, K.; Kang, C.-W. Recent Advances in Colorimetric Detection of Arsenic Using Nanoparticles. *Toxics* **2021**, *9* (6).

(24) Willets, K.; Van Duyne, R. Localized Surface Plasma Resonance Spectroscopy and Sensing. *Annu Rev Phys Chem* **2007**, *58*, 267–297.

(25) Elgrishi, N.; Rountree, J. K.; McCarthy, B. D.; Rountree, E. S.; Eisenhart, T. T. A Practical Beginner's Guide to Cyclic Voltammetry. *JChem Educ* **2018**, *95*, 197–206.

(26) Zoski, C. *Handbook of Electrochemistry*; Elsevier.

(27) Marei, M. M.; Roussel, T. J.; Keyton, R. S.; Baldwin, R. P. Electrochemical and Microfabrication Strategies for Remotely Operated Smart Chemical Sensors: Application of Anodic Stripping Coulometry to Calibration-Free Measurements of Copper and Mercury. *Anal. Chem. Acta* **2013**, *803*.

(28) Princeton Applied Research. Princeton Applied Research. In *Fundamentals of Stripping Voltammetry*.

(29) Determination of Lead at a Thin-Film Mercury Electrode (Formal Report). In *Chem 400A: Voltammetry at a Thin-Film Mercury Electrode*; pp 184–197.

(30) Bolker, B.; Brooks, M.; Clark, C.; Geange, S.; Poulsen, J.; Stevens, H.; White, J.-S. Generalized Linear Mixed Models: A Practical Guide for Ecology and Evolution. *Trend Ecol. Evol.* **2008**, *24* (3).

(31) Bard, A. J.; Faulkner, L. R. *Electrochemical Methods*, 2nd ed.; John Wiley & Sons, 2001.

(32) Konopka, S. J.; McDuffie, B. Diffusion Coefficients of Ferri- and Ferrocyanide Ions in Aqueous Media, Using Twin-Electrode Thin-Layer Electrochemistry. *Anal Chem* **1970**, *42*.

(33) Let's Familiarize Ourselves with the SEM, 2008.

APPENDICES

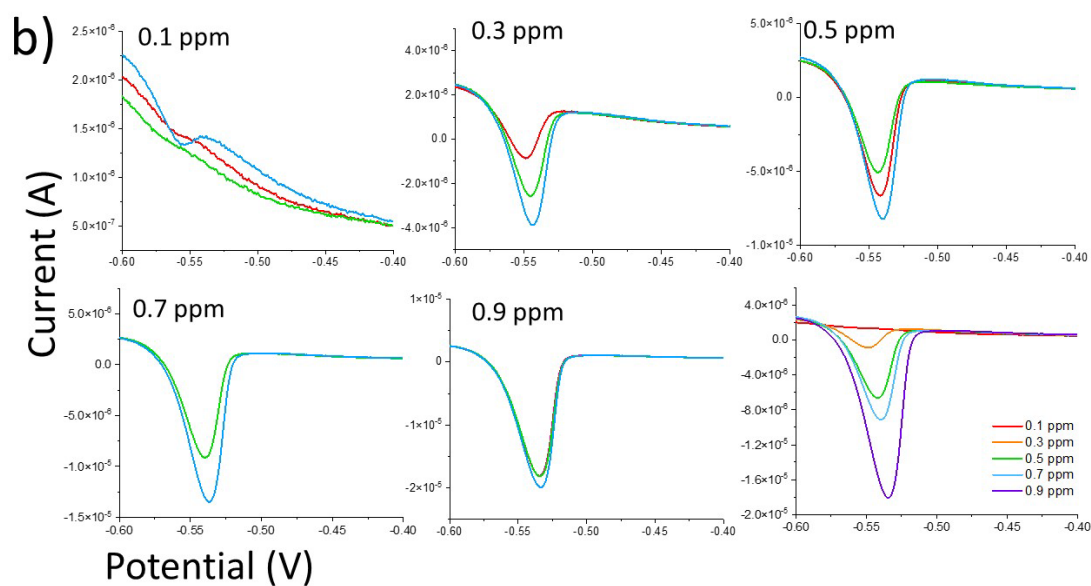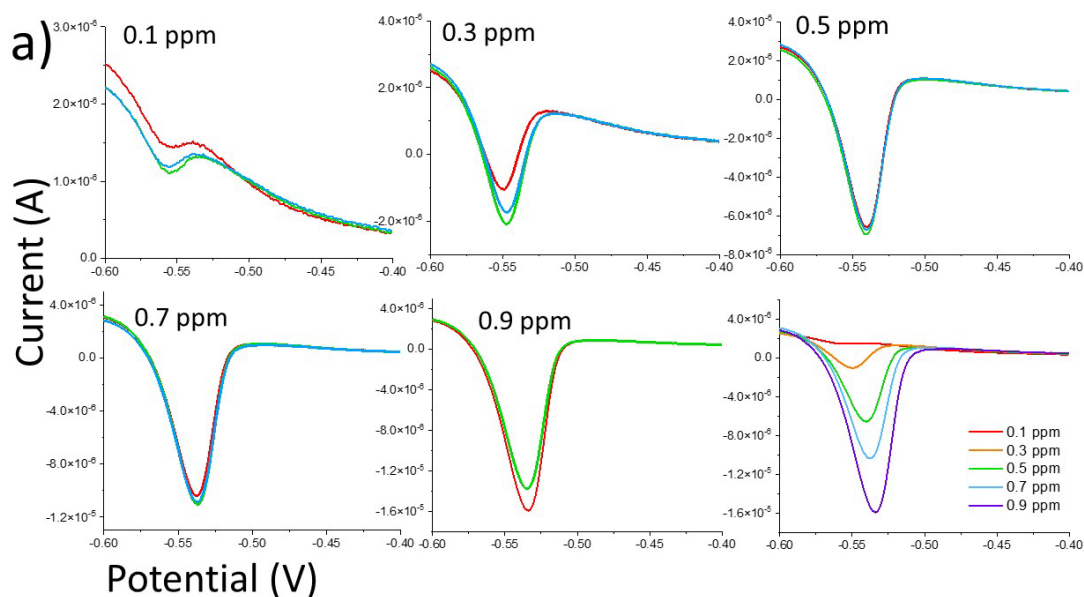Appendix A: Statistical Data For Experiments 2, 3, 4, and 5
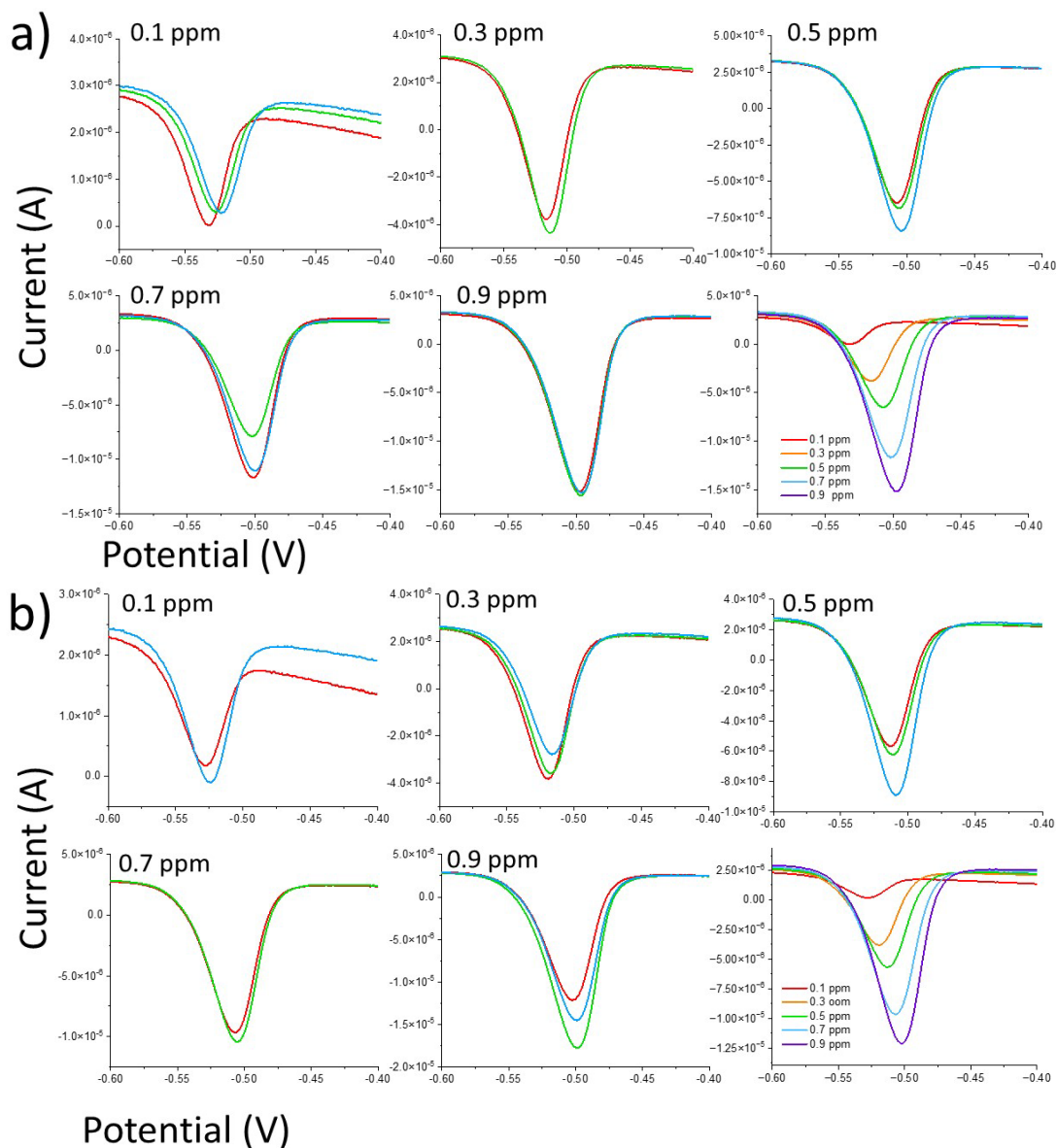
Experiment 2 Anodic Striping Voltammetry oxidation peak overlay for increasing concentrations of lead for Experiment 1 with the counter electrode separated (a) and without separation (b). The peak observed near -0.5 V corresponds to lead. Measurements were taken in triplicate, with the first shown in red, the second in green, and the third in blue. Lastly, an overlay of representative sweep from each concentration is shown to emphasis the increase in current observed as lead concentration increased.
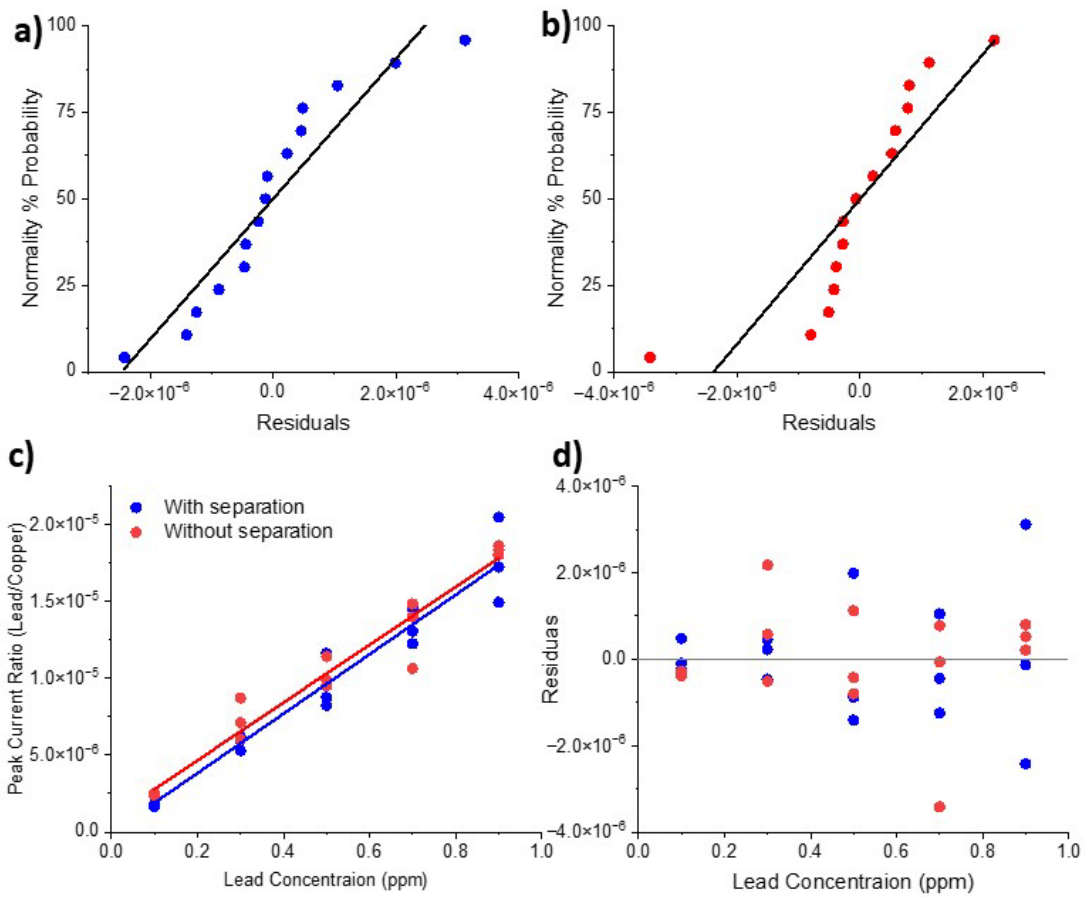
Experiment 2 simple linear regression model and assumptions— pp-plot with separation (a), pp-plot without separation (b), simple linear regression model with least squares regression line with separation (c blue) and without separation (c red), and residual versus lead concentration with separation (d blue) and without separation (d red).
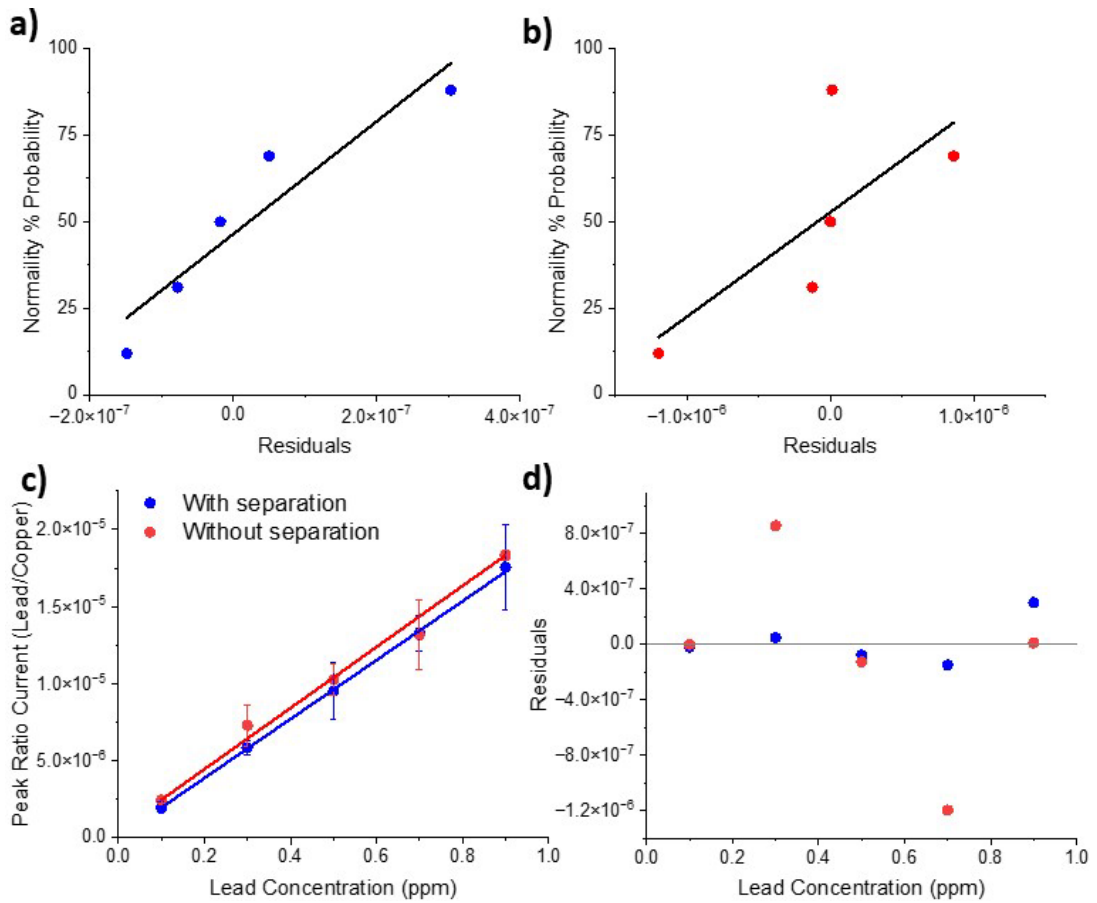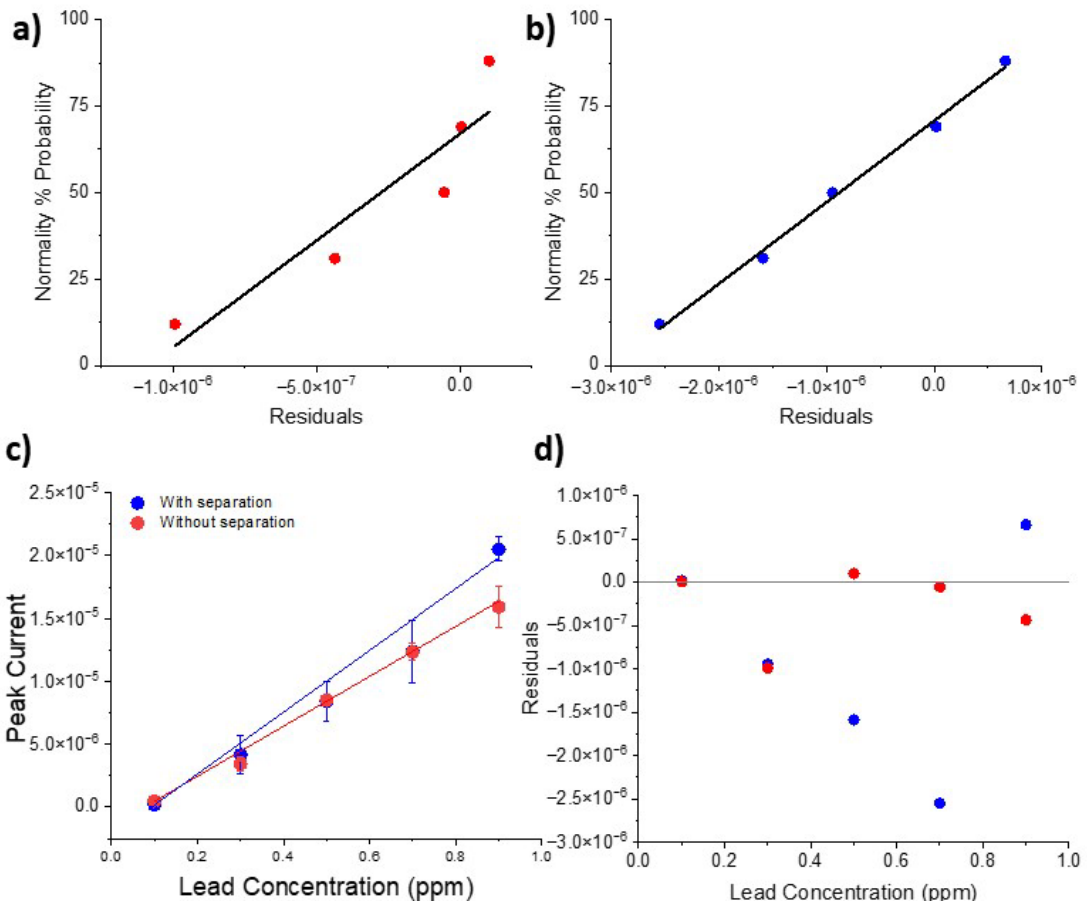
Experiment 2 repeated measures ANOVA model linear regression and assumptions—pp-plot with separation (a), pp-plot without separation (b), repeated measures ANOVA model with least squares regression line with separation (c blue) and without separation (c red), and residual versus lead concentration with separation (d blue) and without separation (d red).

Experiment 3 Anodic Striping Voltammetry oxidation peak overlay for increasing concentrations of lead for Experiment 3 with the counter electrode separated (a) and without separation (b). The peak observed near -0.5 V corresponds to lead. Measurements were taken in triplicate, with the first shown in red, the second in green, and the third in blue. Lastly, an overlay of representative sweep from each concentration is shown to emphasis the increase in current observed as lead concentration increased.
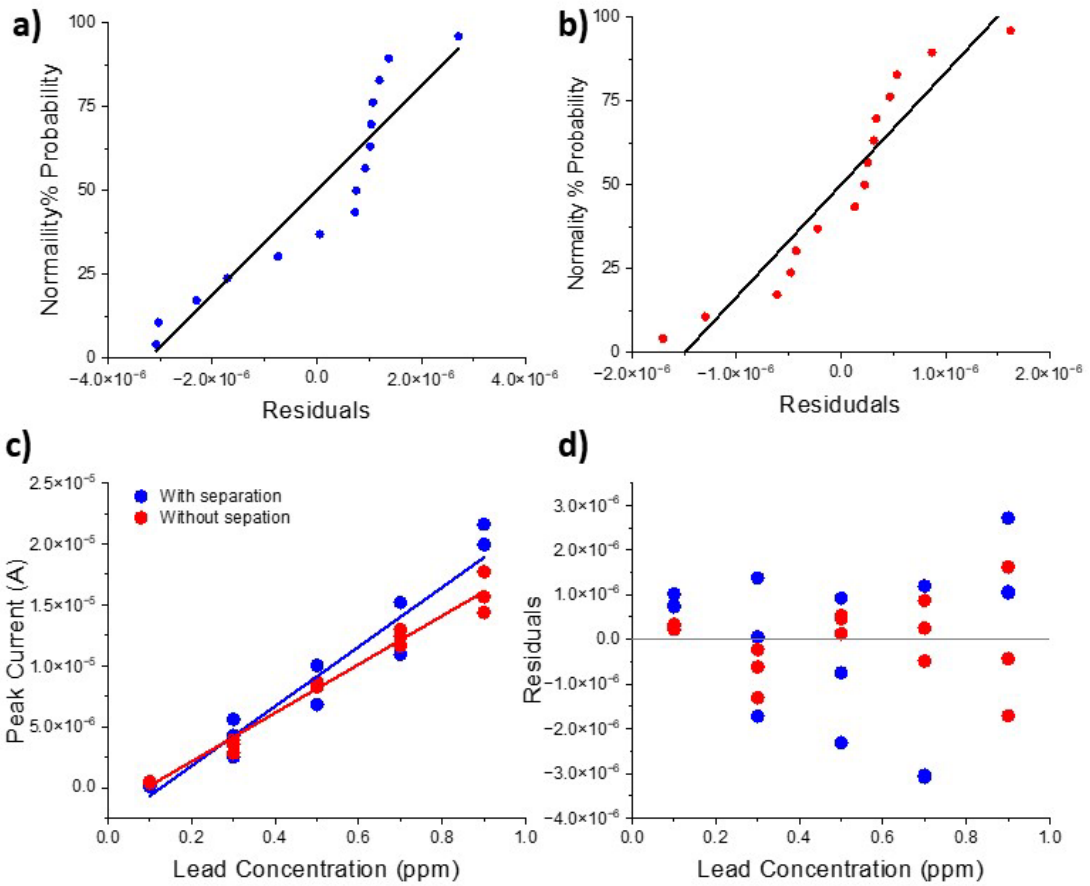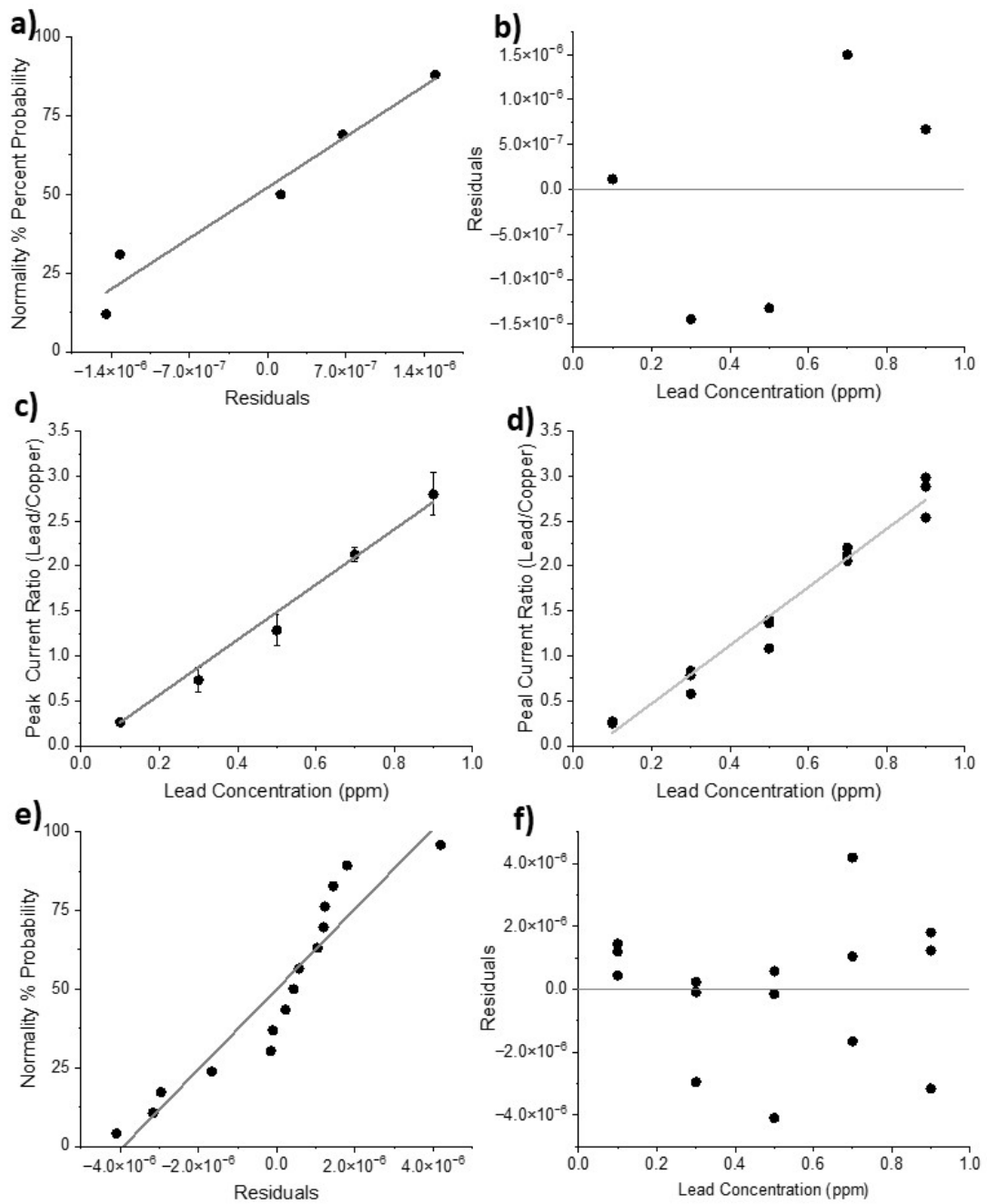
Experiment 3 simple linear regression model and assumptions— pp-plot with separation (a), pp-plot without separation (b), simple linear regression model with least squares regression line with separation (c blue) and without separation (c red), and residual versus lead concentration with separation (d blue) and without separation (d red).

125

Experiment 3 repeated measures ANOVA model linear regression and assumptions—pp-plot with separation (a), pp-plot without separation (b), repeated measures ANOVA model with least squares regression line with separation (c blue) and without separation (c red), and residual versus lead concentration with separation (d blue) and without separation (d red).
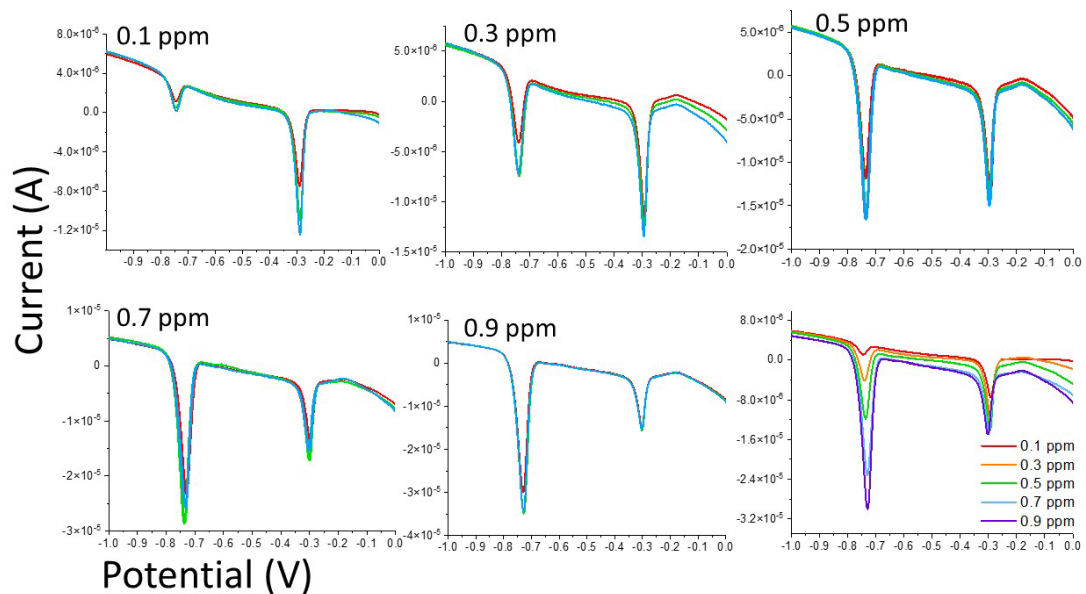
Experiment 4 Anodic Striping Voltammetry oxidation peak overlay for increasing concentrations of lead for Experiment 4. Copper maintained a concentration of 0.1 ppm. The peak observed near -0.5 V corresponds to lead. Measurements were taken in triplicate, with the first shown in red, the second in green, and the third in blue. Lastly, an overlay of representative sweep from each concentration is shown to emphasis the increase in current observed as lead concentration increased.
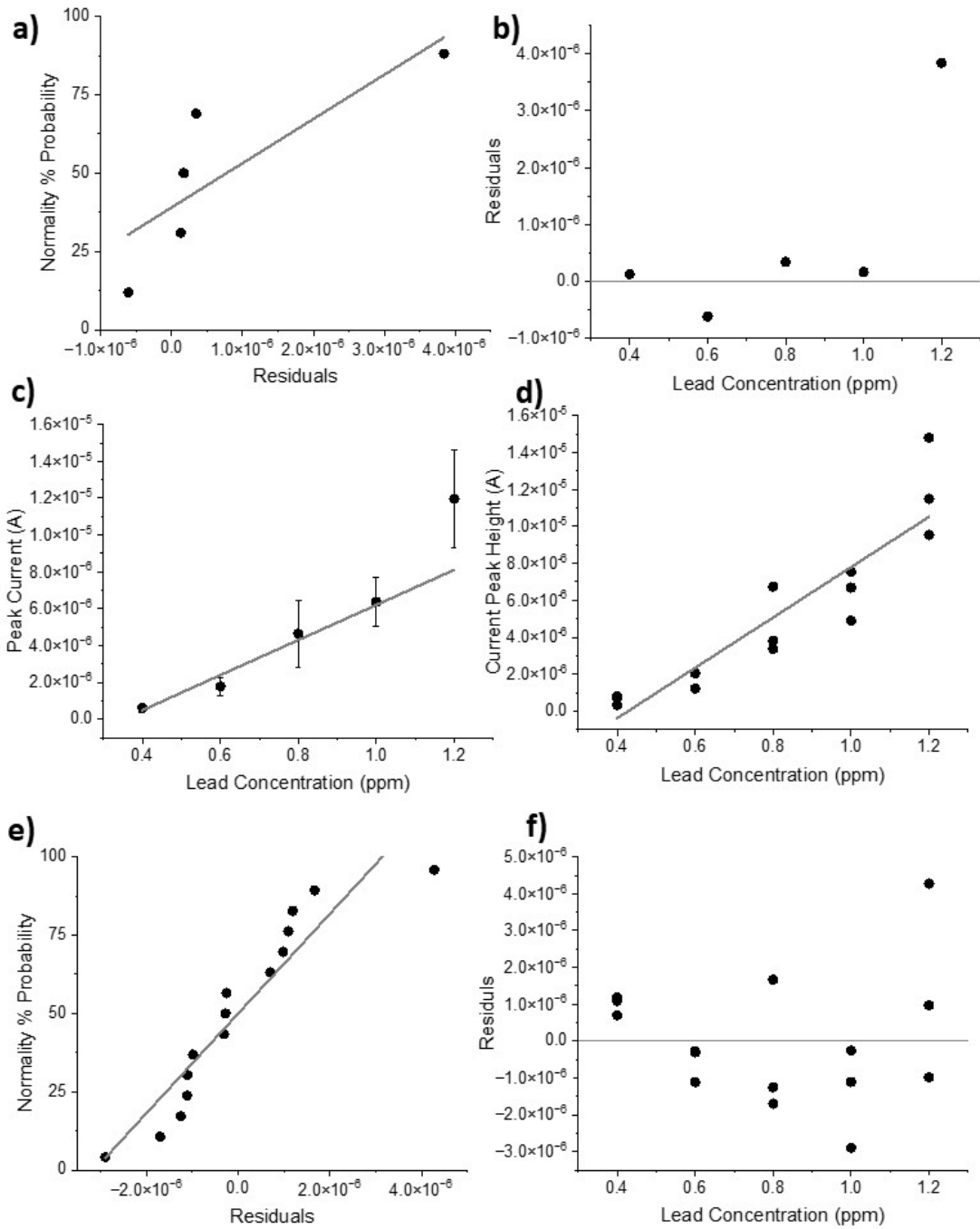
Experiment 4 linear regression and assumptions for the simple linear regression model— pp-plot repeated measures ANOVA (a), residuals versus lead concentration for repeated measures ANOVA (b), and repeated measures ANOVA linear regression model with standard deviation bars (c), simple linear regression model (d), pp-plot simple linear regression model (e), and residuals versus lead concentration for simple linear regression (f),
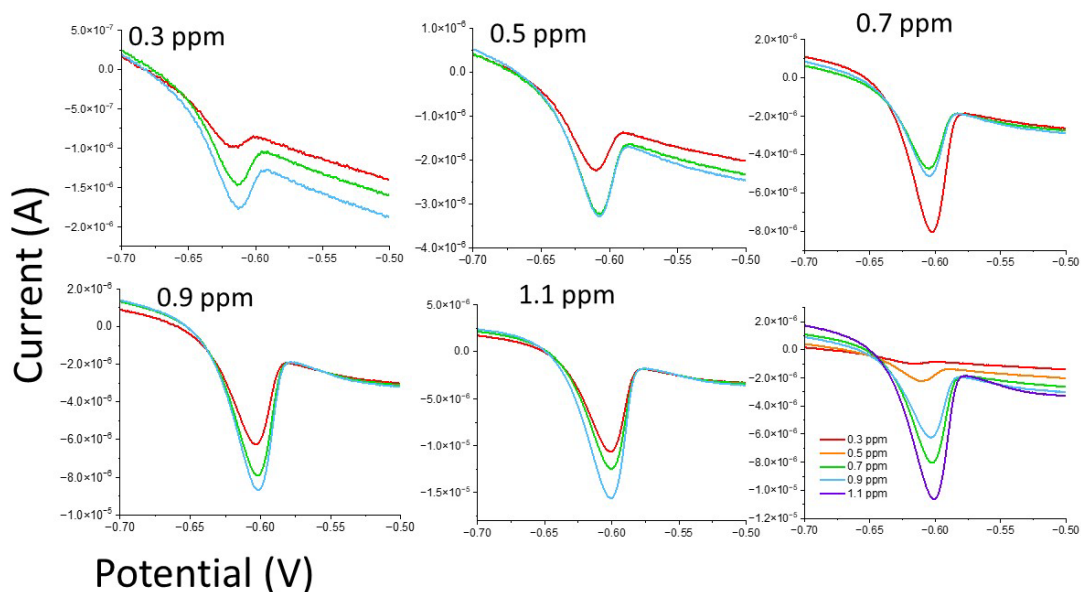
Experiment 5 Anodic Striping Voltammetry oxidation peak overlay for increasing concentrations of lead for Experiment 4. The peak observed near -0.5 V corresponds to lead. Measurements were taken in triplicate, with the first shown in red, the second in green, and the third in blue. Lastly, an overlay of representative sweep from each concentration is shown to emphasis the increase in current observed as lead concentration increased.

Experiment 5 linear regression and assumptions for the simple linear regression model— pp-plot repeated measures ANOVA (a), residuals versus lead concentration for repeated measures ANOVA (b), and repeated measures ANOVA linear regression model with standard deviation bars (c), simple linear regression model (d), pp-plot simple linear regression model (e), and residuals versus lead concentration for simple linear regression (f),